ENERGY MANAGEMENT of ELECTRIC VEHICLE SUPPLY EQUIPMENT IN MULTI-UNIT RESIDENTIAL BUILDINGS

Behrad Jamadi

Thesis submitted to the University of Ottawa in partial fulfillment of the requirements for the degree of

Master of Applied Science, Electrical and Computer Engineering

School of Electrical Engineering and Computer Science
Faculty of Engineering
University of Ottawa

Supervisor: Dr. Javad Fattahi

Abstract

As EV adoption continues to grow, the demand for charging infrastructure is increasing, particularly in multi-unit residential buildings (MURBs), which account for a substantial share of urban housing. However, most existing MURBs were not designed to support the additional electrical demand introduced by EV charging, resulting in limitations in capacity. While electrical upgrades could address these challenges, they are often prohibitively expensive. A more affordable and scalable alternative is the deployment of Energy Management Systems (EMS) dedicated to Electric Vehicle Supply Equipment (EVSEs), which can intelligently allocate power and enhance utilization of existing electrical infrastructure without major physical modifications.

To address these challenges across different electrical topologies, a suite of EMS methods is developed for MURBs. For a single-source feeder supplying EVSEs, we develop a Mixed Integer Linear Programming (MILP) based EMS that explicitly models the two-phase connections of EVSEs in a three-phase system to ensure balanced operation between connected phases. A Nonlinear Auto-Regressive with Exogenous Input (NARX) forecasting model is employed to predict non-EV load consumption, enabling real-time EMS operation. To manage the uncertainties introduced by non-EV load demand and stochastic EV availability across multiple sub-feeders, a Distributionally Robust Optimization (DRO) framework with a Wasserstein ambiguity set is developed to determine the optimal charging profiles for the EVSEs under such uncertain conditions. Furthermore, to better capture the hierarchical

and multi-tier electrical system of MURBs, a game-theoretic EMS based on the Stackelberg model is developed, where the main panel acts as the leader by setting capacity limits, and each sub-feeder, as a follower, maximizes its own consumption. The proposed EMSs are designed to prioritize non-EV loads and allocate the remaining feeder capacity to active EVSEs while adhering to feeder constraints.

Beyond energy allocation, to mitigate excessive curtailment and ensure fairness among EVSEs, a dynamic Round-Robin (d-RR) scheduling mechanism is proposed that can be lightly integrated with the developed EMS methods. By dynamically changing the time quantum, the d-RR approach prevents starvation and equitably distributes charging opportunities across EVs. This scheduler enhances energy utilization and leads to overall customer satisfaction.

Simulation results confirm that the proposed EMSs effectively curtail EVSE loads during high consumption of non-EV loads, which facilitates the integration of EVSEs into existing MURB infrastructures. Moreover, the results of the d-RR scheduler demonstrate that EVSE penetration can increase and provide fair access to the limited charging capacity among EVSEs, without requiring major electrical system reinforcements.

Acknowledgments

I would like to express my deepest gratitude to my supervisor, Dr. Javad Fattahi, for his continuous guidance, encouragement, and invaluable support throughout the course of this research. His insights and expertise have been instrumental in shaping the direction and quality of this work.

I would also like to extend my appreciation to the team at SWTCH Energy Inc. for providing technical resources, practical insights, and collaboration opportunities that greatly enriched this project. This research was supported by Mitacs through the Accelerate program, and I am sincerely grateful for their funding and partnership.

Finally, I wish to thank my family and friends for their unwavering support, patience, and encouragement throughout my academic journey.

Dedication

This thesis is dedicated to my beloved parents and my dear brother, for their unconditional love, support, and sacrifices.

Contents

List of Figures

List of Tables

List of Abbreviations

CMS	Charging Management System
DRO	Distributionally Robust Optimization
d-RR	Dynamic Round-Robin
EMS	Energy Management Systems
EV	Electric Vehicle
EVSE	Electric Vehicle Supply Equipment
FCFS	First-Come First-Served
HEMS	Home Energy Management System
MILP	Mixed Integer Linear Programming
MURB	Multi-Unit Residential Building
NARX	Nonlinear AutoRegressive with Exogenous Inputs
OCPP	Open Charge Point Protocol
RMSE	Root Mean Square Error
RO	Robust Optimization
SO	Stochastic Optimization
SoC	State of Charge

Nomenclature

Sets

$\mathcal{A}$	Set of activated circuits
$\mathcal{C}$	Set of all EVs in the system
$\mathcal{E}$	Set of EVs currently demanding charge
$\mathcal{F}$	Ambiguity set for DRO
$\mathcal{G}_g$	List of circuit indices assigned to group g in d-RR
$\mathcal{L}_{\mathcal{A}}$	Subset of EVSEs currently active
$\mathcal{L}_n$	Set of EVSEs connected to sub-feeder n
$\mathcal{M}$	Set of all breakers across all sub-feeders
$\mathcal{M}_i$	Subset of EVSEs connected to phase i
$\mathcal{M}_n$	Set of breakers connected to sub-feeder n
$\mathcal{M}^k$	Subset of multi-phase EVSEs that require balanced current allocation
$\mathcal{N}$	Set of sub-feeders in the building
P	Set of electrical phases
$\mathbb{P}$	Unknown probability distribution of uncertainties
$\hat{\mathbb{P}}$	Empirical probability distribution estimated from data
$\mathcal{P}_0(\cdot)$	Set of all probability distributions over the uncertain parameters of the system

Indices

g	Group index in d-RR scheduling

i	EV index
$\imath$	Index of the activated circuit within group $\mathcal{G}_g$ in round R
j	Quantum index in d-RR scheduling
m	Index of EVSE or breaker
n	Index of sub-feeder
R	Round index in the d-RR sequence
t	Time-slot index

Parameters / Constants

α_m	Priority coefficient for charger m
$\alpha_{n,m}$	Priority coefficient assigned to DC-connected EVSEs
β	Coefficient ensuring convexity of the objective function
E	Number of EVs currently demanding charge
$I^{\text{ac}}_{n,t}$	Max AC charging current limits for sub-feeder n at time t
I^{dc}	Max DC charging current limits for sub-feeder n at time t
$I^{\max}_m$	Maximum operating current for EVSE m
$I^{\min}_m$	Minimum operating current for EVSE m
κ	Penalty factor in satisfaction formulation
$\mathcal{I}^{\max}$	Maximum total ampacity of the main distribution panel
$l_{n,m}$	EVSE connected to breaker m on sub-feeder n
M_n	Number of EVSEs on sub-feeder n
N	Total number of sub-feeders connected to the main panel
$p^{(i)}$	Ampacity limit (maximum allowable current) of phase i
p_n	Nominal ampacity limit of sub-feeder n
q	Number of circuits/groups selected for concurrent scheduling
r	Coefficient restricting main-panel capacity by the upstream feeder
$\mathcal{S}^{\min}$	Minimum required satisfaction threshold for EV owners
$\mathcal{S}^{\text{thr}}$	Driver satisfaction threshold
t^q	Fixed quantum time per scheduling round
T	Number of time slots in the scheduling horizon
χ_m	Binary indicator of EVSE type (1 = DC, 0 = AC)

$z_{\alpha/2}$	Critical value for the confidence level

Variables

$\bar{i}$	Average requested demand across all EVSEs
i_n	Total current drawn by sub-feeder n
y_m	Operating current assigned to EVSE m
$y_m^{(i)}$	Current allocated to EVSE m on phase i
$y_{n,m,t}$	Charging current allocated to EVSE m on sub-feeder n at time t
z_m	Binary variable indicating whether circuit m is active
$A_{n,m,t}$	Binary indicator for availability of EVSE m on sub-feeder n at time t
$\delta_{n,t}$	Non-EV load on sub-feeder n at time t
δ_n	Non-EV baseload on sub-feeder n
$\delta^{(i)}$	Predicted non-EV load on phase i
i_m	Individual requested demand of EVSE m
$\varepsilon_{n,t}$	Forecast uncertainty for non-EV load on sub-feeder n at time t
$p_{n,m,t}$	Expected availability of EVSE m on sub-feeder n at time t
σ	Standard deviation of predicted non-EV consumption
$\sigma^2_{n,m,t}$	Variance of availability for EVSE m on sub-feeder n at time t

Functions / Derived Quantities

$H(\cdot)$	Heaviside step function
$\lfloor \cdot \rfloor$	Floor function
λ_j	Size of quantum j (EVs allocated to group j)
$\mathcal{Q}_j$	d-RR queue sequence assigned to group j
$\mathcal{S}$	Received SoC before next trip
$\mathcal{S}^{\mathrm{f}}$	SoC of EV after receiving charge
$\mathcal{S}^{\mathrm{f}}_{i,j}$	Final SoC of EV i on day j
$\mathcal{S}^{\mathrm{ini}}$	SoC of EV after daily commute
$\mathcal{S}^{+}$	Overall satisfaction score aggregated over all EVs and time periods
t_i^{δ}	Elapsed charging time of EV i

t_j^d	Dynamic quantum time for group j

Matrices / Arrays

$Z_i(m,m)$	Binary matrix encoding current direction/coupling across phases for EVSE m (phase i)

Contribution of the Work

The research presented in this thesis has resulted in the following publications and conference presentations:

1. **Elsevier Journal (Under Review):**
   B. Jamadi, M. Samadi, and J. Fattahi, "*Multi-tier Electric Vehicle Charging Management using a Non-cooperative Game and Round Robin Scheduling*," *International Journal of Electrical Power and Energy Systems*, submitted in Sep 2024.

2. **IEEE PES Conference Papers:**
   B. Jamadi, EB. Onural, and J. Fattahi, "*Electrification in Residential Buildings using Distributionally Robust Optimization*," in *IEEE Power & Energy Society General Meeting (PESGM)*, 2025.

3. **IEEE EPEC Conference Paper:**
   EB. Onural, B. Jamadi, and J. Fattahi, "*Rethinking Smart Grid Mesh Network with Dual Border Routers for Asset Integration*," in *IEEE Electrical Power and Energy Conference (EPEC)*, 2025.

4. **IEEE PES Conference Papers:**
   EB. Onural, M. Bazyari, B. Jamadi, and J. Fattahi, "*Real-Time AI-Driven EV Charger Load Management for Residential Electrification*," in *IEEE Power & Energy Society General Meeting (PESGM)*, 2025.

5. **SYSTEMS AND METHODS FOR ELECTRIC VEHICLE (EV) MESH CONNECTIVITY AND ENERGY MANAGEMENT:**
filed in 2025 by **SWTCH Energy Inc.**.

Chapter 1

Introduction

1.1 Motivation

The Government of Canada has set 2050 as the target year to achieve net-zero greenhouse gas emissions, aligning with global efforts to combat climate change and transition toward a cleaner energy future [1]. The growing electrification of energy consumption across the residential, commercial, and industrial sectors would be a key pathway toward achieving this transition. Electrification refers to the process of replacing fossil fuel-operated systems with electric alternatives, which can reduce greenhouse gas emissions. By shifting the energy demand of end-users to electricity generated by renewable resources, societies can accelerate the transition toward a more sustainable future [2].

Electrification in the residential sector comprises upgrading thermal and transportation loads. The thermal loads, such as heat pumps and electric water heaters, replace conventional gas-based systems for space and water heating, contributing to building decarbonization, while transportation electrification replaces conventional combustion engine vehicles with Electric Vehicles (EVs).

Driven by advances in battery technology, decreasing manufacturing costs, and supportive government policies, global EV adoption has accelerated over the past decade [3]. Annual EV sales increased from fewer than 100,000 units in 2012 to over 14 million in 2023, representing approximately 18% of all vehicle sales worldwide [4]. According to the International Energy Agency (IEA), the global EV stock is projected to surpass 250 million by 2030 under current policy scenarios [5]. Along with this global movement, the government of Canada also aims for all new vehicles sold by 2035 to be zero emission [6].

The affordability and convenience of charging EVs are recognized as the main factors influencing the adoption of electric vehicles [7, 8]. According to Canadian statistics, approximately one-eighth of households reside in condominium units, predominantly located in metropolitan areas characterized by a deep dependence on vehicles for daily commuting [9]. To ensure equitable infrastructure access, it is imperative that lower-income communities in Canada have access to approximately 30% of EVSEs by 2030 [10]. To this end, the charging infrastructure network must expand its coverage to cater to a wider range of drivers [5]. Meeting this ambitious target will increase electricity demand and require upgrades to existing infrastructure. Most of the MURBs and condominiums in Canada were constructed years ago [11], and were designed with limited electrical capacity. Most of the MURBs in Canada are not designed to handle the extra load from EV charging. Peak electricity demand often coincides with residents returning home and using high-power appliances and EV chargers [12]. This overlap between household peak demand and EVSE utilization heightens the risk of feeder overloads, raising concerns regarding infrastructure upgrade costs and the affordability of charging technologies in MURBs.

Although upgrading electricity infrastructure in MURBs could address the issue, implementing an energy management approach to regulate the additional demand from electrification is more cost-effective and sustainable in the long run [13], which is the focus of this thesis.

1.2 Thesis Outline

This thesis introduces a suite of near-real-time online EMS solutions to enable the cost-effective integration of EVSE into MURBs without requiring major electrical upgrades. To better frame the proposed solution, Section 1.3 provides an in-depth review of the background and previous studies on energy management across various grid applications. Subsection 1.3.1 then classifies the architectures of different electrical systems in MURBs and identifies the key constraints and functional requirements for an effective EMS. Building on this understanding, the thesis outlines four methods suitable for MURBs, presented across the subsequent chapters.

In Chapter 3, a dynamic Round-Robin (d-RR) scheduling mechanism is introduced as a simple but efficient near real-time solution for managing concurrent EV charging sessions in MURBs. We derive the formulation and present the algorithm for the d-RR method, explaining how it dynamically adjusts charging intervals based on the number of active EVSEs to ensure fair access to the available feeder capacity. A case study is also presented to compare its performance with conventional approaches such as First-Come-First-Served (FCFS) scheduling and Regular charging, showing improvements in fairness and energy utilization.

In Chapter 4, a centralized EMS based on a Mixed-Integer Linear Programming (MILP) formulation is developed for MURBs in which all EVSEs are connected to a single sub-feeder. The modeling of two-phase EVSE connections in a three-phase distribution system is described, along with the integration of a short-term non-EV load prediction model into the optimization process. A case study using real building data is provided to illustrate the EMS operation and demonstrate its computational efficiency under deterministic conditions.

In Chapter 5, an EMS based on Distributionally Robust Optimization (DRO) is developed to ensure reliable operation under uncertainties such as variations in non-EV load consumption and unpredictable EV availability across different sub-feeders in the MURB electrical system. The mathematical formulation of the Wasserstein-based ambiguity set is provided to capture these uncertainties, and a case study is conducted to validate that the developed DRO framework can effectively balance robustness and efficiency.

In Chapter 6, a hierarchical Energy Management System (EMS) based on a non-cooperative Stackelberg game formulation is introduced to represent multi-tier electrical structures in MURBs. This chapter explains how the Stackelberg framework models the leader–follower interaction between the main panel and sub-feeders to enable coordinated energy allocation across the building network. It presents the mathematical formulation of the game with the proof of equilibrium existence using Kakutani's fixed-point theorem. A case study is also provided to demonstrate how the proposed hierarchical EMS can effectively coordinate sub-feeder operation and integrate with the d-RR scheduling mechanism introduced earlier.

1.3 Background and Literature Review

The concept of an Energy Management System (EMS) emerged in the early 1970s as utilities began computerizing generation, transmission, and intertie coordination; by the mid-1970s, EMS were formalized in control-center practice and literature [14, 15, 16]. An EMS can be defined as a framework that monitors, controls, and optimizes the generation, distribution, and consumption of energy across different scales of the power system. Traditionally, EMS were developed for electric utilities to supervise power generation, transmission, and distribution, with the primary objective of maintaining reliability and minimizing operational costs at the grid level. Later, advances in Information and Communication Technologies (ICT) have enabled the deployment of EMS solutions at the consumer and building levels, and led to emergence of concepts such as smart buildings, Home Energy Management Systems (HEMS), and smart grids, which aim to enhance electricity efficiency, provide grid services, and lower operational costs for both grid operators and end-users [17, 18, 19]. In the following sub-sections, we will review different EMS architectures and various methods applied to residential and non-residential applications.

1.3.1 Energy Management System Architectures

From a control-theoretic perspective, the architecture of an EMS determines how information is processed and how control decisions propagate through the system. Depending on system hierarchy and communication topology, EMS frameworks are broadly categorized as centralized, decentralized, or distributed [20]. Figure 1.1 illustrates the structural differences among these paradigms.

Centralized architecture places decision authority in a single control unit that gathers data from all nodes (e.g., appliances, EVSEs, or DERs) and optimizes operations globally. Reference [21] used a centralized energy management scheme for grid-connected DC microgrids. Their model is structured hierarchically into three control layers. The primary layer directly regulates converters and loads, the secondary layer maintains power balance and bus voltage, and the tertiary layer performs optimization tasks such as PV-BESS utilization and load shedding. Furthermore, a centralized control scheme is proposed in [22], where a central controller collects voltage, current, and state-of-charge (SoC) data, processes them, and makes global decisions regarding source prioritization, load allocation, and charging/discharging strategies in a hybrid microgrid. Although central architecture is more effective at global optimization and enables simpler control of the whole system, it faces challenges of computational scalability and vulnerability to single points of failure [23].

In decentralized EMS architectures, decision authority is distributed among multiple local controllers, and each controller optimizes its own resources. This reduces communication congestion and computational burden compared to centralized approaches, and enhances resilience to failures. For example, Wynn *et al.* proposed a decentralized EMS for microgrids under renewable energy and demand uncertainties, demonstrating how local controllers could efficiently manage resources while participating in demand response programs [24]. Additionally, [25] developed a decentralized multi-agent EMS for EV charging in low-voltage microgrids. Another work in [26] utilized a decentralized architecture for urban charging hubs with multiple V2G aggregators, where local aggregators coordinated EV routing and real-time charging. It should be noted that a decentralized scheme can lead to suboptimal global solutions due to the limited coordination among local controllers. In distributed EMS architectures, local controllers manage their own subsystems while exchanging limited information with neighboring units to achieve coordination across the system. This structure provides a balance between centralized global optimization and decentralized autonomy [27]. However, they are mostly expensive and difficult to implement due to the participation of multiple entities, and they require reliable communication networks to ensure convergence and system stability [20].

The authors of [28] implemented a multi-agent swarm optimization model where generators, storage systems, and EV charging stations act as autonomous agents that exchange solutions with neighbors and learn from the most effective ones. They showed that this cooperative process enables the system to balance supply and demand and gradually reach consensus without relying on a central controller. Moreover, to preserve the privacy of individual energy systems, paper [23] proposed a peer-to-peer distributed framework for multi-energy systems. Each subsystem operator optimizes locally and shares only boundary information through optimality condition decomposition, while blockchain consensus ensures secure coordination. Similarly, Umar *et al.* introduced a distributed EMS based on blockchain for community microgrids, in which prosumers directly trade energy using smart contracts and consensus mechanisms, enabling secure and transparent peer-

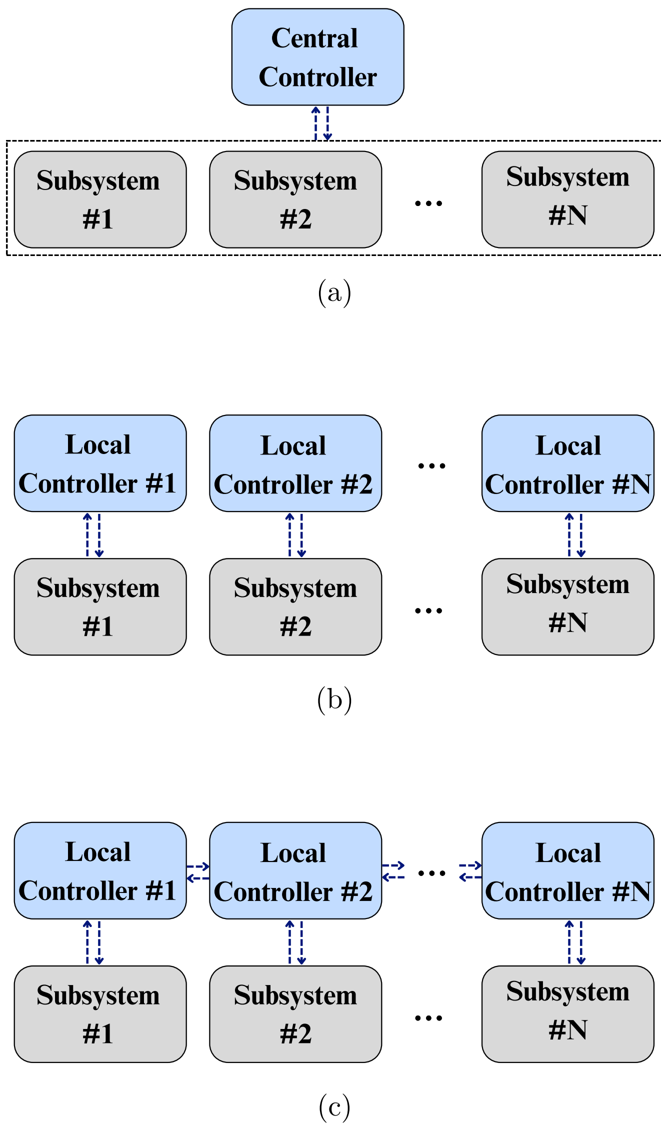

Figure 1.1: Different EMS architectures based on the level of control centralization and information exchange among system entities: (a) Centralized, (b) Decentralized, and (c) Distributed.

to-peer energy management [29].

1.3.2 Energy Management Strategies

A proper EMS strategy must be employed within a defined architecture. The architecture defines the level of centralization in control and coordination among components of the system, whereas the strategy determines the decision-making mechanism applied within that structure. In centralized architectures, since global information is available and a single controller manages the entire system, strategies typically rely on global optimization to determine control actions. As the system transitions toward more distributed or decentralized architectures, decision-making becomes shared among multiple controllers or agents with localized objectives. In such cases, strategies must enable coordination and interaction among these entities through iterative or cooperative mechanisms.

Developing an effective EMS requires the identification of a suitable control and coordination framework that aligns with the desired decision variables and operational objectives. This selection largely depends on the nature of the energy resources within the system, including both generation and consumption. Generally, resources can be classified as controllable, where the EMS can directly influence their operation, or non-controllable, which exhibit stochastic behavior due to factors such as user demand patterns and variability in environmental or other exogenous conditions. Controllable resources within an EMS are typically categorized based on the nature of their flexibility. The main categories include discrete-controllable, continuous-controllable, and shiftable loads. Discrete-controllable resources operate in distinct states (e.g., on/off), continuous-controllable resources allow modulation of power consumption within specified bounds, and shiftable resources permit temporal rescheduling of operation without degrading performance. Many end-use devices, such as dishwashers and energy storage systems, combine more than one of these properties [20]. For these types of resources, Mixed-Integer Linear Programming (MILP)-based EMS frameworks under a centralized architecture are commonly employed. MILP is an optimization technique in which the objective function and constraints are linear, but the decision variables are of mixed type, consisting of both continuous and discrete components. In MILP, binary variables are utilized to represent on/off states of controllable resources[18].

Employing MILP in HEMS has been widely explored to optimally schedule home appliances and energy storage systems, aiming to minimize electricity costs while ensuring user preferences and grid constraints are satisfied [30, 31]. Additionally, a centralized EMS for distributed and interconnected microgrids based on a MILP formulation is proposed in [32] to take advantage of compatibility with open-source solvers. Their EMS coordinates local generation, storage, and controllable loads across multiple microgrids while preserving data privacy and reducing overall operational costs. Furthermore, reference [33] managed active and reactive power flows in microgrids by formulating the problem as an MILP model, where binary variables represented the on/off states of distributed generators and storage units, and continuous variables captured their active and reactive power outputs. Their approach enabled optimal unit commitment and power dispatch while ensuring voltage stability, power factor compliance, and operational limits.

When the number of energy resources increases, and the system grows in scale, the EMS problem can become mathematically complex and computationally demanding for optimization techniques such as MILP [34]. In addition, when the behavior of energy resources exhibits uncertainty, and there is limited data to develop accurate predictive models, model-based approaches may not perform effectively due to the lack of reliable forecasts or complete system information. Under these circumstances, heuristic and metaheuristic approaches are widely adopted for energy management applications [35]. These approaches operate without requiring precise system models or detailed forecasts. Instead, they rely on readily available information, simple decision rules, or iterative search mechanisms to identify near-optimal solutions[18, 36].

A heuristic-based EMS for HVAC systems in university buildings was proposed in [37] to minimize electricity cost while maintaining thermal comfort. The authors first formulated the problem as an MILP model, where HVAC ON/OFF states and temperature levels were defined as decision variables dependent on uncertain parameters such as room temperature and occupancy. They demonstrated that solving this MILP is NP-hard, making exact optimization computationally infeasible for large systems, and therefore proposed a heuristic control strategy to achieve near-optimal results efficiently. Furthermore, the study in [38] utilized metaheuristic algorithms for a HEMS due to their capability in solving large-scale, nonlinear problems. They considered a typical smart home with ten appliances, PV generation, and an energy storage system, and performed a simulation under a 24-hour Time of Use pricing scheme to achieve cost savings and Peak to Average Ratio (PAR) reduction. Similarly, a meta-heuristic HEMS using a genetic algorithm (GA) was proposed in [39] to minimize residential electricity costs under Time of Use (ToU) tariffs. The authors used GA because the charging power functions of the energy storage system (ESS) and plug-in electric vehicle (PEV) were formulated as discrete and nonlinear functions, which are computationally inefficient to solve with MILP. Additionally, Farias *et al.* in [35] proposed an energy management in EV charging stations (EVCS) that combines Evolutionary Particle Swarm Optimization (EPSO) for day-ahead scheduling with a rule-based controller for real-time operation to achieve cost savings and reduced PAR. In their method, EPSO is responsible for generating an optimized charging schedule in advance, and during operation in real-time, the heuristic layer adjusts this schedule to handle uncertainties related to the stochastic behavior of the EV.

For systems that include shiftable energy resources and where sufficient data are available to develop reliable forecasting models, predictive control can enhance operational planning. The model predictive control (MPC) optimizes system operation by forecasting future behavior over a specified time horizon. At each control step, MPC solves an optimization problem that minimizes a cost function subject to system constraints, implements the first control action, and then repeats the process as new measurements and forecasts become available. MPC inherently provides a degree of robustness against uncertainties, as its feedback mechanism continuously corrects deviations between predicted and actual performance. However, precision in MPC depends on accurate models and forecasts, and solving an optimization problem at every step can be computationally demanding for large-scale systems [40].

MPC is used for a centralized EMS to coordinate PV generation, energy storage systems (ESS), and EV charging within a home nanogrid [41]. Employed MPC optimized power flow to minimize operating costs and ensure full overnight EV charging. In their study, they assumed perfect knowledge of future information, including electricity prices, load demand, PV generation, and EV arrival and departure times, for their predictive scheduling. They also compared their method with a heuristic approach and showed that MPC achieved lower operating costs, reduced grid stress, and provided better overall performance, especially under variable electricity pricing. Instead of assuming perfect knowledge of future information, dynamic state equations of the system components can be derived to construct a predictive model for forecasting system behavior in smart buildings [42]. Additionally, data-driven approaches such as symbolic regression [43] and regression-based model error compensation [44] can be utilized for forecasting in MPC frameworks. A comparison between MPC and a heuristic method was also presented in [45] for an off-grid microgrid, showing superior performance of MPC by reducing fossil fuel use, increasing renewable utilization, and enabling smaller equipment sizing while maintaining comfort. Reference [46] compared machine learning and MPC methods for optimizing battery energy storage systems within HEMS. A case study was conducted on a German low-voltage distribution grid with 13 households over a full year, evaluating performance in terms of peak shaving, grid constraint violations, and computational burden. The results show that MPC achieves results in terms of objective function value and constraint, but at a high computational cost, while machine learning methods provide faster results with slightly reduced accuracy.

Achieving affordable electrification in MURBs requires installing EVSEs for tenants within the existing electrical infrastructure, without costly upgrades to feeders or panels. This can be accomplished through EMS approaches that dynamically allocate and curtail charging power in real time according to the available electrical capacity. However, existing EMS frameworks have not been specifically dedicated to EVSE management in MURBs and often overlook the distinct electrical characteristics of EVSEs. EVSEs behave as nonlinear, elastic loads, typically connected to two phases of a three-phase system, which introduces the need to maintain phase balance among EVSEs. In addition, real-time EMS operation requires fast and computationally efficient optimization methods to ensure safe operation. As discussed earlier, MILP is well-suited for this purpose, as it can effectively model binary phase-assignment decisions while maintaining tractable computation times, making it ideal for real-time EMS implementation. For this purpose, in Chapter 4, we propose a central EMS based on MILP for the case where all EVSEs are installed on a single sub-feeder. The proposed model explicitly accounts for the phase connections of EVSEs within the three-phase system, ensuring balanced operation among EVSEs while maximizing the utilization of the available electrical capacity. Additionally, since a real-time EMS cannot operate solely using instantaneous metering data, a forecasting model is utilized to predict load consumption ahead of time.

Supervised and unsupervised machine learning approaches are widely used to develop prediction models in energy systems [47]. Unsupervised learning methods such as K-means clustering and principal component analysis (PCA) operate without labeled target outputs and aim to extract hidden structures or statistical patterns from historical data. These approaches are commonly used for clustering similar consumption profiles and anomaly detection, where the objective is to understand the data structure rather than predict a specific future value [48], [49]. Supervised learning, in contrast, relies on labeled input–output pairs, where historical measurements are used to train a model to estimate a desired target variable. The model learns a nonlinear mapping between these variables by minimizing prediction error during training [47]. In this work, since the aim is to predict the future non-EV load, and the building's historical consumption measurements are available, the forecasting problem is formulated within a supervised learning framework. Past load observations serve as input data, while the corresponding future load value represents the target output.

Among supervised learning models, classical statistical methods such as the Autoregressive Integrated Moving Average (ARIMA) model are commonly used for time-series prediction. ARIMA captures linear temporal dependencies based on past observations and stochastic error terms, and has demonstrated effectiveness in stationary or near-stationary load profiles. However, its performance may degrade when the underlying system exhibits strong nonlinear behavior or rapidly changing dynamics [50].

In addition to statistical models, neural network-based approaches such as the Multilayer Perceptron (MLP) have been adopted for regression-based forecasting problems. An MLP is a feedforward neural network capable of approximating complex nonlinear mappings between inputs and outputs. While MLPs provide improved flexibility compared to linear models such as ARIMA, they do not inherently capture temporal dynamics unless lagged observations are explicitly included in the input layer. As a purely feedforward architecture, an MLP lacks internal feedback connections and does not explicitly model system memory [51].

Other supervised models such as Support Vector Regression (SVR) and

Random Forest regression networks, have also been applied in load forecasting literature [50],[52]. Support Vector Regression is a kernel-based method capable of modeling nonlinear relationships between input variables and load demand; however, its performance is sensitive to the selection of model parameters and kernel functions. Random Forest can handle high-dimensional data and nonlinear patterns, but it may suffer from overfitting and requires careful tuning of hyperparameters. Although these models can capture nonlinear relationships, they do not inherently represent temporal dependencies in time-series data and therefore require the temporal structure of the data to be explicitly encoded through engineered lag features.

To better capture sequential dynamics, recurrent neural network architectures such as Long Short-Term Memory (LSTM) networks have been introduced. LSTM models are capable of learning long-term temporal dependencies in time-series data [50]. However, their training process typically requires large datasets and significant computational resources, which may limit their applicability in some forecasting environments. Another recurrent architecture used for time-series prediction is the Nonlinear Autoregressive model with Exogenous Inputs (NARX). The NARX model incorporates delayed input and output signals directly into the model formulation, and captures temporal dependencies and nonlinear system dynamics in time-series data. In addition, exogenous variables such as environmental or operational factors can be included as external inputs to improve prediction accuracy [53]. Similar to other neural network models, the training of NARX networks may also require considerable computational effort depending on the dataset size. In this work, the NARX model is adopted to forecast non-EV load consumption.

In energy systems with decentralized decision-making, where several autonomous agents (e.g., prosumers, microgrids, or distributed generators) determine their own operational strategies, game-theoretic models offer a structured means of analyzing their interactions and equilibrium behavior. In this framework, each resource acts as a player that optimizes its own objective function, such as minimizing cost, maximizing utility, or balancing SoC while considering the influence of the decisions of players on energy supply/demand balance, or market price. Through iterative strategy updates or distributed optimization, the system converges toward an equilibrium state (e.g., a Nash equilibrium) in which no participant can further improve its outcome unilaterally. These methods are typically applied to shiftable and elastic responsive resources, enabling coordinated yet autonomous decision-making within distributed EMS architectures. Game-theoretic formulations are broadly categorized as cooperative, when agents share common objectives, and non-cooperative, when each agent pursues its own interests [54].

An EMS based on a cooperative game for interconnected microgrids was presented in [55] to reduce total operating costs and enhance renewable energy utilization. In the developed game, participants (microgrid) formed a coalition to jointly schedule generation, storage, and demand. Additionally, authors in [56] modeled the Local Energy Community (LEC) as a coalition cooperative game, where participants engaged in P2P energy trading. They considered a community with 100 peers (50 consumers and 50 prosumers), a shared battery, and 15 EV chargers. The stability of cooperation was maintained by ensuring it was Nash-stable, which means none of the participants had an incentive to leave since all achieved better outcomes within the coalition. This enabled consumers to lower their electricity bills, prosumers to increase revenues, and the community to improve renewable utilization.

In [57], the real-time operation of a heat-electricity integrated energy system (HE-IES) was modeled as a non-cooperative Stackelberg game. The energy service provider acted as the leader and set dynamic electricity, heat, and demand response prices, while users acted as followers and adjusted their consumption to minimize their own costs. The existence and uniqueness of a Stackelberg equilibrium were also analyzed by authors to show that the game leads to a stable and feasible solution. A Stackelberg game was utilized to capture hierarchical interaction between system operators and end-users in multi-community integrated energy systems [58]. In this framework, the operator sets electricity and heat prices to maximize profit. On the other hand, users responded to these price signals by adjusting flexible and interruptible loads to minimize their individual costs. Additionally, authors proposed an iterative algorithm to achieve convergence to a Stackelberg equilibrium and demonstrated environmental and economic benefits for the operator and users.

It is worth mentioning that despite the advantages of game theory approaches in modeling the hierarchical interaction in power management applications, they often suffer from high computational complexity and coordination challenges among distributed decision makers as the system scale grows. Moreover, game theory typically assumes that players behave rationale, but in reality, users may prioritize comfort over cost and act unpredictably [59]. For cases where EVSEs are installed across multiple sub-feeders, different EMS approaches are required to ensure coordinated and safe operation throughout the system. Unlike single-source installations, MURB electrical infrastructures are inherently distributed and hierarchical, consisting of feeders, sub-feeders, and branches operating at different voltage levels and transformer ratios. Each sub-feeder supplies a subset of EVSEs and non-EV loads. Effective management requires maintaining balanced operation within each sub-feeder while ensuring compliance with the overall capacity limits imposed by the main panel. Since decisions made at one sub-feeder can affect the available capacity of others, a hierarchical coordination mechanism is needed to manage interactions between the main panel and the sub-feeders.

A non-cooperative game can be used to model the electrical system in MURBs, where the main panel (leader) regulates capacity limits and each sub-feeder (follower) seeks to maximize its own operational benefit. Accordingly, in Chapter 6, a real-time EVSE energy management solution based on a hierarchical non-cooperative Stackelberg game framework is proposed to capture this decentralized leader–follower interaction between the main panel and sub-feeders.

While deterministic EMS formulations assume perfect knowledge of system variables and constraints, real-world operation is often affected by significant uncertainty in renewable generation, demand, and resource availability. To address these challenges, stochastic and robust optimization frameworks have been developed to explicitly account for such variability. Among them, Stochastic Optimization (SO) and Robust Optimization (RO) are two widely adopted approaches, particularly within centralized EMS frameworks. SO model uncertain parameters through probability distributions or scenario generation and optimize for expected performance [60].

A scenario-based SO model was developed in [61] for real-time EV charging scheduling under uncertainty in arrival/departure times and state of charge (SoC). In their work, they utilized Inhomogeneous Markov Chains to generate scenarios, and to reduce the computation burden, they used a scenario reduction technique. They showed SO produces charging schedules that follow the desired load-flattening profile more closely and avoid large deviations in total demand compared with a deterministic model that only uses expected values. Therefore, it achieves lower peak demand and smoother load profiles, leading to better peak shaving performance. Similarly, [62] utilized a Monte Carlo simulation approach to generate stochastic scenarios of EV arrivals and departures. Furthermore, [63] proposed a stochastic optimization model for scheduling residential microgrid and took into account uncertainties in renewable generation and EV charging behavior, achieving lower operating costs and better load flattening compared to the deterministic model. However, SO typically requires a large number of scenarios to ensure reliable out-of-sample results, leading to high computational complexity. In addition, it depends on a precise probability distribution, which may not be available in practical applications [64].

The RO uses deterministic sets or distribution bounds to characterize the range of variability of the uncertain parameters [65]. The optimization then seeks solutions that remain feasible under the worst-case realization within these sets. However, this often leads to conservative solutions, as a single uncertainty set cannot fully represent the diversity of possible probability distributions [60]. The RO has been applied in HEMS equipped with PV–battery storage and EV chargers, while also integrating demand response strategies such as Time of Use and Real-time pricing [66]. The uncertainties in PV output and household demand were modeled using the column-and-constraint generation (C&CG) algorithm, and demonstrated that their approach can lead to grid stability. In microgrid management with uncertain EV loads, a two-stage RO model was proposed in [67]. The upper layer optimized microgrid operation under worst-case conditions to minimize costs, while the lower layer controlled EV charging to mitigate power fluctuations and maintain charging safety. To reduce excessive conservatism from unrealistic worst-case scenarios, a data-driven uncertainty set was constructed using a trained neural network, which also improved convergence speed. To take advantage of both RO and SO, a hybrid stochastic–robust optimization framework is presented in [68] for future energy planning problems. RO is used to guarantee reliability in critical aspects, such as always meeting peak demand, while SO is applied to handle future uncertainties in demand, renewable costs, and technology improvements using scenarios.

Distributionally Robust Optimization (DRO) bridges the gap between SO and RO by balancing robustness and probabilistic modeling. It assumes that the true distribution of uncertain parameters is unknown but belongs to an ambiguity set of candidate distributions. Optimization is then performed against the worst-case distribution within this set [69]. Furthermore, DRO is well-suited for decentralized and distributed EMS architectures, where decision-making is shared among multiple agents operating under uncertainty. For instance, a fully decentralized (distributed) EMS based on DRO was developed in [70] for multi-agent distribution systems, where each agent optimized its local operation and peer-to-peer energy trading under renewable generation uncertainty. DRO was also applied for the optimization problem between the distributed system operator and the energy management agents of microgrids to consider uncertainties in renewable generation, load demand, and electricity prices [71]. It should be noted that the performance of DRO heavily depends on the proper construction of the ambiguity set, as an overly large set may lead to conservative solutions, while an underspecified one may fail to capture true distributional shifts [72, 73]. Furthermore, DRO models often suffer from high computational complexity, particularly when dealing with high-dimensional data or non-convex loss functions [69]. Two widely used approaches to construct ambiguity sets are *moment-based* and *distance-based* ambiguity sets. Moment-based sets rely on known statistical properties of uncertain parameters, such as means and variances, and are particularly effective when reliable moment estimates are available. A moment-based DRO framework was proposed in [74] for energy management in islanded microgrids. The ambiguity set was constructed by allowing the true mean of the uncertain wind generation to vary within an ellipsoid around the empirical mean, and the true covariance was constrained to lie within a scaled version of the empirical covariance matrix. On the other hand, distance-based ambiguity sets are constructed by measuring how close a candidate distribution is to a nominal one, which is typically an empirical distribution obtained from historical data. Among these, Wasserstein ambiguity sets have gained popularity due to their favorable theoretical and practical properties. The application of DRO in energy dispatch problems under uncertainty has been studied in [75, 64, 76]. Non-probabilistic and Wasserstein-based ambiguity sets were used to capture imprecision in probability distributions and reformulate the problems into tractable forms (e.g., MILP, bilinear, or SDP). The studies demonstrated that DRO outperforms scenario-based stochastic programming in terms of robustness and practical performance. The sensitivity of the Wasserstein radius in adjusting conservatism and confidence levels has been discussed in [77]. An enhanced microgrid resiliency framework was developed using DRO to address cyber-physical threats. Such events are diverse, and historical data are often limited; the approach integrates risk-based event prediction with a Wasserstein ambiguity set. The model mitigates excessive conservatism by selecting policy modes that consider only a subset of potential events while maintaining robustness to distributional uncertainty [78]. A few studies have applied DRO to EV charging stations integrated with photovoltaic (PV) systems, including uncertainties in EV demand and PV generation. To solve these problems, the models were reformulated into convex optimization programs using duality theory [79, 80]. Duality theory, introduced in [81, 72], provides a mathematical framework that transforms complex optimization problems into equivalent dual formulations that are easier to analyze and computationally tractable.

The performance of an EMS is usually affected by uncertainties such as variations in non-EV load consumption and unpredictable EV availability in an MURB. To enable the EMS to make robust and reliable decisions under such conditions, a DRO-based EMS is proposed in Chapter 5. The model determines a global, robust charging profile for all EVSEs across the system by employing a Wasserstein ambiguity set to represent these uncertainties.

While above mentioned EMS offer advantages in optimizing energy usage, they often fall short in addressing the real-time scheduling of EVSEs and the uncertainties associated with on-demand EV usage, including user driving habits and arrival times in MURBs, which are inherently probabilistic. A scheduling mechanism can mitigate these challenges by intelligently deferring EV charging to off-peak periods. This is particularly beneficial when the number of concurrent charging requests exceeds available capacity, as it reduces the need for aggressive curtailment by the EMS. Unlike existing optimization-based scheduling methods, which are time-dependent and computationally intensive for large numbers of EVSEs, simpler queue-based strategies such as First-Come First-Served (FCFS), Shortest Job First (SJF), and Shortest Remaining Time First (SRTF) have also been studied [82]. However, when shorter tasks continually arrive, longer charging sessions may be repeatedly postponed, leading to starvation and unfair resource allocation, as well as challenges in accurately predicting task durations [82]. To address this limitation, the Round Robin (RR) scheduling approach has been adopted for its fairness and simplicity. RR provides a flexible and scalable framework that can be readily integrated with real-time EMS operations. It has been widely used to address communication capacity constraints, mitigate data congestion, ensure periodic measurement transmission, support state estimation in nonlinear uncertain systems, enable distributed Nash equilibrium computation, perform recursive filtering, facilitate finite-horizon H_∞ state estimation, and coordinate distributed cooperative control [83, 84, 85, 86, 87, 88, 89, 90].

Enhanced RR variants have been developed to improve adaptability and efficiency. The Enhanced Round Robin (ERR) algorithm dynamically adjusts the time quantum based on the mean burst time to optimize resource utilization and response time under variable workloads [91]. Similarly, RR with Adaptive Priority Scheduling (RRAPS) integrates priority-oriented logic with RR to improve task execution and resource utilization in real-time systems [92]. The Median Mean Round Robin (MMRR) algorithm further refines this concept by computing a dynamic time quantum based on the median and mean burst times within each cluster [93].

Despite its broad adoption in other domains, the use of the Round Robin (RR) algorithm for managing EVSEs remains largely unexplored. In Chapter 3, this gap is addressed through the implementation of a dynamic Round Robin (d-RR) algorithm.

Chapter 2

Electrical System Topologies and System Models in Multi-Unit Residential Buildings

Integrating EVSE into an existing building's electrical infrastructure requires careful assessment of the system's capacity and compliance with relevant electrical codes. According to Rule 8-106(9) of the Canadian Electrical Code, when additional loads such as EVSEs are introduced to an existing service or feeder, the total load may be calculated by summing the new loads, applying demand factors as permitted, along with the maximum demand of the existing installation measured over the most recent 12-month period. EVSEs are considered as continuous loads and must be connected using a demand factor of 100% (Rule 8-302). The resulting calculated load must comply with the limits outlined in Rules 8-104(5) and 8-104(6), which define how much continuous load can be connected based on the rating of the overcurrent protection. In cases where historical consumption data is unavailable, it is a common practice that the main panel has been designed to include a small reserve capacity for future expansion.

Beyond load capacity constraints, National Electrical Code Rule 408.54 states that panelboards shall not be used with more overcurrent devices than the number for which they are designed, rated, and listed. Furthermore, as specified in NEC 110.3(B), only breakers that are listed and approved for use with a specific panelboard (typically from the same brand and model family) can be installed. In cases where higher-capacity breakers are required to support EVSEs, NEC 240.4 mandates that the feeder conductors must also be resized to match the new breaker rating. These technical requirements often result in higher installation costs, even when only a limited number of EVSEs can be added to the remaining available capacity. As a result, the need to share a small number of chargers among multiple tenants, combined with significant installation expenses, reduces the willingness of residents to embrace electrification within MURBs.

An EMS enables the installation of more EVSE within a building, allowing each tenant to have a dedicated charger rather than relying on shared units, which enhances convenience and user satisfaction. Moreover, supporting more chargers without costly upgrades, the installation expenses, including breaker upgrades, wiring modifications, and compliance costs, can be distributed across multiple users, improving cost-efficiency on a per-tenant basis.

EMS that directly interact with a building's electrical infrastructure, such as controlling breakers, relays, or load curtailment devices, must undergo certification by nationally recognized testing laboratories (e.g., CSA, UL, or ETL). These systems are considered part of the electrical installation and must comply with safety standards outlined in national codes. However, obtaining certification for such systems can be costly and time-consuming. The approval process often involves rigorous testing, documentation, and coordination with certified hardware manufacturers, which can delay deployment and limit flexibility in design. In contrast, EMS solutions that are online/cloud-based operate entirely through software without direct physical connection to electrical equipment and do not require certification; instead, they gather data from metering devices and communicate with certified hardware over secure network protocols, making them more scalable and easier to deploy, especially in residential buildings.

Therefore, the EMS proposed in this thesis adopts a cloud-based architecture. The overall system architecture is demonstrated in Figure 2.1, which follows a scalable and pervasive communication infrastructure and does not need any additional communication means.

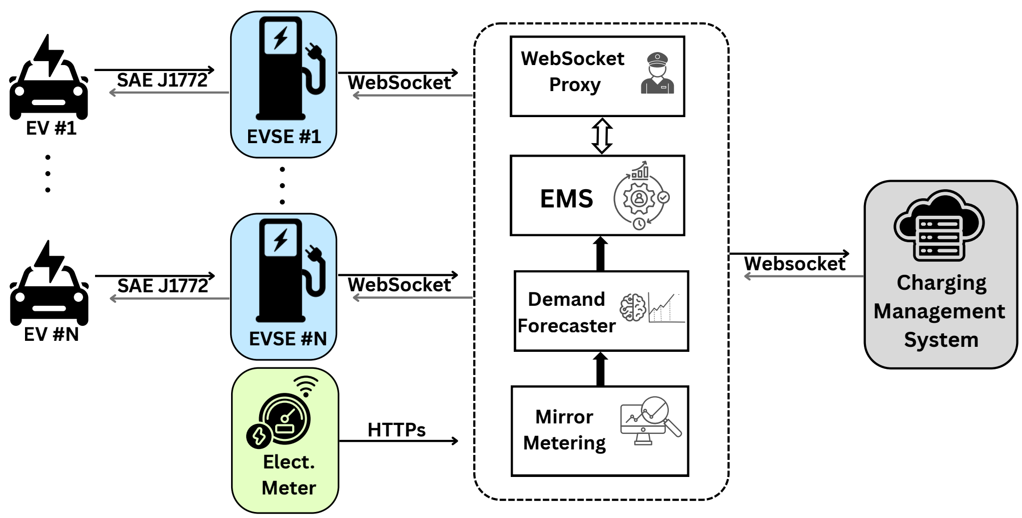

Figure 2.1: Illustration of cloud-based EMS architecture of this work.

In our proposed architecture, SAE J1772 is employed as the communication standard between EVs and EVSEs, which is the most widely adopted interface for AC chargers in North America [94]. J1772 specifies the signaling protocol between the EV and EVSE, which supports functions such as detecting EV connection via the proximity pin and defining the maximum operating current through the pilot signal [95].

To coordinate the communication between EVSEs and the EV charging management system, our chargers are compliant with the Open Charge Point Protocol (OCPP). OCPP essentially acts as the common language and communication channel between EVSEs and the charging management system (CMS) [96], which handles services such as user authentication, session control, and billing. Different OCPP messages are used for specific functions. For example, *StatusNotification* to report charger status, *StartTransaction/StopTransaction* to initiate or terminate charging sessions, and *MeterValues* to exchange consumption data.

The use of OCPP-certified hardware and software offers advantages, such as allowing operators to switch backend systems or replace EVSEs without vendor lock-in, which provides flexibility in the long term and supports future expansion plans. Furthermore, by enforcing common standards for processes such as session initiation, authorization, payment, and billing, OCPP reduces system complexity and ensures a smoother and more consistent charging experience for EV owners [97].

The OCPP protocol relies on the WebSocket communication standard, which enables real-time, two-way data exchange over a single persistent connection [96]. In the proposed system, the proxy, hosted in the cloud, functions as middleware between EVSEs and the CMS. This proxy maintains two types of WebSocket connections: one upstream with the CMS and one downstream with the EVSEs. From the CMS perspective, the proxy behaves like an OCPP client, forwarding EVSE OCPP messages. On the other hand, to the EVSEs, it acts as a server, issuing charging profile (named ChargingProfile in OCPP) sets with their corresponding profile limits and holding the charging schedule [98].

As depicted in Figure 2.1, the proxy consists of several functions. The non-EV load consumption of the building is monitored through metering equipment, and this data is transmitted via HTTP requests to the *Mirror Metering* function. This function detects changes in consumption (both EV and non-EV) and provides inputs to the forecasting model. The forecasting model predicts future non-EV loads and forwards this information to the EMS module, which is further detailed in subsequent chapters. The WebSocket unit in the figure is responsible for message exchange in both directions towards the CMS and the EVSEs. In fact, the proxy monitors and records EVSE status events such as authorization, start, metering, suspended, and stop by parsing OCPP messages over WebSocket connections. It then determines the optimal system response to EVSE requests.

The proxy maintains an inventory of all available EVSEs within each tenant, and stores information such as their phase connections, operational states, rated capacities, current consumption, and their paired WebSocket links to both the EVSEs and the CMS. When an EV is plugged into an EVSE, the vehicle's presence is detected through the SAE J1772 pilot signal. At this point, the EVSE transitions from the *Available* state to the *Preparing* state. This results in a *StatusNotification* message being sent to the proxy, which updates the EVSE's state in the inventory and forwards the notification to the CMS.

The charging session is initiated once the user authenticates (by tapping an RFID card or using a mobile application). Upon successful authorization by the CMS, the EVSE issues a *StartTransaction* message to the proxy. The proxy forwards the start request to the CMS, which responds by assigning a unique transaction ID to track this charging session. This event triggers the EMS function within the proxy, which determines an appropriate charging profile for the EVSE based on the building's available capacity. With this exchange complete, the EVSE enters the *Charging* state, and energy begins to flow from the EVSE to the vehicle. The charging process is regulated by the pilot signal in coordination with the vehicle's onboard charging system.

Throughout the charging process, the EVSE periodically transmits updates such as sending the *MeterValues*, and *StatusNotification* OCPP messages to show the current consumption and operational state, respectively.

The proxy records these updates in the EVSE inventory and relays the information to the CMS to ensure synchronization across the system.

If a new EV connection is established, the corresponding EVSE issues another *StartTransaction* message. This triggers the EMS optimization process again, recalculating charging profiles for all connected EVSEs to reflect the updated system demand. It is important to note that the EMS optimization is also triggered by sudden changes in non-EV load consumption detected by the building meters, prompting the system to re-evaluate and adjust the charging allocations.

Once a charging session ends, the EVSE sends a *StopTransaction* message followed by a *Finishing* state notification to the proxy. This again triggers the EMS optimization to reassign charging profiles among the remaining EVSEs. The EVSE also provides final *MeterValues* so that the CMS can log the session's total energy consumption and duration. Following this, the EVSE transitions back through the *Preparing* state to the *Available* state, once again becomes idle and ready for the next vehicle.

The choice of an appropriate method for formulating the EMS problem is reliant on the underlying topology of the electrical system. Consider a MURB equipped with multiple sub-feeders, each responsible for supplying various non-EV loads. The building owner decides to install a new EVSE to serve the residents' charging needs. In some buildings, the initial design may include unused sub-feeders reserved for future expansions. If such a sub-feeder is available, it can be dedicated to the new EVSE loads, meaning that this sub-feeder does not share its capacity with any other non-EV loads in the building. We refer to this as the Dedicated mode. In case there is no unused sub-feeder available, the EVSEs must be connected to an existing sub-feeder that already supplies non-EV loads. In this case, the sub-feeder must support both EV and non-EV loads concurrently without exceeding its rated capacity. This configuration is referred to as mixed mode.

Figure 2.2a and Figure 2.2b illustrate the Dedicated and Mixed configurations, respectively. Let the main panel of the building be connected to N sub-feeders, denoted by the set $\mathcal{N} = \{1, 2, \ldots, N\}$. We focus on a specific sub-feeder $n \in \mathcal{N}$, which operates in either Dedicated or Mixed mode and draws a total current of i_n to supply its connected loads. Sub-feeder n consists of a set of breakers $\mathcal{M}_n = \{m_1, m_2, \ldots, m_M\}$. The EVSEs are connected to these breakers and are denoted by the set $\mathcal{L}_n = \{l_1, l_2, \ldots, l_M\}$, where each $l_m \in \mathcal{L}_n$ corresponds to a specific breaker $m \in \mathcal{M}_n$. The aggregated charging demand of EVSEs can exceed the sub-feeder's capacity in these topologies.

In the Dedicated mode, the EVSEs are connected to a specific sub-feeder, and their energy consumption occurs within that sub-feeder's capacity, without impacting the loads supplied by other sub-feeders in the building's electrical system. Therefore, a separate metering device is not required, as the entire capacity of the sub-feeder is allocated to EVSEs only, with their consumption reported via OCPP *MeterValues* messages. The only requirement in this configuration is to ensure that the total EV load does not exceed the sub-feeder's rated capacity. On the other hand, in the Mixed mode, since the EVSEs share a sub-feeder with non-EV loads, it becomes necessary to install a meter at the sub-feeder level. This meter records the total current drawn by all loads on the feeder. By subtracting the known EV loads from the total measured current, the non-EV load time series is obtained and fed to the forecaster, which estimates the upcoming non-EV demand using a rolling-window approach on the meter data to predict the total upcoming load. The detailed formulation of the forecasting model will be discussed in Section 4.2. Then, the EMS evaluates the constraints and allocates the optimized energy to the EVSE.

It should be noted that the EMS in these frameworks operates at the sub-feeder level and does not control the entire building's electrical system. Its decision-making is confined to the selected sub-feeder n, regardless of whether it operates in Dedicated or Mixed mode.

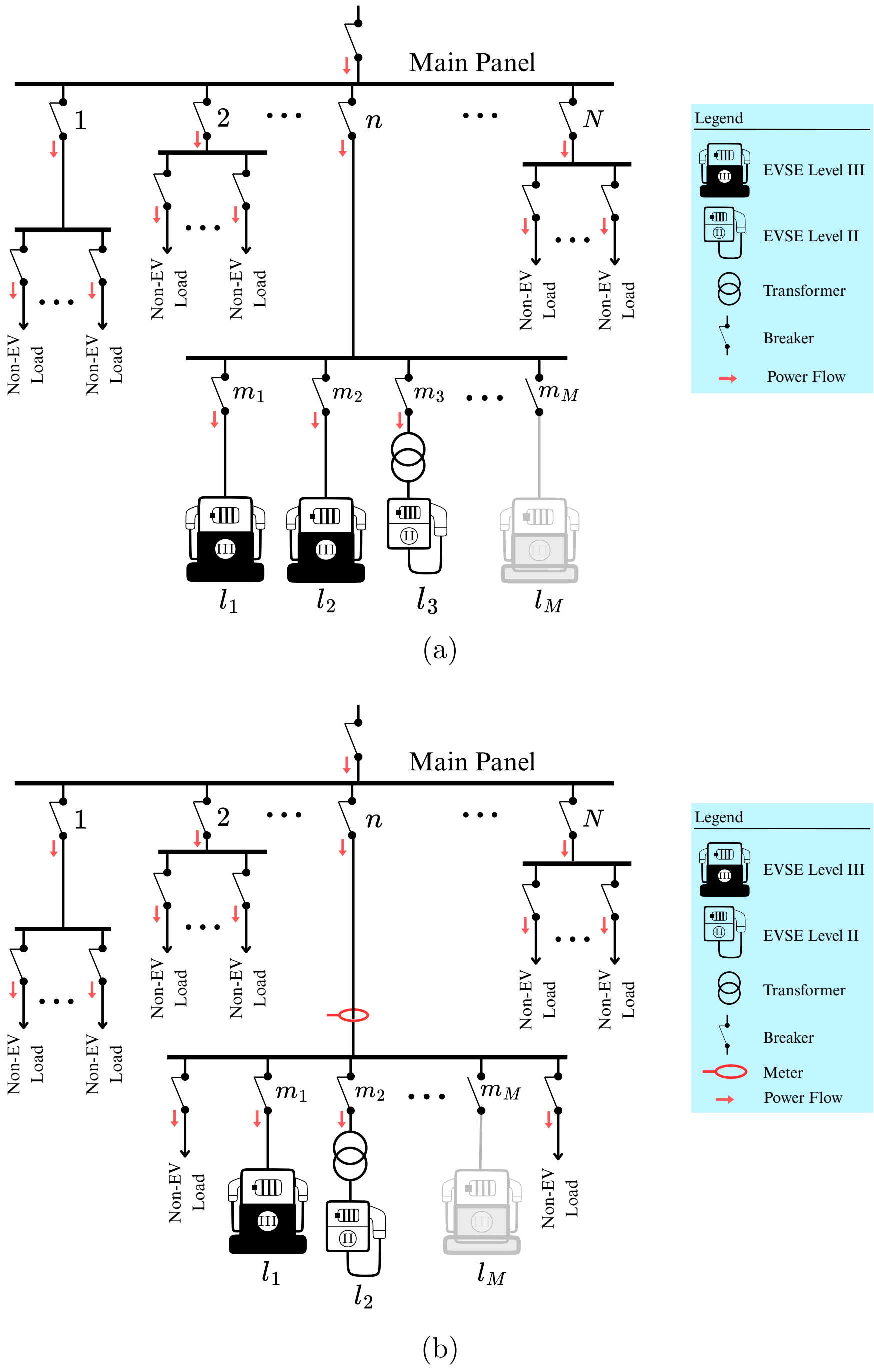

Figure 2.2: EVSE installation configurations on a single sub-feeder: (a) Dedicated mode, where the sub-feeder supplies only EVSEs, and (b) Mixed mode, where EVSEs share the sub-feeder with non-EV loads.

The goal is to develop a real-time EMS that enables the integration of EVSEs into either a dedicated or mixed sub-feeder while adhering to the feeder's constraints. Since EVSEs behave as nonlinear and elastic loads, typically connected across two phases of a three-phase network, we propose in Chapter 4 a MILP-based centralized EMS that captures the phase-assignment decisions using binary variables. The proposed model enables real-time curtailment of EVSEs during periods of high non-EV load consumption to ensure that the total load on each phase remains within the feeder's capacity limits.

A more general multi-tiered electrical system for an MURB application is shown in figure 2.3, comprising a main distribution panel, multiple feeders with different voltage levels, step-down transformers, residential loads, meters, and a collection of Level II and Level III EVSEs on sub-feeders. In this setup, the main panel is connected to N sub-feeders, where $\mathcal{N} = \{1, \ldots, N\}$ denotes the set of sub-feeders in the power distribution. Each sub-feeder $n \in \mathcal{N}$ requires an amperage of i_n to feed to both non-EV loads and EVSEs. Sub-feeder n has an associated set of breakers $\mathcal{M}_n = \{m_{n,1}, \ldots, m_{n,M_n}\}$. The breaker $m_{n,j}$ refers to the j-th breaker connected to feeder n. The set of all circuits (breakers) in the network is denoted by $\mathcal{M} = \bigcup_{n \in \mathcal{N}} \mathcal{M}_n$. Among these, a subset $\mathcal{A} \subseteq \mathcal{M}$ represents the activated circuits. The activated circuits can be defined as $\mathcal{A} = \{m_{n,j} \in \mathcal{M}_n \mid \text{Circuit } m_{n,j} \text{ is activated}\}$. The set of EVSEs is denoted by $\mathcal{L}_n = \{l_{1,1}, l_{1,2}, \ldots, l_{n,M_N}\}$, where each EVSE $l_{n,m} \in \mathcal{L}_n$ is connected to one of the circuits $m_{n,j} \in \mathcal{M}_n$ on sub-feeder n. The subset of activated EVSEs is denoted by $\mathcal{L}_\mathcal{A} \subseteq \mathcal{L}_n$. The set of all EVs in the system is represented by $\mathcal{C} = \{c_1, \ldots, c_C\}$ and $\mathcal{E} = \{\epsilon_1, \ldots, \epsilon_E\}$ is defined as the set of EVs currently demanding charges where $\mathcal{E} \subseteq \mathcal{C}$.

In MURBs, there are many sources of uncertainty in electrical consumption, and they are distributed across the system. These uncertainties can arise from variations in non-EV load consumption on different sub-feeders due to factors such as user behavior, seasonal effects, and time-of-day patterns.

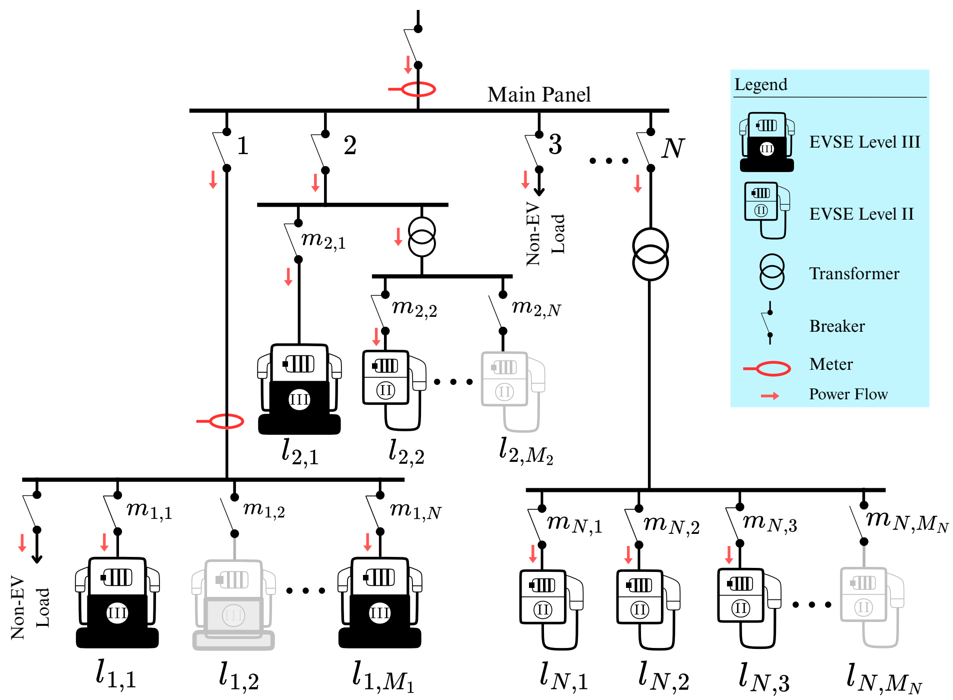

Figure 2.3: Schematic diagram of a multi-tiered electrical system in MURBs.

The integration of EV loads further compounds this uncertainty, mostly due to differences in driving habits and charging requirements. We discussed that enabling a real-time EMS solely by relying on meter readings is insufficient, and a forecasting model is required to estimate consumption ahead of time. However, the aforementioned uncertainties inevitably limit the forecasting model's accuracy, and reliance on predicted values can lead to safety risks. Specifically, during certain hours of the day, such as evenings, when many EV owners return from work and begin charging their vehicles, and non-EV load consumption is simultaneously high and volatile, a sudden spike in non-EV load during such periods can overload the system and trip breakers. Consequently, deterministic optimization approaches such as MILP, which do not account for these uncertainties, are prone to safety risks.

To address this limitation, we will provide an EMS based on DRO to account for the uncertainties present in MURBs. DRO aligns well with the distributed nature of MURB electrical systems. By utilizing the Wassestein ambiuity set, we capture the uncertainties in non-EV load consumption and EVSEs availability on each sub-feeder and generate globally optimized set-points for EVSEs across the system. The detailed mathematical formulation of the proposed model is presented in Chapter 5.

From Figure 2.3, it can be observed that the electrical systems in MURBs are not a simple single-source configuration; they are often highly distributed and multi-tiered, with many sub-feeders and branches. Allocating energy demand within the setup is challenging due to the need to balance load across systems with varying voltage levels and transformer ratios. Furthermore, identifying a globally optimal operation for all distributed EVSEs, regardless of their type (DC, AC level II, etc.) and voltage level, is challenging. To manage such systems with conflicting constraints, game-theoretic methodologies are particularly appealing as they provide a conceptual framework for the formal description of the interactions between independent rational players. An electrical system in MURBs can be formulated as a conventional non-cooperative game, where the main panel (the leader) has the authority to regulate the limits, and all other sub-feeders (the followers) move afterward to maximize their benefit.

To this end, we formulate our EMS problem using a Stackelberg game model. The aim is to create a holistic EMS that integrates EVSE into existing building infrastructure while managing limited electrical capacity, adjusting EV demand in response to non-EV load changes, and ensuring optimal and fair operating. The core regulatory principle of this model is to initially fulfill the requirements of non-EV loads and subsequently adjust the current to EVSEs based on real-time demands. This prioritization strategy is essential for ensuring that consumers' primary needs are adequately met before allocating resources to EVSEs. The detailed mathematical formulation of the proposed Stackelberg game-based EMS is presented in Chapter 6.

The decision-making process in this setup can be implemented through a distributed control application, consisting of multiple threads that are loosely coupled via a redundant publish-subscribe (pub-sub) database. Each thread logs its actions to a central database and listens for notifications through unique identifiers. It should be noted that EV chargers act as passive agents in this framework; they respond to control commands, including curtailment decisions. Even in the presence of very fluctuating non-EV loads, the EV charging profiles are decoupled and dynamically adjust within their corresponding sub-feeder allocated capacity.

While proposed EMS offer distinct advantages in optimizing energy usage and ensuring compliance with infrastructure constraints, they often fall short in addressing the real-time scheduling of EVSEs and the uncertainties inherent to on-demand EV usage in MURBs, such as user driving habits and arrival times, which are inherently probabilistic. Specifically, when feeder capacity is limited, and the number of EVs requesting charging exceeds this capacity, the EMS may impose excessive curtailment on individual EVs. According to the SAE J1772 standard [95], which mostly governs AC charging in North America, there is a minimum allowable current that an EVSE can advertise to an EV (typically 6 A). If the allocated current drops below this threshold, the charging session will be rejected by the EV, leading to unsuccessful charging attempts and reduced user satisfaction.

A scheduling mechanism can address these challenges by intelligently deferring EV charging to off-peak periods. Thus, Chapter 3 proposes a Dynamic Round Robin (d-RR) algorithm with a variable time quantum for managing the charging of EVs in a queue. The proposed d-RR is particularly useful in EMS frameworks where task characteristics and system loads fluctuate frequently. It achieves a balance between responsiveness and fairness, making it a practical choice for dynamic EVSE scheduling. This formulation allows the EV charging problem to be decoupled into two dimensions: power allocation through an EMS and time scheduling via d-RR. To demonstrate the effectiveness of the d-RR when coupled with real-time EMS strategies, its integration is evaluated in the Stackelberg EMS case study, highlighting its capability to increase the penetration of installed EVSEs and enhance user satisfaction.

Chapter 3

Dynamic Round Robin Scheduling

The increasing number of EVs in MURBs has led to frequent instances where simultaneous charging requests exceed the available electrical capacity. To manage this growing demand, an effective and fair scheduling mechanism is required to coordinate charging access among multiple EVSEs. This chapter introduces a dynamic Round Robin (d-RR) scheduling algorithm designed to address this challenge by distributing charging opportunities cyclically among EVSEs within a group. The proposed d-RR approach ensures fairness, prevents monopolization of charging resources, and maintains consistent utilization of available capacity. Unlike conventional Round Robin methods that operate with a fixed time quantum, the proposed d-RR algorithm dynamically adjusts its time quantum based on the number of active EVSEs. This adaptive feature allows the scheduling process to remain responsive under varying load conditions and to ensure equitable access for all users.

A case study is presented to evaluate the performance of the proposed d-RR scheduler and compare it against alternative FCFS scheduling. The evaluation examines key performance indicators, including fairness, EVSE utilization, and user satisfaction. Additionally, we discuss the integration capability of d-RR into real-time EMS frameworks to enhance coordination between scheduling and power allocation. This integration and its effectiveness are later demonstrated in the Stackelberg EMS framework discussed in Chapter 6.

The remainder of this chapter is organized as follows. Section 3.1 describes the system model and the formulation of the proposed d-RR scheduling algorithm. Section 3.2 presents the case study, performance evaluation, and comparative analysis with alternative scheduling approaches.

3.1 System model

Round Robin real-time task management is recognized as one of the simplest, fairest, and most widely adopted scheduling algorithms, particularly designed for time-sharing systems [99]. It operates by assigning specific time intervals, known as time quantum, to tasks within a ready queue. Each process is allocated an identical time quantum; those with burst times exceeding the time quantum are interrupted and moved to the end of the queue while the next process begins execution [100]. This cycle continues until all processes are completed. Upon finishing execution, a process is removed from the ready queue [101].

Implementing a d-RR algorithm in EV charging stations has the potential to enhance charging capacity by increasing the number of EVSE units in a given area. In a d-RR algorithm, based on certain triggers, the time quantum is adjusted for tasks to reflect their current needs and system conditions. The dynamic adjustment of the time quantum helps optimize resource utilization by minimizing idle times and improving system throughput.

To better understand the operation of the d-RR scheduler and how it achieves the aforementioned advantages, Figure 3.1 illustrates the charging sequence of four EVs over a four-hour period and compares its performance with the conventional First-Come First-Served (FCFS) method. In the FCFS

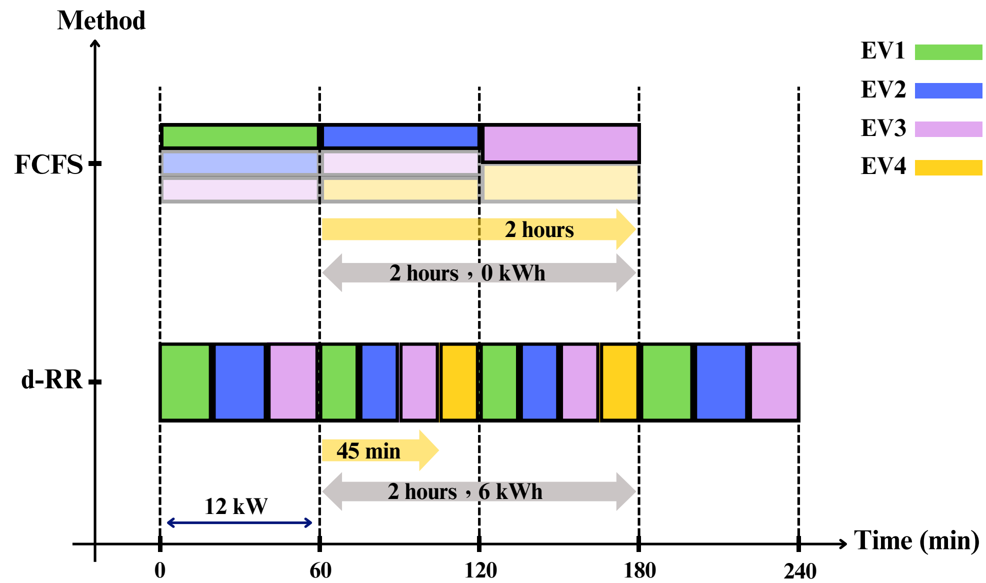

Figure 3.1: Comparison of the FCFS and d-RR charging scheduling methods in terms of energy allocation and waiting time for four EVs over a four-hour period.

strategy, EVs are charged sequentially based on their arrival order, with only one EV receiving power at a time, while others wait until the preceding ones are fully charged. It has been assumed that each EV requires 12 kWh of energy to reach full charge, and the maximum deliverable power by feeder is 12 kW per hour. Therefore, each EV requires approximately one hour of charging to become fully charged. At hour 1, EV1 to EV3 are available, and the fourth EV joins the group at hour 2, being placed at the end of the queue. However, EV4 is assumed to depart at hour 4.

As shown in the upper part of Figure 3.1, in the FCFS method, only one EV receives the full 12 kW charging power at any given time, while the remaining EVs remain idle. Consequently, EV4 experiences a waiting period of two hours without receiving any energy before leaving the queue. This highlights the limitation of the FCFS approach, which results in long waiting times and reduced fairness among EVs. On the other hand, during the two hours that EV4 is available in the queue, the d-RR method divides each one-hour scheduling window ($t^q = 1hr$) into four dynamic time quanta of 20 minutes ($t^d = 20min$) each, cyclically assigning the available 12 kW of power among all active EVs. Therefore, EV4 receives two charging intervals before leaving the queue, corresponding to approximately 6 kWh, or 50% of its full charge. Compared to the FCFS method, this strategy substantially reduces waiting times, improves energy distribution fairness, and enables even late-arriving EVs to obtain an adequate level of charge before departure. In the following, we proceed with the formulation of the d-RR scheduler.

As illustrated in Fig. 2.3, the electrical system of an MURB consists of multiple feeders and sub-feeders, each supplying a group of EVSEs and non-EV loads. For $\mathcal{E}$ EVs on demand, there are $\mathcal{L}_{\mathcal{A}}$ active EVSEs under circuits $\mathcal{A}$, electrically connected to feeder n. The i^{th} EV can be connected to one of these active EVSEs and placed in the scheduling queue. The d-RR scheduling can be applied to multiple groups of EVSEs in $\mathcal{L}_{\mathcal{A}}$. Figure 3.2 illustrates this process for a representative sub-feeder n within the multi-tier MURB structure. For the group $\mathcal{L}_{\mathcal{A},j}$, the d-RR queue sequence $\mathcal{Q}_j$ has the size of,

$$\lambda_j = \begin{cases} \left\lfloor \frac{E}{q} \right\rfloor & \text{for } j \neq q, \\ E - \left\lfloor \frac{E}{q} \right\rfloor \times (q-1) & \text{for } j = q. \end{cases} \tag{3.1}$$

where λ_j is the size of quantum j, E is the number of EVs currently demanding charges, q is the number of circuits selected, and symbol $\lfloor\rfloor$ represents the floor function. Let's consider a constant quantum time t^q assigned to each $\mathcal{M}_n$, then the dynamic quantum time t^d represents the time varying during each round of charging EVs and can be calculated by

$$t_j^d = \frac{t_j^q}{\lambda_j} \tag{3.2}$$

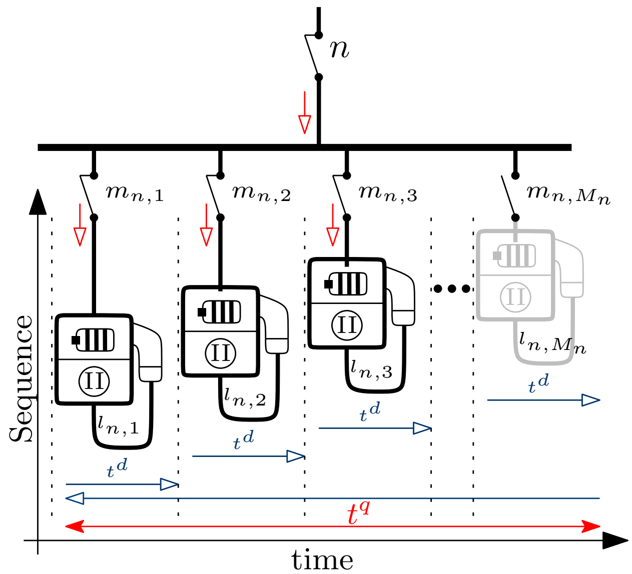

Figure 3.2: Sequential operation of EVSEs on sub-feeder n under the d-RR scheduler, where a fixed quantum t^q is divided into dynamic time slices t^d across the active EVSEs.

Algorithm 1 presents the d-RR process, where the d-RR algorithm starts by identifying the EVs on demand $\mathcal{E} \subseteq \mathcal{C}$, the number of permitted circuits q, and the fixed time quantum t^q. The dynamic time quantum for each group j, denoted as t_j^d, can then be calculated using (3.2). The charge elapsed time for every EV $\epsilon_i \in \mathcal{E}$ will be recorded as t_i^δ, which tracks the time each EV has been actively charging. If an EV is not fully charged after receiving its initially assigned time quantum t^q, it will be kept in a new queue with additional time, and this process continues until the EV is fully charged. If a vehicle becomes fully charged before completing its assigned burst time, it is disconnected from the EVSE, and a new time quantum t^q is calculated for the remaining vehicles.

During the charging process of the i^{th} EV, if a new EV request arrives or if a charging process is terminated, the dynamic time quantum t_j^d for group j must be recalculated. The charging process for all EVs must proceed according to the revised time quantum t^q. To avoid looping on individual

Algorithm 1 Dynamic Round Robin Scheduling for EVSEs

Require: EVs on demand $\mathcal{E}$, active EVSEs $\mathcal{L}_{\mathcal{A}}$
1: set λ_j using (3.1)
2: **for** each feeder $n \in \mathcal{N}$ and connected EVSEs $\mathcal{L}_{\mathcal{A}}$ to it **do**
3:     update t_j^d using (3.2) ,
4:     **while** EV $\epsilon_i \in \mathcal{E}$ is in queue $\mathcal{Q}_j$ **do**
5:         **while** $t_i^\delta < t_j^d$ **do**
6:             keep charging EV ϵ_i and update t_i^δ,
7:             **if** new EV on demand or terminated **then**
8:                 go to Step 3,
9:             **end if**
10:         **end while**
11:     **end while**
12:     do a right circular shift on $\mathcal{Q}_j$,
13:     go to Step 3,
14: **end for**

EVSEs due to repetitive connection and disconnection requests from the EVs in the group, the elapsed charging time t_i^δ will be counted for each quantum block. Therefore, if the group size changes due to the addition or removal of a charging request, a new dynamic time quantum t_j^d will be quickly recalculated. If the i^{th} EV has been charged for a duration exceeding t_j^d, it will be paused and pushed to the back of the queue $\mathcal{Q}_j$. Otherwise, it will continue receiving a charge until $t_i^\delta < t_j^d$. Priority is assigned to other waiting EVs in the queue, and all new EV requests will be handled on a first-come-first-served basis.

3.2 Case Study

To illustrate the effectiveness of the proposed d-RR, we consider a MURB with 322 units, where 56 residents own an EV with a dedicated EVSE installed at their parking slot. It is assumed that no EMS is deployed. Therefore, EV charging must be planned conservatively based on the minimum capacity available after accounting for the building's non-EV loads. To ensure operational safety under this worst-case assumption, the total capacity allocated to EV charging is restricted to a maximum of 15 kW. The EV drivers depart between 7:00 AM and 9:00 AM, and arrive at the charging station daily between 6:00 PM and 10:00 PM, with arrival and departure times determined randomly. To calculate the SoC of EVs after a daily commute, we employ $\mathcal{S}^{\text{ini}} = 1 - \eta_d l E_b / P_b$, where l represents the daily commute distance for each EV, modeled using a log-normal distribution with parameters $\mu = 4.08$ and $\sigma = 0.745$, as detailed in [102]. E_b is the normalized EV energy consumption per kilometer (kWh/km), randomly assigned within the range of 0.15 to 0.22 kWh/km. The battery size P_b is randomly selected within the range of 65 to 120 kWh. η_d is the EV driving efficiency, which depends on driving style, speed, and daily traffic, and is assumed to be 0.8. Given that, we use the SoC_{ini} to calculate the SoC of the EV after charging using $\mathcal{S}^{\text{f}} = \mathcal{S}^{\text{ini}} + T E_c \eta_c / P_b$, where E_c is the optimal kW power assigned to each EVSE, T represents the charge duration, and η_c is the EVSE charge efficiency, assumed to be 0.9.

To provide a comparison between the proposed d-RR and other benchmark scheduling methods, we studied two other scenarios of no scheduling (Regular) and FCFS scheduling. In the regular mode, we considered no scheduling mechanism and the availability of 1-10 EVSEs in specific parking spots for EVs. The earliest arriving EV receives the charge, and the other EVs can reserve the EVSEs for the next available time slot. We assumed EV owners are generally unwilling to plug in their cars after midnight, so there will be no reservations after 1:00 AM due to inconvenience. In the FCFS approach, users book the next available time through a user-facing system and are placed in a queue, with all subsequent requests processed in the order received, regardless of other conditions. However, for the FCFS and d-RR scenarios, each EV owner has a dedicated EVSE installed at their parking slot, meaning the number of EVSEs equals the number of EVs, but not all of them can be activated simultaneously. This setup allows all customers to plug in their vehicles as soon as they arrive at the charging station. We define the customer satisfaction metric equal to received SoC before the next trip.

$$\mathcal{S} = \left(\mathcal{S}^{\mathrm{f}}_{i,j} - \kappa\right) \tag{3.3}$$

where $\mathcal{S}^{\mathrm{f}}_{i,j}$ represents the $\mathcal{S}^{\mathrm{f}}$ of the i^{th} EV on the j^{th} day, and $\kappa = \max(0, \mathcal{S}^{\mathrm{min}} - \mathcal{S}^{\mathrm{f}}_{i,j})$ is penalty factor subtracted from $\mathcal{S}^{\mathrm{f}}_{i,j}$ if it falls below the minimum satisfaction score $\mathcal{S}^{\mathrm{min}}$. We also defined the overall satisfaction score by

$$\mathcal{S}^{+} = \frac{100}{ET} \sum_{i=1}^{E} \sum_{j=1}^{T} H\left(\mathcal{S}^{\mathrm{f}}_{i,j} - \mathcal{S}^{\mathrm{thr}}\right) \tag{3.4}$$

where H is the Heaviside step function, which is 1 when $\mathcal{S}^{\mathrm{f}}_{i,j}$ is greater than the driver satisfaction threshold $\mathcal{S}^{\mathrm{thr}}$ and 0 otherwise. The results indicate that the d-RR and FCFS algorithms significantly outperform the regular method.

Figures 3.3 to 3.5 show the yearly satisfaction score ($\mathcal{S}^{+}$) with a minimum satisfaction threshold of $\mathcal{S}^{\mathrm{min}} = 30\%$ and a satisfaction threshold $\mathcal{S}^{\mathrm{thr}} = 30\%$, with 56 EVSEs ($E$) over 365 days ($T$) for the Regular, FCFS, and d-RR scenarios, respectively. It should be noted that the first two rows in the heatmaps are shaded in gray, indicating that no simulations were conducted for those cases. This is because the total feeder capacity was limited to $15kW$ in the absence of EMS. When only one or two EVSEs are active simultaneously, this capacity would need to be divided equally among them, which would exceed the typical rated limit of individual Level II chargers. Therefore, these cases were excluded from the analysis to ensure realistic and safe operating conditions. Figure 3.3 illustrates a heatmap that captures the overall customer satisfaction score ($\mathcal{S}^{+}$) in the Regular scenario, where no centralized scheduling algorithm is used, and EVs are charged based on availability. This method is all about a first-available, non-prioritized service model, which can lead to less-than-ideal resource use, especially when demand is high. The figure reveals that the peak satisfaction score of 50.9%

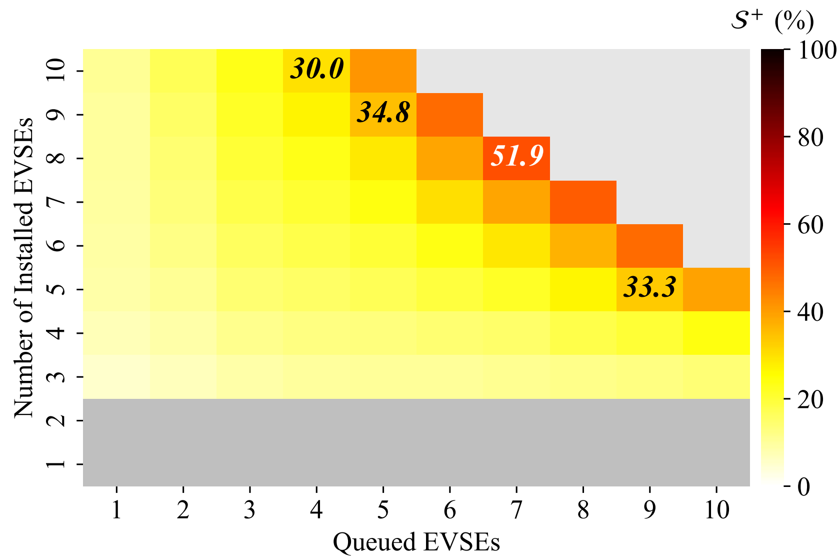

Figure 3.3: Customer satisfaction S^+ as a function of the number of installed EVSEs and queued EVSEs for the regular case with no EMS

is achieved when there are 8 active EVSEs and a queue size of 7. This queue is not a physical queue; rather, it reflects the average number of daily charging requests happening throughout the year. In this setup, the number of EVs competing for service is modest relative to the available infrastructure, allowing most vehicles to achieve a final SoC above the minimum satisfaction threshold. However, if the number of active EVSEs drops or the queue size increases, the system's ability to meet customer charging needs takes a significant hit. For instance, when we cut the active EVSEs down to 5 and with the best queue size 9, the satisfaction score drops to 32.6%. Thus, without a scheduling system in place, resources can't be allocated dynamically based on demand, resulting in a higher frequency of charging sessions that fall short of the required SoC threshold.

Figure 3.4 shows the satisfaction for the FCFS scheduling case, which is a common central scheduling approach for managing EV fleets. This scenario requires a central system to manage charge requests and loitering, which

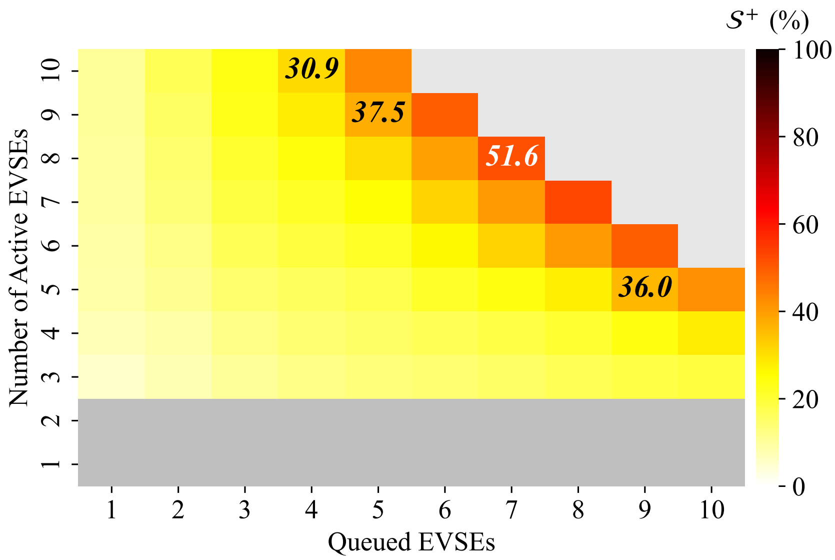

Figure 3.4: Customer satisfaction S^+ as a function of the number of installed EVSEs and queued EVSEs for the FCFS method with no EMS

might necessitate a more complex integration with the local real-time EMS. Assuming the existence of such integration and coordination, FCFS shows a better overall satisfaction score compared to the Regular case. With 8 active EVSEs and an EV queue size of 7, an average satisfaction score of around 51.5% can be achieved. In this setting, the number of concurrent charging requests is slightly below the available infrastructure, allowing the FCFS scheduler to allocate chargers to vehicles with minimal delay. As EVs are served in arrival order and the demand stays within system limits, waiting times remain short, and most vehicles can achieve their target SoC before departure, and therefore resulting in high satisfaction. For all other cases, enabling such scheduling enables the efficient use of available time and power resources, making it feasible to install and dedicate up to twice as many EVSEs to individual users compared to the Regular case. Figure 3.5 presents the results for the d-RR scheduling strategy, which distributes charging time fairly across EVs. It manages to achieve a slightly higher satisfaction score of 53.7% under the same conditions (with 8 EVSEs and a queue size of 7) and demonstrates better resilience during periods of light demand. In both d-RR and FCFS setups, a total of 56 EVSEs are installed and ready to plug upon arrival, while only 8 are enabled at a time. Taking the availability of a charger upon arrival and sufficient SoC for the next day as a measure of convenience and satisfaction, this indicates the value of coordinated scheduling in maximizing perceived service quality with limited infrastructure.

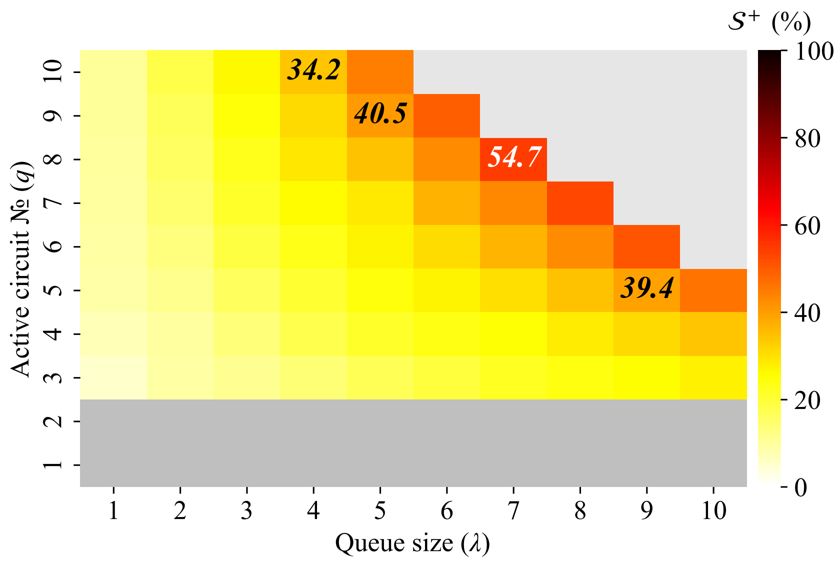

Figure 3.5: Customer satisfaction S^+ as a function of the number of installed EVSEs and queued EVSEs for the d-RR method with no EMS

Although the d-RR scheduler enhances EVSE utilization and improves charging fairness, its performance can be further improved through the integration of an EMS. Without an EMS, the charging process does not account for the dynamic variations in building loads, which can lead to conservative power allocation. By incorporating an EMS, the system can dynamically adjust charging power based on real-time load conditions, increasing energy utilization and ensuring safe and coordinated operation between EV and non-

EV loads. In the following chapters, different EMS frameworks are presented to further enhance system performance and adaptability under various operating conditions. The effectiveness of the d-RR scheduler integrated with an EMS is further discussed in the case study of Chapter 6.

3.3 Conclusion

This chapter presented a d-RR scheduling mechanism for EVSE management in MURBs. The proposed d-RR algorithm dynamically allocates charging opportunities among EVSEs by adapting its time quantum based on the number of active EVSEs. Through simulation studies, the d-RR scheduler demonstrated superior performance compared to traditional unsupervised (Regular) and FCFS approaches. The results confirmed that d-RR achieves higher overall user satisfaction and better fairness. While FCFS can offer comparable satisfaction levels under moderate demand, its reliance on static queue ordering limits its adaptability. In contrast, d-RR dynamically responds to real-time changes in EV arrivals and terminations, ensures fair access to limited feeder capacity, and avoids monopolization by individual EVs. Overall, the findings highlight the potential of d-RR as a lightweight scheduling mechanism that increases EVSE penetration, enhances customer satisfaction, and improves perceived fairness. Furthermore, the design of the d-RR algorithm allows integration with real-time EMS, where it can complement power allocation strategies to achieve both optimal scheduling and energy coordination.

Next we propose and examine different EMS approaches to determine the optimal power allocation among EVSEs under varying electrical system topologies and operational conditions. The next chapter covers a centralized EMS for EVSE integration in both dedicated and mixed panel configurations.

Chapter 4

Centralized Energy Management for EVSE Integration in Dedicated and Mixed Panels

Efficient coordination of EVSE operation in MURBs is essential to prevent feeder overloading and maintain phase balance under increasing charging demand. This chapter introduces a real-time EMS formulated using MILP to optimize EVSE power allocation while ensuring compliance with electrical capacity and balance constraints. The proposed framework provides a centralized control mechanism that dynamically distributes available power among EVSEs within existing infrastructure limits. To enable proactive decision-making, the EMS incorporates an NARX-based forecasting model for non-EV building loads. Forecasts are integrated into the MILP formulation to continuously adjust EVSE power levels, mitigating the impact of fluctuating non-EV consumption and preserving near-symmetrical phase loading. The proposed system is validated using real data from a MURB in the Lower Mainland region of Vancouver, Canada. The chapter also examines user charging performance through state-of-charge (SoC) analysis and evaluates the computational efficiency of the approach to demonstrate its suitability for real-time implementation. In the next section, the MILP formulation of the proposed EMS is derived for coordinating EVSE operation in mixed-mode configurations. Section 4.2 introduces the NARX forecasting model used to predict non-EV building loads and integrate them into the control framework. Finally, a case study based on real residential data is presented to evaluate the performance and practicality of the proposed approach.

4.1 MILP formulation

The electrical infrastructure of an MURB consists of a three-phase feeder supplying multiple EVSEs that behave as nonlinear, elastic loads. Each EVSE typically connects to two of the three available phases, making the distribution of charging current across phases a critical factor in maintaining system balance and avoiding phase overloading. Building on this structure and its load characteristics of EVSEs, the following section formulates a MILP model to optimally allocate charging currents among EVSEs operating in both Mixed and Dedicated modes (described in Chapter 2), while considering feeder capacity constraints. Since the Mixed mode represents a more comprehensive configuration than the Dedicated mode, the proposed model can also be applied to the Dedicated mode. The difference lies in the absence of non-EV load consumption in the Dedicated mode, which eliminates the need for a forecasting model. Therefore, this thesis focuses exclusively on the Mixed mode. Let's consider a single feeder operating in Mixed Mode as shown in Figure 2.2b. Let $P = \{A, B, C\}$ denote the set of electrical phases in a MURB, and let $\mathcal{M} = \{1, 2, \ldots, M\}$ represent the set of EVSE units installed in the building. Each EVSE $m \in \mathcal{M}$ is connected to one or more electrical phases, and the current allocated to EVSE m on phase $i \in P$ is denoted by the decision variable $y_m^i \in \mathbb{R}_{\geq 0}$.

The objective of the proposed MILP-based EMS is to maximize the total current allocated to all EVSEs such that the total demand remains within the capacity of each phase, while ensuring balance across phases and satisfying per-EVSE operational bounds. This can be expressed as the following maximization problem:

$$\max_{y_m^i} \quad \sum_{m\in\mathcal{M}} \sum_{i\in P} \left(\alpha_m \chi_m + (1-\chi_m)\right) y_m^i \tag{4.1}$$

subject to:

$$\sum_{m\in\mathcal{M}} y_m^i \leq p^{(i)} - \delta^{(i)}, \quad \forall i \in P \tag{4.1a}$$

$$y_m^i = 0, \quad \forall m \notin \mathcal{M}_i, \forall i \in P \tag{4.1b}$$

$$\sum_{i\in P} Z_i(m,m)\, y_m^i = 0, \quad \forall m \in \mathcal{M}^k \tag{4.1c}$$

$$I_m^{\min} \leq y_m^i \leq I_m^{\max}, \quad \forall m \in \mathcal{M}, \forall i \in P \tag{4.1d}$$

The variable χ_m in (4.1) is defined as a binary indicator of EVSE type, where $\chi_m = 1$ represents DC fast chargers and $\chi_m = 0$ denotes AC chargers. The coefficient α_m provides a degree of fairness by assigning higher priority to users with more urgent demands, such as those returning with a low state of charge (SoC) or requiring a faster turnaround.

In constraint (4.1a), the term $p^{(i)}$ represents the ampacity limit of phase $i \in P$, and $\delta^{(i)}$ is the predicted non-EV load on phase i, obtained from the NARX forecasting model. This constraint ensures that the total EVSE current allocated to each phase remains within the available margin after accounting for other loads. It should be noted that, in the *Dedicated mode*, since there are no non-EV loads connected to the feeder, $\delta^{(i)} = 0$, which simplifies the constraint to $\sum_{m\in\mathcal{M}} y_m^i \leq p^{(i)}$.

Constraint (4.1b) enforces phase connection of chargers. Specifically, if

EVSE $m \in \mathcal{M}$ is not physically connected to phase i, then no current can be allocated on that phase. The set $\mathcal{M}_i \subset \mathcal{M}$ contains all EVSEs connected to phase i, and the constraint guarantees that $y_m^i = 0$ for all $m \notin \mathcal{M}_i$.

Constraint (4.1c) addresses phase balancing for EVSEs that draw current from multiple phases. The subset $\mathcal{M}^k \subset \mathcal{M}$ denotes the set of multi-phase EVSEs that require balanced current allocation. The binary matrix $Z_i(m, m) \in \{-1, 1\}$ captures the direction of current flow across connected phases for each EVSE, and this constraint enforces that the difference in allocated currents remains zero, maintaining symmetry across the involved phases.

Finally, the bounds constraint (4.1d) specifies the limits on the current allocation y_m^i. Each y_m^i must lie within the interval $[I_m^{\min}, I_m^{\max}]$, denoting the lower and upper limits of power that can be allocated to charging point m on phase i.

This MILP formulation ensures balanced allocation of charging current to EVSEs in real time while respecting infrastructure constraints and operational safety requirements.

4.2 Proactive Predictive State Awareness

In MURBs, non-EV load consumption is heavily influenced by human behavior and external conditions (e.g., weather), resulting in unpredictable load profiles. A real-time EMS cannot rely solely on instantaneous metering data to make decisions, as this approach may lead to overloading the transformer due to over-allocation of EV charging current in the presence of sudden non-EV load changes. To address this, integrating a prediction model into the EMS enhances its ability to make informed, proactive decisions by predicting non-EV current consumption ahead of time.

The NARX model is used as a short-term forecasting model to predict nonlinear functions of past observations and exogenous variables. It enables the capture of temporal dependencies while incorporating external factors such as environmental and temporal drivers of electricity consumption. In addition, it utilizes a recursive autoregressive structure in which previously predicted values are fed back into the model as inputs, allowing the dynamic evolution of demand to be represented over time. Implemented as a feedforward neural network, the NARX model provides strong nonlinear modeling capability while maintaining efficient computational complexity, making it suitable for real-time applications [53].

By tracking short-term historical ampacity and its temporal trends, NARX model predicts near-future non-EV load demand within a configurable prediction horizon (typically between 5 and 30 seconds), allowing the system to proactively adjust the permitted charging capacity in real time.

The architecture of the proposed NARX model is illustrated in Fig. 4.1. The model receives lagged values of past load consumption together with selected exogenous variables at its input layer. Specifically, the autoregressive input set consists of a predefined collection of past demand values $y(t-\ell)$, where $\ell \in \{1, 2, 3, 6, 12, 18, 24, 48, 72, 168\}$, capturing both short-term temporal dependencies and longer periodic consumption patterns.

Exogenous variables describing environmental and temporal conditions are also included in the input layer. In particular, ambient temperature $T(t)$, hour of the day $h(t)$, day of the week $d(t)$, and seasonal indicators $s(t)$ are used to capture external factors influencing residential electricity consumption. To properly represent the periodic nature of calendar variables, the temporal inputs $h(t)$, $d(t)$, and $s(t)$ are transformed using sine and cosine cyclical encodings. Furthermore, polynomial interaction features among the exogenous variables are generated to allow the model to capture nonlinear relationships between environmental conditions and load behavior.

The nonlinear mapping between the input features and future load demand is modeled using a feedforward neural network composed of three fully connected hidden layers with 128, 64, and 32 neurons, respectively. Each

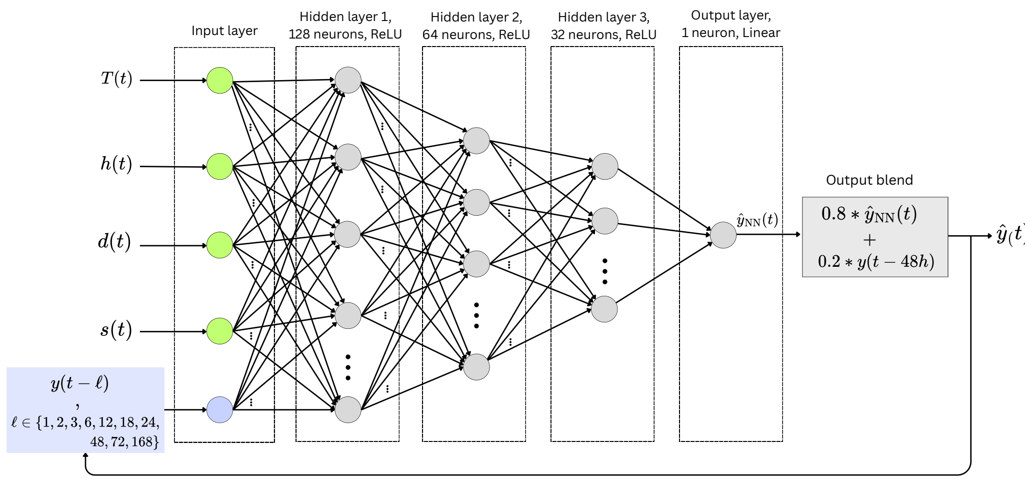

Figure 4.1: Architecture of the NARX neural network used for non-EV load forecasting.

hidden layer employs the Rectified Linear Unit (ReLU) activation function to capture complex nonlinear relationships within the data. The output layer consists of a single neuron with a linear activation function that produces the predicted load demand for the next time step. Model parameters, including weights and biases, are optimized during training using the backpropagation algorithm with the Adam optimizer to minimize the prediction error. The NARX forecasting model can therefore be expressed as

$$\begin{gathered} \hat{y}_{NN}(t) = f\Big(y(t-\ell),\, u(t);\, \alpha\Big), \\ \ell \in \{1, 2, 3, 6, 12, 18, 24, 25, 48, 72, 168\} \end{gathered} \tag{4.2}$$

where $\hat{y}_{NN}(t)$ denotes the demand predicted by the neural network at time t, $y(t-\ell)$ represents the selected lagged demand inputs, and $u(t)$ denotes the vector of exogenous variables including temperature and temporal features. The function $f(\cdot)$ represents the nonlinear mapping implemented by the neural network, and α denotes the set of trainable parameters (weights and biases).

To improve prediction robustness and account for strong daily periodicity in building load profiles, the neural network output is combined with a historical reference value from 48 hours earlier. The final prediction is therefore computed as

$$\hat{y}(t) = 0.8\,\hat{y}_{NN}(t) + 0.2\,y(t-48) \tag{4.3}$$

where $y(t-48)$ represents the observed demand value from the same hour two days earlier.

It should be noted that prior to training, the dataset undergoes a preprocessing stage to address missing or corrupted smart-meter readings caused by sensor malfunctions or communication interruptions. Linear interpolation is used to fill short consecutive gaps by estimating intermediate values between adjacent measurements while preserving the temporal continuity of the load profile. For isolated missing values or longer gaps where interpolation could distort the underlying consumption pattern, mean imputation is applied to maintain statistical consistency within the dataset.

To evaluate the forecasting performance of the model, the Root Mean Squared Error (RMSE) can be utilized as the primary metric, defined as:

$$\text{RMSE} = \sqrt{\frac{1}{n}\sum_{i=1}^{n}\left(y_i - \hat{y}_i\right)^2} \tag{4.4}$$

where, y_i and $\hat{y}_i$ denote the actual and predicted values, respectively, and n is the number of samples in the evaluation set. RMSE provides a quantitative measure of the average magnitude of prediction error, with lower values indicating more accurate forecasts.

4.3 Case Study

To evaluate the performance of the proposed approach, we chose a multi-residential building from the dataset [103] for our study to validate the pro-

Table 4.1: Summary of system parameters and assumptions for the MILP-based EMS case study.

Parameter	Variable	Assumption / Value
Feeder capacity (per phase)	p	200A (20% safety margin)
Number of residential units in building	–	8
Number of EVSEs	N	6 Level II EV chargers ($\chi_m = 0$)
Max. operating current of EVSE m	$I_m^{\max}$	[32, 22, 24, 26, 28, 30] A for chargers 1–6
Min. operating current of EVSE m	$I_m^{\min}$	1A for all chargers
Priority coefficient	α_m	All chargers have equal priority ($\alpha_m = 1$)

posed model. This building is situated in the Lower Mainland area of Vancouver, Canada, and consists of eight units, with 75% of the residents being EV owners who have requested EVSE infrastructure for the building. The building's capacity per phase is 200 A, and to ensure safety, a 20% margin is reserved as unavailable. Therefore, we aim to limit the maximum usage to 160 A per phase. The building's non-EV loads are connected to all three phases. Six EVSEs from various brands were considered, each is connected to two phases with maximum current capacity ($I_m^{\max}$) ranging from 22 A to 32 A. Table 4.1 summarizes the parameters and assumptions used in this case study. Our predictive NARX model receives the past 10 time steps of building consumption data, obtained from smart meters, and predicts the next time step using a rolling window technique. This rolling window continuously monitors both the actual consumption and its rate of change, enabling the system to proactively anticipate upcoming load conditions. Developed NARX model allows us to define a 90% probability range, meaning we can expect an accurate estimation to fall within this range with a certain level of confidence. Figure 4.2 illustrates the actual versus predicted values for solar generation and household power consumption over a 24-hour period, complete with hourly error annotations. The blue and red markers indicate lower and upper errors, respectively, while the shaded pink area represents the error range. The solid orange line depicts the predictions, and the blue line shows the actual test values, emphasizing the model's predictive accuracy. The RMSE for the predicted energy consumption profile was 0.3779 kW, and

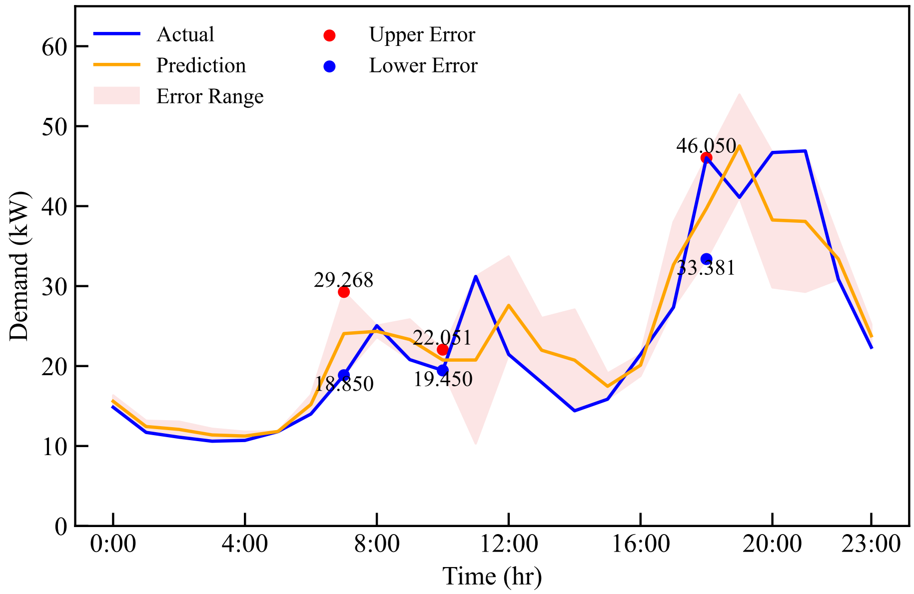

Figure 4.2: Predicted vs. actual building power consumption over a 24-hour period using the NARX model, including upper and lower error bounds.

analyzing predicted profiles over 30 randomly selected days throughout the year yields an average RMSE of 0.5297 kW for the building. As shown in Figure 4.2, the maximum non-EV load consumption of the building is about 46 KW. Considering 57.6 KW (160 Amp) total allowable capacity of the building, it leaves only 11.6 KW effective room for EVSE utilization, meaning that without an EMS in place, roughly two typical level-II EVSEs can work at full power simultaneously. On the other hand, when an automatic EMS is used, we can oversubscribe the service panel with more loads. Using EMS dynamically extends the room for utilizing more EVSEs while it prevents overloading the electrical system.

We set the minimum EVSE charge rate $I_m^{min} = 1\,\text{A}$, and Figure 4.3 shows the optimal power distribution and operation schedule for each charger, along with the total power consumption of the building. The charger demand from 7:00 AM to 5:00 PM is set randomly; however, after 6:00 PM, it is assumed

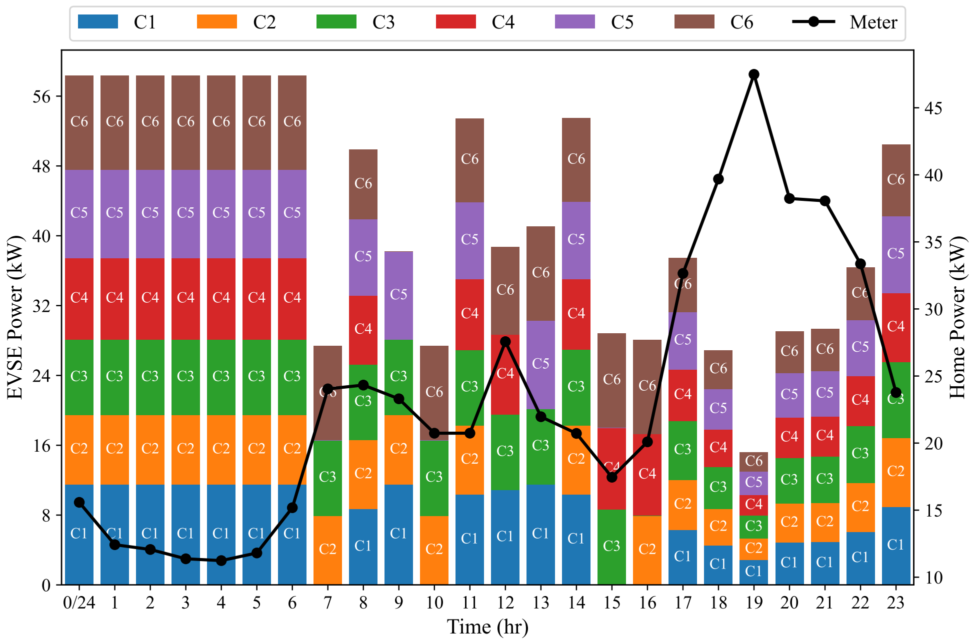

Figure 4.3: Hourly power assigned to each EVSE with respect to the building's non-EV load under the MILP-based EMS.

that demand arises from all EVs. The proposed optimization model effectively allocates the charging profile to each EVSE. Adhering to the overall feeder constraints, when the demand on other non-EV loads is high, the EVSE charge profiles are curtailed to accommodate the feeder limit. However, they are prioritized for a higher charging profile during lower consumption periods, such as nighttime. Furthermore, Figure 4.4 illustrates the real-time energy management response at a more detailed time scale for each phase. Considering that sending too many requests in a short period can trigger the EV's security mechanism (SuspendedEV mode), users can adjust data sampling and response intervals based on their specific requirements. As shown in Figure 4.4, our system supports granular, real-time constraints that enable precise load management while maintaining EVSE stability. As a parameter of user satisfaction, whether drivers receive sufficient energy for

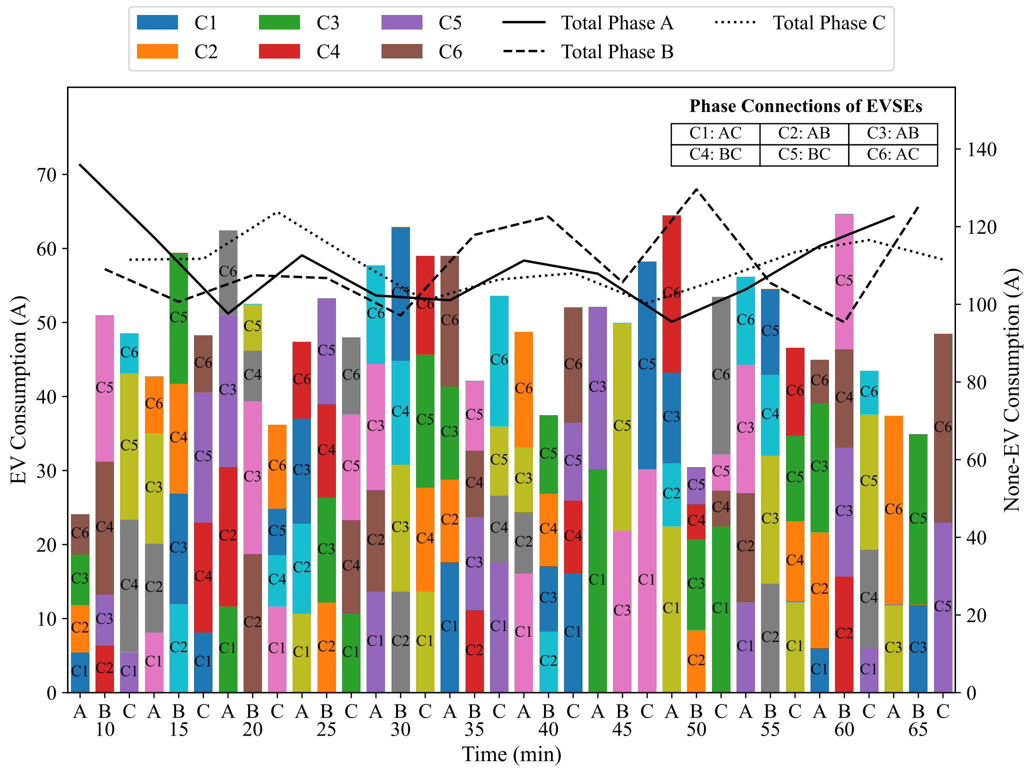

Figure 4.4: Granular phase current distribution of EVSEs. The solid, dashed, and dotted lines are the current consumption of non-EV loads.

the next trip despite EVSE curtailments, we simulated the SoC evolution of six EVs over a 30-day period. The result of this study is demonstrated in Figure 4.5. Each day, every driver departs the building between 7–9 AM and, after a daily commute, returns between 5–7 PM. The trip pattern typically includes three segments: a morning commute, an optional lunch errand, and an evening return. To calculate the SoC of EVs after a daily commute, we employ

$$\mathcal{S}^{\text{ini}} = \mathcal{S}^{\text{start}} - \frac{\eta_d \, l \, E_b}{P_b}$$

Where $\mathcal{S}^{\text{start}}$ denote the SoC at the start of the day (i.e., before the morning commute), l represents the daily commute distance for each EV, modeled

Table 4.2: Parameters and assumptions for the 30-day EV SoC evolution simulation.

Parameter	**Variable**	**Assumption / Value**
Departure time window	–	07:00–09:00 (random)
Arrival time window	–	17:00–19:00 (random)
Daily commute parameters	–	Total distance $l \sim \mathcal{LN}(\mu = 4.08, \sigma = 0.745)\,\text{km}$ [102]
Energy per km	E_b	$[0.15, 0.22]$ kWh/km
Battery size	P_b	$[65, 120]$ kWh
Driving efficiency	η_d	0.8
Charging efficiency	η_c	0.9
Charge slowdown threshold	–	$SoC > 90\%$

using a log-normal distribution with parameters $\mu = 4.08$ and $\sigma = 0.745$, as detailed in [102]. E_b is the normalized EV energy consumption per kilometer (kWh/km), randomly assigned within the range of 0.15 to 0.22 kWh/km. The battery size P_b is randomly selected within the range of 65 to 120 kWh. η_d is the EV driving efficiency, which depends on driving style, speed, and daily traffic, and is assumed to be 0.8. Given that, we use the SoC_{ini} to calculate the SoC of the EV after charging using

$$\mathcal{S}^{\text{f}} = \mathcal{S}^{\text{ini}} + \frac{T E_c \eta_c}{P_b}$$

where E_c is the optimal kW power assigned to each EVSE and obtained from our proposed EMS, T represents the charge duration, and η_c is the EVSE charge efficiency, assumed to be 0.9. To mimic real EV behaviour, the charging rate tapers above 90% SoC. Table 4.2 summarizes the study parameters. It can be observed from Figure 4.5 that all vehicles maintain a high SoC throughout the 30-day period despite occasional curtailments. To better visualize the SoC evolution pattern, the zoomed-in inset highlights a representative 24-hour window. The average final SoC values shown in the figure represent the mean SoC of each EV at the end of all 30 simulated days, confirming that all EVs reach nearly full charge by morning departure. These results demonstrate that the proposed EMS effectively respects feeder and phase constraints while ensuring user satisfaction.

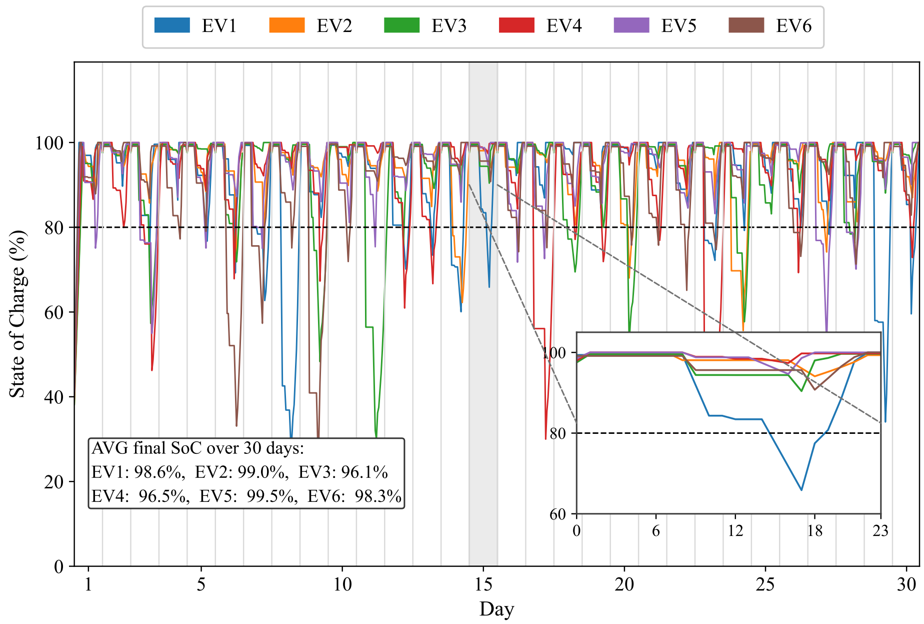

Figure 4.5: SoC evolution of EVs over 30 days, along with the average final SoC of each EV before the morning departure over the 30 days. The inset shows the detailed profiles for day 15.

To demonstrate the efficacy of our optimization model, the computation time for calculating the optimal setpoints as the number of EVSEs increases is presented in Figure 4.6. In order to reduce randomness, we repeated each setting 10 times and reported the mean. The runtime grows gently as N increases (approximately linear), and remains around 6 ms for N=50, which shows the algorithm is fast and efficient.

4.4 Conclusion

This chapter introduced a MILP-based EMS for EVSE integration in both dedicated and mixed electrical system topologies within an MURB. The proposed EMS aims to maximize the total current allocation to EVSEs while ensuring adherence to per-phase feeder capacity limits and maintaining cur-

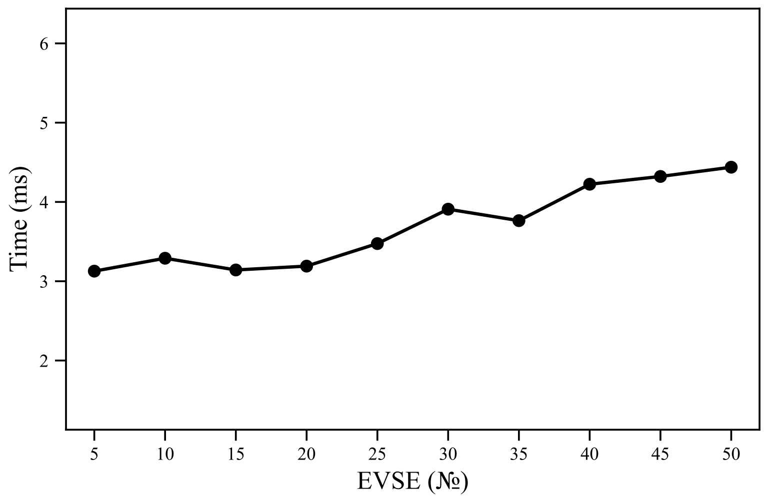

Figure 4.6: Computation time for calculating optimal setpoints using the proposed MILP-based EMS as the number of EVSEs increases.

rent balance across multi-phase EVSE connections. By incorporating an NARX forecasting model to estimate non-EV loads, the EMS dynamically adapts to real-time building consumption conditions. The results of the conducted case study demonstrate that the EMS effectively curtails EVSE current during periods of high non-EV demand and reallocates charging power during off-peak periods, optimizing the use of available capacity without exceeding feeder constraints. Furthermore, the system's responsiveness under real-time conditions was validated through a fine-grained analysis. In addition, the SoC evaluation confirmed that the proposed strategy preserves user satisfaction by maintaining acceptable charge levels across EVs. Finally, the computational time analysis verified the efficiency of the method, showing that it scales well with the number of EVSEs and remains suitable for real-time implementation. Although the proposed EMS demonstrates effective performance under deterministic conditions, practical operation in MURBs may involve uncertainties in non-EV load consumption and EV availability. To address this aspect, the next chapter introduces an EMS based on DRO to ensure reliable EVSE operation under such uncertainties.

Chapter 5

Uncertainty-Driven Energy Management for Robust EVSE Operation

Energy management in MURBs is challenged by uncertainties such as fluctuating non-EV loads and unpredictable EV user behavior. These factors limit the effectiveness of deterministic or standard stochastic models. DRO addresses this by optimizing the worst-case expected outcome over an ambiguity set of plausible distributions, offering a balanced alternative to overly conservative robust methods and unreliable stochastic approaches.

In this chapter, we present a real-time EMS based on a DRO framework designed for MURBs. The proposed model addresses the challenge of integrating EVSEs into existing building infrastructures that may lack sufficient capacity to support simultaneous charging for all EV-owning residents. The EMS accounts for key uncertainties, including the stochastic availability of EVs and fluctuations in building load profiles. To capture these uncertainties, we construct a Wasserstein-based ambiguity set, enabling the EMS to optimize for the worst-case expected performance over a range of plausible probability distributions. The NARX prediction model, proposed in section 4.2, is employed to forecast power demand, which informs a dynamic curtailment strategy. This also enables the calculation of the uncertainty set and offers valuable insights for implementing curtailment strategies of EVSEs. The proposed method was tested on an MURB located on Vancouver Island. Confidence levels were calculated at each time step to quantify the uncertainty. The results show that during periods of high uncertainty, the EMS adopted a more conservative strategy by curtailing EVSE consumption more aggressively, while under lower uncertainty, it allowed more flexible charging, thereby improving infrastructure utilization.

5.1 Real-time DRO formulation

To manage uncertainties in EVSE availability and non-EV load fluctuations, we formulate the energy allocation problem using a DRO framework. The term *distribution* here refers to the probability distribution of uncertain parameters and is not a distributed system architecture. One can adopt DRO to a centralized EMS architecture and accounts for the uncertainties by optimizing against the worst-case probability distribution within a specified ambiguity set constructed from historical records. This enables robust performance without requiring exact knowledge of the underlying distribution, while also avoiding the overly conservative outcomes typical of traditional robust methods.

Consider the hierarchical topology demonstrated in Figure 2.3, which consists of a main distribution panel connected to N sub-feeders, indexed by the set $\mathcal{N} = \{1, 2, \ldots, N\}$. Each sub-feeder $n \in \mathcal{N}$ serves a set of M_n EVSEs. Let $y_{n,m,t}$ denote the current (in amperes) allocated to EVSE m on sub-feeder n at time t, and let $A_{n,m,t}$ be a binary variable indicating its availability at that time. The parameter $\chi_{n,m} \in \{0, 1\}$ indicates whether the EVSE is connected to a DC ($\chi_{n,m} = 1$) or AC ($\chi_{n,m} = 0$) sub-panel. The coefficient $\alpha_{n,m}$ is assigned to DC-connected EVSEs to prioritize urgent demand. The objective is to minimize the worst-case expected total weighted current drawn over a scheduling horizon T, across all EVSEs and sub-feeders:

$$\min_{y} \sup_{\mathbb{P}\in\mathcal{F}} \mathbb{E}_{\mathbb{P}} \left[\sum_{n\in\mathcal{N}} \sum_{m=1}^{M_n} \sum_{t=0}^{T-1} \left(\alpha_{n,m}\chi_{n,m} + (1-\chi_{n,m}) \right) A_{n,m,t}\, y_{n,m,t} \right] \tag{5.1}$$

subject to:

$$I^{\min}_{n,m,t} \le y_{n,m,t} \le I^{\max}_{n,m,t}, \quad \forall n \in \mathcal{N},\ \forall m \in \{1,\dots,M_n\},\ \forall t \tag{5.1a}$$

$$\sum_{m=1}^{M_n} A_{n,m,t}\, y_{n,m,t} + \delta_{n,t} + \varepsilon_{n,t} \le p_n, \quad \forall n \in \mathcal{N},\ \forall t \tag{5.1b}$$

$$\sum_{n\in\mathcal{N}} \left(\sum_{m=1}^{M_n} A_{n,m,t}\, y_{n,m,t} + \delta_{n,t} + \varepsilon_{n,t} \right) \le \mathcal{I}^{\max}, \quad \forall t \tag{5.1c}$$

$$\sum_{m=1}^{M_n} \chi_{n,m}\, y_{n,m,t} \le I^{\mathrm{dc}}_{n,t}, \quad \forall n \in \mathcal{N},\ \forall t \tag{5.1d}$$

$$\sum_{m=1}^{M_n} (1-\chi_{n,m})\, y_{n,m,t} \le I^{\mathrm{ac}}_{n,t}, \quad \forall n \in \mathcal{N},\ \forall t \tag{5.1e}$$

Here, $I^{\min}_{n,m,t}$ and $I^{\max}_{n,m,t}$ represent the minimum and maximum allowable charging current for EVSE m, connected to sub-feeder n at time t, respectively. The decision variable $y_{n,m,t}$ denotes the current allocated to each EVSE. The term $\delta_{n,t}$ is the uncertain non-EV load consumption on sub-feeder n at time t, while p_n denotes the nominal ampacity available to sub-feeder n. The term $\varepsilon_{n,t}$ represents a time-dependent forecast uncertainty and is computed as defined in (5.2), where σ denotes the standard deviation of the predicted consumption, and $z_{\alpha/2}$ is the critical value associated with the desired confidence level. These values are derived from the prediction results discussed in Section 4.2.

$$\varepsilon_{n,t} = z_{\alpha/2}\sqrt{\sigma^2} \tag{5.2}$$

Constraint (5.1a) ensures that all EVSEs operate within their physical charging limits. Constraint (5.1b) enforces a per-sub-feeder capacity limit by ensuring that the total current drawn by EVSEs, together with the forecasted non-EV load and its associated uncertainty, does not exceed the nominal ampacity p_n of each sub-feeder. In parallel, Constraint (5.1c) imposes a system-wide constraint that aggregates all EVSE currents and non-EV loads across all sub-feeders, ensuring the total demand remains within the main panel's capacity $\mathcal{I}^{\max}$. Constraints (5.1d) and (5.1e) separately bound the cumulative current drawn by DC and AC EVSEs, respectively, to ensure adherence to their corresponding sub-feeder capacity limits.

Solving optimization problem in (5.1) requires the distributions of the uncertain variables $A_{n,m,t}$ and $\delta_{n,t}$ to be characterized. The ambiguity set $\mathcal{F}$ defines a family of plausible probability distributions for these random variables, constrained by their empirical first and second order moments obtained from historical data. The following expression presents the proposed ambiguity set:

$$\mathcal{F} = \left\{ \mathbb{P} \in \mathcal{P}_0\left(\mathbb{R}^{\left(\sum_{n\in\mathcal{N}} M_n + |\mathcal{N}|\right)\cdot T}\right) \;\middle|\; \begin{array}{l} \mathbb{E}_{\mathbb{P}}[A_{n,m,t}] = p_{n,m,t}, \quad \forall n \in \mathcal{N},\ \forall m \in \{1,\ldots,M_n\},\ \forall t, \\ \mathbb{E}_{\mathbb{P}}\left[(A_{n,m,t} - p_{n,m,t})^2\right] \le \sigma^2_{n,m,t}, \quad \forall n,m,t, \\ \mathbb{E}_{\mathbb{P}}[\delta_{n,t}] = \mu_{n,t}, \quad \forall n,t, \\ \mathbb{E}_{\mathbb{P}}\left[(\delta_{n,t} - \mu_{n,t})^2\right] \le \left(\sigma^L_{n,t}\right)^2, \quad \forall n,t \end{array} \right\}. \tag{5.3}$$

where, $p_{n,m,t}$ is the expected activity of EVSE m connected to sub-feeder n at time t, $\sigma^2_{n,m,t}$ is the variance of the availability of EVSE m, $\mu_{n,t}$ is its expected consumption of non-EV loads on sub-feeder n, and $(\sigma^L_{n,t})^2$ is its variance. In the objective function (5.1) and the constraints (5.1b)–(5.1c), the uncertain variables $A_{n,m,t}$ and $\delta_{n,t}$ are realized through their statistical moments defined in (5.3), where the expected values $p_{n,m,t}$ and $\mu_{n,t}$ represent their average behaviors, and the variance bounds $\sigma^2_{n,m,t}$ and $(\sigma^L_{n,t})^2$ capture the allowable deviation around these expectations.

Solving the optimization problem (5.1) is challenging due to the infinite dimension of the ambiguity set $\mathcal{F}$, which can lead to intractable solutions for standard convex optimization solvers. To enable practical implementation and ensure computational efficiency, we reformulate the problem into a finite-dimensional convex program. The details of this reformulation are presented in the following subsection.

5.2 Reformulation of DRO problem into a Finite Convex Program

We reformulate the problem in (5.1) as a finite-dimensional convex program by replacing the moment-based ambiguity set in (5.3) with a Wassestein ball centered at the empirical distribution of the uncertain variables. Let

$$\xi = \Big(A_{n,m,t},\ \delta_{n,t}\Big)_{n\in\mathcal{N},\ m\in\{1,\dots,M_n\},\ t=0,\dots,T-1} \in \mathbb{R}^d \tag{5.4}$$

where $d = \left(\sum_{n\in\mathcal{N}} M_n + |\mathcal{N}|\right) T$, and let $\hat{\xi}^{(i)} = \Big(\hat{A}^{(i)}_{n,m,t},\ \hat{\delta}^{(i)}_{n,t}\Big)$, $i = 1,\dots,N_{\text{data}}$, denote historical samples of EVSE availability and non-EV load. The empirical distribution is $\hat{\mathbb{P}}_{N_{\text{data}}} := \frac{1}{N_{\text{data}}} \sum_{i=1}^{N_{\text{data}}} \delta_{\hat{\xi}^{(i)}}$. We define a Wasserstein ambiguity set

$$\mathcal{F}_W = \left\{\mathbb{P} \in \mathcal{P}_0(\Xi) \,\Big|\, W_2\Big(\mathbb{P}, \hat{\mathbb{P}}_{N_{\text{data}}}\Big) \le \rho\right\}, \tag{5.5}$$

where $W_2(\cdot,\cdot)$ is the 2-Wasserstein distance induced by the Euclidean norm, $\Xi \subseteq \mathbb{R}^d$ is the support of ξ, and $\rho > 0$ is the Wasserstein radius. In the remainder, we approximate the original DRO problem by replacing $\mathcal{F}$ with $\mathcal{F}_W$.

From an operational standpoint, the set $\mathcal{F}_W$ can be interpreted as the collection of all load and availability distributions that are not too far from the historical data. The empirical distribution $\hat{\mathbb{P}}_{N_{\text{data}}}$ captures how EVSEs and non-EV loads have behaved in the past, while the radius ρ determines how much we allow future behavior to deviate from these historical patterns. A small ρ means we trust the past data almost literally; a larger ρ means we hedge against more severe shifts in EV usage or building load. For a given decision vector y, all the uncertain terms in our model (objective and constraints) depend on the random vector ξ only through weighted sums of its components. To capture this common structure, we introduce a generic function:

$$f(\xi, y) = \beta(y)^\top \xi + \gamma(y). \tag{5.6}$$

where $\beta(y) \in \mathbb{R}^d$ is the vector of weights applied to the uncertain quantities and $\gamma(y) \in \mathbb{R}$ is a deterministic offset. In other words, for fixed y, the function $f(\cdot, y)$ is linear in the uncertain vector ξ.

Let

$$\hat{\mathbb{E}}[f(\xi, y)] := \frac{1}{N_{\text{data}}} \sum_{i=1}^{N_{\text{data}}} f\left(\hat{\xi}^{(i)}, y\right), \tag{5.7}$$

denote the empirical expectation of f under the historical samples $\hat{\xi}^{(i)}$. A standard result in Wasserstein distributionally robust optimization then states that the worst-case expected value of f over the Wasserstein ball (5.5) can be written in closed form as

$$\sup_{\mathbb{P} \in \mathcal{F}_W} \mathbb{E}_{\mathbb{P}}[f(\xi, y)] = \hat{\mathbb{E}}[f(\xi, y)] + \rho \|\beta(y)\|_2. \tag{5.8}$$

This representation holds under standard assumptions on the support Ξ and the transportation cost defining W_2 (e.g., $\Xi = \mathbb{R}^d$ and a quadratic cost induced by the Euclidean norm); see, for example, standard references on Wasserstein distributionally robust optimization.

Intuitively, the vector $\beta(y)$ collects how strongly the function f reacts to each uncertain component of ξ, and the norm $\|\beta(y)\|_2$ measures the overall sensitivity of f to uncertainty. Equation (5.8), therefore, says that the worst-case expectation is equal to the empirical average performance $\hat{\mathbb{E}}[f(\xi, y)]$ plus a robustness margin $\rho\|\beta(y)\|_2$ that grows with both the Wasserstein radius ρ and the sensitivity of the function to the uncertain loads and availabilities.

In other words, (5.8) says that the worst-case expected value under all plausible distributions in $\mathcal{F}_W$ equals an average over historical scenarios plus a "robustness penalty." The first term, $\frac{1}{N_{\text{data}}}\sum_i f(\hat{\xi}^{(i)}, y)$, is simply the empirical performance of a given allocation y on past days. The second term, $\rho\|\beta(y)\|_2$, acts like a safety margin that grows with both the radius ρ (how conservative we want to be) and the sensitivity vector $\beta(y)$ (how strongly the function reacts to changes in the uncertain loads and availabilities). If the allocation y makes the system highly sensitive to uncertainty, $\|\beta(y)\|_2$ is large and the worst-case penalty becomes significant.

Thus, every worst-case expectation of a linear functional of ξ can be expressed as an empirical mean plus a norm-regularization term.

We now apply the generic result in (5.8) to the objective (5.1). The quantity inside the expectation in (5.1) is the total weighted current drawn by all EVSEs over the horizon. For compactness, we write this objective term as a function of the uncertainty vector ξ and the decision vector y:

$$f_{\text{obj}}(\xi, y) = \sum_{n\in\mathcal{N}} \sum_{m=1}^{M_n} \sum_{t=0}^{T-1} C_{n,m} A_{n,m,t}\, y_{n,m,t}, \tag{5.9}$$

with

$$C_{n,m} := \alpha_{n,m}\chi_{n,m} + (1-\chi_{n,m}). \tag{5.10}$$

For fixed y, this function is linear in the availability variables $A_{n,m,t}$ and does not depend on the non-EV loads $\delta_{n,t}$. In the notation of (5.8), this corresponds to a coefficient vector $\beta(y) = c(y) \in \mathbb{R}^d$ and offset $\gamma(y) = 0$, where the entry of $c(y)$ associated with $A_{n,m,t}$ equals $C_{n,m}y_{n,m,t}$ and all entries associated with $\delta_{n,t}$ are zero. In other words,

$$f_{\text{obj}}(\xi, y) = c(y)^\top \xi. \tag{5.11}$$

Substituting $f = f_{\text{obj}}$ and $\beta(y) = c(y)$ into (5.8) yields

$$\sup_{\mathbb{P}\in\mathcal{F}_W} \mathbb{E}_{\mathbb{P}}[f_{\text{obj}}(\xi, y)] = \frac{1}{N_{\text{data}}} \sum_{i=1}^{N_{\text{data}}} \sum_{n\in\mathcal{N}} \sum_{m=1}^{M_n} \sum_{t=0}^{T-1} C_{n,m} \hat{A}^{(i)}_{n,m,t}\, y_{n,m,t} + \rho\, \|c(y)\|_2. \tag{5.12}$$

Here, each coefficient $c(y)$ entry quantifies how much the objective increases If a particular EVSE becomes available and we allocate it current $y_{n,m,t}$. The empirical term averages this total weighted current over historical availability patterns, while the robustness term $\rho\|c(y)\|_2$ penalizes schedules that are very sensitive to who actually plugs in, thereby encouraging more conservative and stable charging profiles. Intuitively, if we schedule large currents $y_{n,m,t}$ on many EVSEs simultaneously, the norm $\|c(y)\|_2$ becomes large, and the optimizer "feels" that this plan is fragile to changes in who actually plugs in, leading to a higher robust cost.

The worst-case expected objective therefore reduces to an empirical average of the weighted charging currents plus an ℓ_2-regularization term that captures distributional robustness.

Consider the sub-feeder constraint (5.1b),

$$\sum_{m=1}^{M_n} A_{n,m,t} y_{n,m,t} + \delta_{n,t} + \varepsilon_{n,t} \;\le\; p_n, \qquad \forall n \in \mathcal{N},\, \forall t. \tag{5.13}$$

To ensure robustness against distributional uncertainty, we require that the worst-case expected value of the random part of the left-hand side does not exceed the available capacity margin:

$$\sup_{\mathbb{P}\in\mathcal{F}_W} \mathbb{E}_{\mathbb{P}}\left[\sum_{m=1}^{M_n} A_{n,m,t} y_{n,m,t} + \delta_{n,t}\right] + \varepsilon_{n,t} \;\le\; p_n, \qquad \forall n, t. \tag{5.14}$$

Here, $A_{n,m,t}$ denotes the random availability of EVSE m on sub-feeder n at time t, $y_{n,m,t}$ is the scheduled charging current, $\delta_{n,t}$ is the random non-EV load on sub-feeder n, $\varepsilon_{n,t}$ is the forecast uncertainty margin, and p_n is the nominal ampacity of sub-feeder n. Define

$$H_{n,t}(\xi, y) := \sum_{m=1}^{M_n} A_{n,m,t} y_{n,m,t} + \delta_{n,t}, \tag{5.15}$$

which is again linear in ξ. Let $h_{n,t}(y) \in \mathbb{R}^d$ denote the coefficient vector of ξ in $H_{n,t}(\xi, y)$. Specifically, $h_{n,t}(y)$ has entries $y_{n,m,t}$ corresponding to the availability variables $A_{n,m,t}$ (for the fixed sub-feeder n and time t), entry 1 corresponding to the non-EV load $\delta_{n,t}$, and zeros elsewhere. In other words, each component of $h_{n,t}(y)$ measures how much the sub-feeder loading $H_{n,t}(\xi, y)$ would change if the associated uncertain quantity (an EVSE becoming active or the non-EV load increasing) were to increase by one unit. Using (5.8), we obtain

$$\sup_{\mathbb{P} \in \mathcal{F}_W} \mathbb{E}_{\mathbb{P}} \left[H_{n,t}(\xi, y) \right] = \frac{1}{N_{\text{data}}} \sum_{i=1}^{N_{\text{data}}} \left(\sum_{m=1}^{M_n} \hat{A}_{n,m,t}^{(i)} y_{n,m,t} + \hat{\delta}_{n,t}^{(i)} \right) + \rho \| h_{n,t}(y) \|_2, \tag{5.16}$$

and hence (5.14) is equivalent to the deterministic convex constraints

$$\frac{1}{N_{\text{data}}} \sum_{i=1}^{N_{\text{data}}} \left(\sum_{m=1}^{M_n} \hat{A}_{n,m,t}^{(i)} y_{n,m,t} + \hat{\delta}_{n,t}^{(i)} \right) + \rho \| h_{n,t}(y) \|_2 + \varepsilon_{n,t} \ \leq \ p_n, \qquad \forall n, t. \tag{5.17}$$

In (5.17), the left-hand side is the expected loading on sub-feeder n at time t, augmented by two distinct safety buffers. The empirical term captures the average historical current drawn by EVSEs and non-EV loads, while the robust term $\rho \| h_{n,t}(y) \|_2$ accounts for model uncertainty in how many EVSEs are actually active and how non-EV loads evolve. Finally, $\varepsilon_{n,t}$ is the forecast margin derived from the load prediction model. Together, these three components ensure that the chosen currents $y_{n,m,t}$ respect the feeder rating p_n not only on a typical day, but also under adverse yet plausible realizations of EV charging behavior and building demand.

Similarly, the main panel constraint (109d) can be written as

$$\sum_{n \in \mathcal{N}} \left(\sum_{m=1}^{M_n} A_{n,m,t} y_{n,m,t} + \delta_{n,t} + \varepsilon_{n,t} \right) \leq I^{\max}, \qquad \forall t. \tag{5.18}$$

We impose the Wasserstein-robust form

$$\sup_{\mathbb{P} \in \mathcal{F}_W} \mathbb{E}_{\mathbb{P}} \left[\sum_{n \in \mathcal{N}} \left(\sum_{m=1}^{M_n} A_{n,m,t} y_{n,m,t} + \delta_{n,t} \right) \right] + \sum_{n \in \mathcal{N}} \varepsilon_{n,t} \leq I^{\max}, \qquad \forall t. \tag{5.19}$$

Here, $A_{n,m,t}$ is the random availability of EVSE m on sub-feeder n at time t, $y_{n,m,t}$ is the scheduled current, $\delta_{n,t}$ is the random non-EV load on sub-feeder n, $\varepsilon_{n,t}$ is the forecast uncertainty margin for that feeder and time, and $I^{\max}$ denotes the capacity (ampacity) of the main distribution panel.

Define

$$K_t(\xi, y) := \sum_{n \in \mathcal{N}} \left(\sum_{m=1}^{M_n} A_{n,m,t} y_{n,m,t} + \delta_{n,t} \right), \tag{5.20}$$

which represents the total instantaneous current seen by the main panel at time t for a given realization of the uncertainties ξ and decision vector y. Since $K_t(\cdot, y)$ is linear in ξ, there exists a coefficient vector $\mathbf{k}_t(y) \in \mathbb{R}^d$ such that

$$K_t(\xi, y) = \mathbf{k}_t(y)^\top \xi. \tag{5.21}$$

The entries of $\mathbf{k}_t(y)$ are $y_{n,m,t}$ for all availability variables $A_{n,m,t}$ at time t, and 1 for all non-EV loads $\delta_{n,t}$, with zeros elsewhere. In other words, each component of $\mathbf{k}_t(y)$ represents how much the total main panel loading $K_t(\xi, y)$ would change if the corresponding uncertain quantity (an EVSE becoming active or a feeder's non-EV load) were to increase by one unit.

Applying (5.8) with $f = K_t$ and $\beta(y) = \mathbf{k}_t(y)$ yields

$$\sup_{\mathbb{P} \in \mathcal{F}_W} \mathbb{E}_{\mathbb{P}}[K_t(\xi, y)] = \frac{1}{N_{\text{data}}} \sum_{i=1}^{N_{\text{data}}} \left[\sum_{n \in \mathcal{N}} \sum_{m=1}^{M_n} \hat{A}^{(i)}_{n,m,t} y_{n,m,t} + \hat{\delta}^{(i)}_{n,t} \right] + \rho \|\mathbf{k}_t(y)\|_2. \tag{5.22}$$

and therefore (5.19) is equivalent to

$$\frac{1}{N_{\text{data}}}\sum_{i=1}^{N_{\text{data}}}\left[\sum_{n\in\mathcal{N}}\left(\sum_{m=1}^{M_n}\hat{A}^{(i)}_{n,m,t}y_{n,m,t}+\hat{\delta}^{(i)}_{n,t}\right)\right]+\rho\|\mathbf{k}_t(y)\|_2+\sum_{n\in\mathcal{N}}\varepsilon_{n,t} \ \le \ I^{\max}, \qquad \forall t. \tag{5.23}$$

At the main panel level, (5.23) plays the same role but now aggregates all sub-feeders. The empirical term reflects the average total building current (all EVSEs plus non-EV load), the robust margin $\rho\|\mathbf{k}_t(y)\|_2$ captures system-wide sensitivity to worst-case deviations in EV plug-in patterns and base load, and forecasting uncertainty (captured by $\sum_{n\in\mathcal{N}}\varepsilon_{n,t}$) adds the forecast uncertainty from each feeder. In electrical terms, this is analogous to sizing the main panel schedule so that even if several feeders experience higher-than-expected demand at the same time, the total current remains below the nameplate limit $I^{\max}$.

Combining (5.12), (5.17), and (5.23) with the deterministic constraints (5.1a), (5.1d), and (5.1e), We obtain the following finite-dimensional convex optimization problem:

$$\begin{aligned}\min_{y} \quad & \frac{1}{N_{\text{data}}}\sum_{i=1}^{N_{\text{data}}}\sum_{n\in\mathcal{N}}\sum_{m=1}^{M_n}\sum_{t=0}^{T-1}C_{n,m}\hat{A}^{(i)}_{n,m,t}y_{n,m,t}+\rho\|c(y)\|_2 \\ \text{s.t.} \quad & (5.17), \quad (5.23),\end{aligned} \tag{5.24}$$

$$I^{\min}_{n,m,t}\le y_{n,m,t}\le I^{\max}_{n,m,t}, \qquad \forall n,m,t. \tag{5.25a}$$

$$\sum_{m=1}^{M_n}\chi_{n,m}y_{n,m,t}\le I^{\text{dc}}_{n,t}, \qquad \forall n,t. \tag{5.25b}$$

$$\sum_{m=1}^{M_n}(1-\chi_{n,m})y_{n,m,t}\le I^{\text{ac}}_{n,t}, \qquad \forall n,t. \tag{5.25c}$$

In (5.24), all decision variables are finite-dimensional (the charging currents $y_{n,m,t}$), and all constraints are either linear or involve an ℓ_2-norm such as $\|c(y)\|_2$, $\|h_{n,t}(y)\|_2$, and $\|\mathbf{k}_t(y)\|_2$. Each of these norm terms is convex and can be represented by a standard second-order cone (SOC) constraint by introducing an auxiliary scalar variable s and enforcing $\|v\|_2 \leq s$, for the appropriate vector v. As a result, the Wasserstein DRO approximation (5.24) can be written as a second-order cone program (SOCP), whose size grows linearly with the number of historical samples N_{data}. Such SOCPs are a well-studied class of convex optimization problems and can be efficiently solved using off-the-shelf conic solvers (e.g., MOSEK, Gurobi, ECOS), in contrast to the original infinite-dimensional DRO formulation over the ambiguity set $\mathcal{F}$.

5.3 Case Study

We studied a residential building with eight units located in Vancouver, Canada, using the publicly available AMPds dataset [103]. Each unit, along with its associated EVSE, is connected to an individual sub-feeder rated at 50 A. To comply with electrical safety standards, a 20% safety margin is applied to each sub-feeder, resulting in a usable capacity of 40 A per unit. All sub-feeders are connected to a main distribution panel with a total ampacity of 250 A. Each unit is equipped with a Level II EVSE, resulting in a total of eight EVSEs installed in the building. All EVSEs are assumed to be Level II ($\chi_{n,m} = 0$) and are sourced from different vendors, offering a maximum current capacity ranging from 25 A to 32 A, with a minimum operational threshold of 6 A. To realistically reflect uncertainties in EV charging behavior, we consider that each EVSE has a 70% probability of being available at any given time, simulating variability due to user behavior. It is assumed that charge requests drop to 20% during the daytime period between 8:00 A.M. and 3:00 P.M. Table 5.1 summarizes the parameters used in this case study.

Table 5.1: Summary of system parameters and assumptions for the DRO-based EMS case study.

Parameter	**Variable**	**Value / Assumption**
Location	–	Vancouver, Canada
Number of Residential Units	–	8
Number of EVSEs	–	8 (1 per unit)
Number of Sub-Feeders	N	8 (1 per unit)
Sub-Feeder Nominal Capacity	p_n	50A each (40A after 20% safety margin)
Main Feeder Capacity	$\mathcal{I}^{\max}$	250
EVSE Type	$\chi_{n,m}$	Level II ($\chi_{n,m} = 0$)
EVSE Max. Operating Current	$I_{n,m,t}^{\max}$	25–32 A
EVSE Min Operating Current	$I_{n,m,t}^{\min}$	6 A for all EVSEs
EVSE Availability Probability	$A_{n,m,t} \sim \mathbb{P}$	10%-70%

The proposed EMS leverages a predictive model of the building, described in subsection 4.2, to integrate hourly energy demand forecasts for each residential unit, while explicitly accounting for the uncertainties introduced in (5.2). The forecasting model is trained using a dataset that is partitioned into training, validation, and test subsets. To improve the accuracy of the NARX, we incorporate temperature, day of the week, and season as exogenous variables.

Figure 5.1 presents the predicted 24-hour energy consumption profile for one unit on a representative day in February, with a corresponding Root Mean Square Error (RMSE) of 0.3779 kW. To assess the model's performance more broadly, we evaluate its predictions over 30 randomly selected days throughout the year. The resulting average RMSE across these days is approximately 0.5297 kW, indicating a consistent level of forecasting accuracy suitable for EMS integration.

A noticeable deviation is observed in the predicted peak power around 6 P.M., indicating considerable uncertainty in power consumption during this period across different days. This variability renders deterministic load management strategies insufficiently reliable. Therefore, the use of a DRO framework becomes essential to enable more conservative and reliable decision-making during such peak hours.

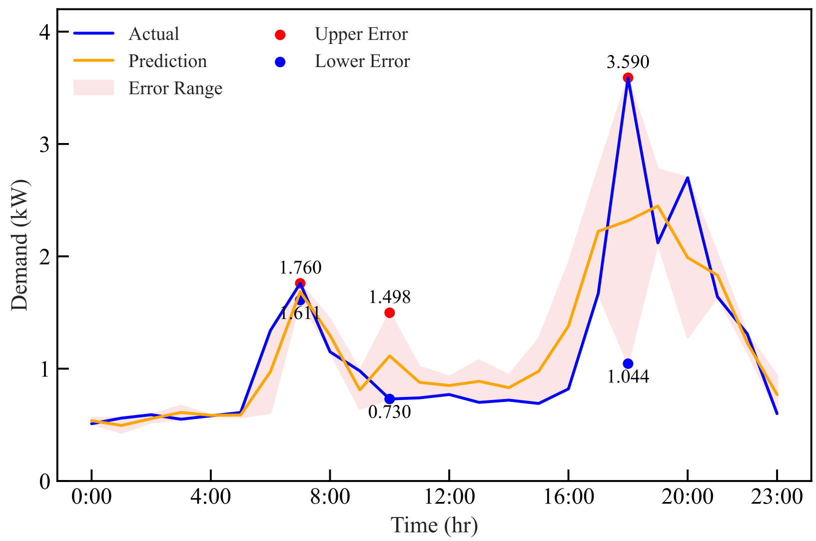

Figure 5.1: Forecasted 24-hour power consumption for a residential unit compared with actual measurements, including upper and lower error bounds.

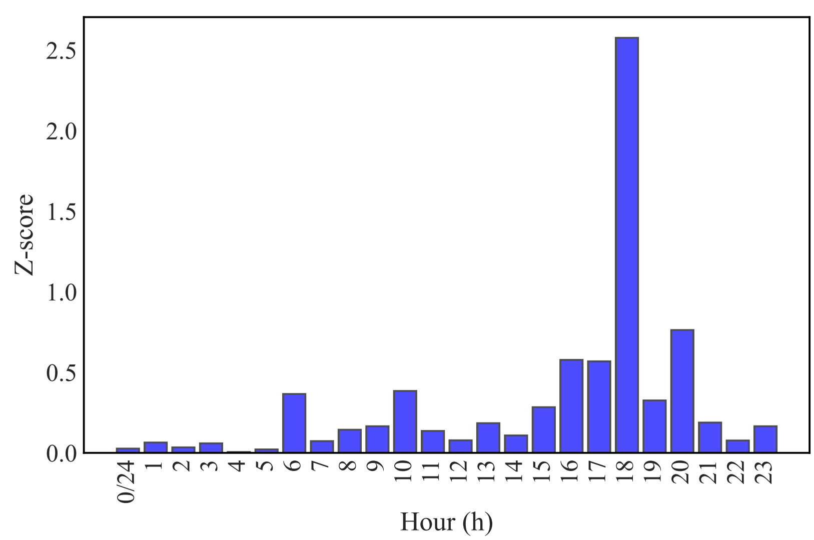

Figure 5.2: Z-score of the prediction error for each hour of the day.

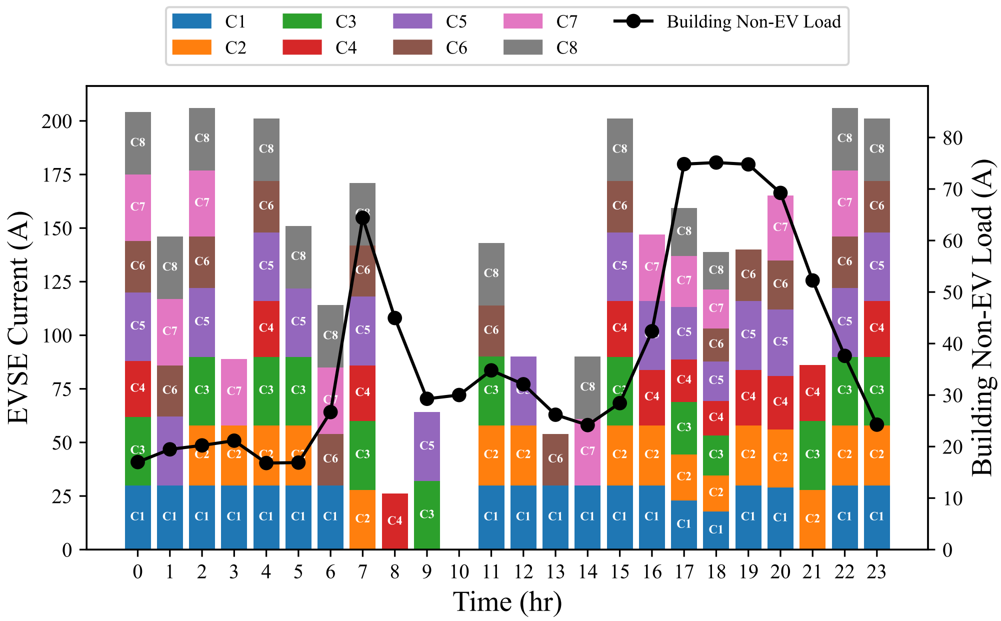

Figure 5.3: Current allocated to each EVSE over the day under the DRO-based EMS, shown alongside the building's non-EV load.

To examine the distributed uncertainties throughout the hours of a day, we analyzed the z-scores related to each predicted value for every hour. Therefore, the error between actual and predicted values can be used as a confidence level to calculate the Wasserstein radius using (5.2) and then introduce it into the DRO model presented in (5.1). The z-score at each hour of the day, shown in Figure 5.2, constructs the ambiguity set of common loads in the building. Figure 5.3 presents the results of the DRO-based optimization. As shown, the model dynamically adjusts the power allocated to EVSEs while adhering to the feeder capacity constraint. During periods of high non-EV building load, the optimization reduces EV charger allocations to ensure the total demand remains within the allowable limit.

To further analyze the detailed load dynamics, Figures 5.4 (a–h) present the minute-level consumption profiles of all eight sub-feeders in the building during the period from 6:00 P.M. to 8:00 P.M. This high-resolution view is obtained by converting the hourly data into a minute-based frequency using linear interpolation. Each subplot illustrates the allocated EVSE current, non-EV load, total load, allowable deviation, and feeder capacity for the corresponding unit. The annotation "Remained Capacity" in each plot denotes the portion of feeder capacity that remained unutilized during the two-hour window due to the stochastic nature of non-EV load behavior. The figure highlights that the DRO effectively captures the uncertainty of each sub-feeder and determines globally coordinated charge profiles for all EVSEs. This minute-level resolution demonstrates the real-time adaptability of the proposed EMS in managing rapidly changing residential loads.

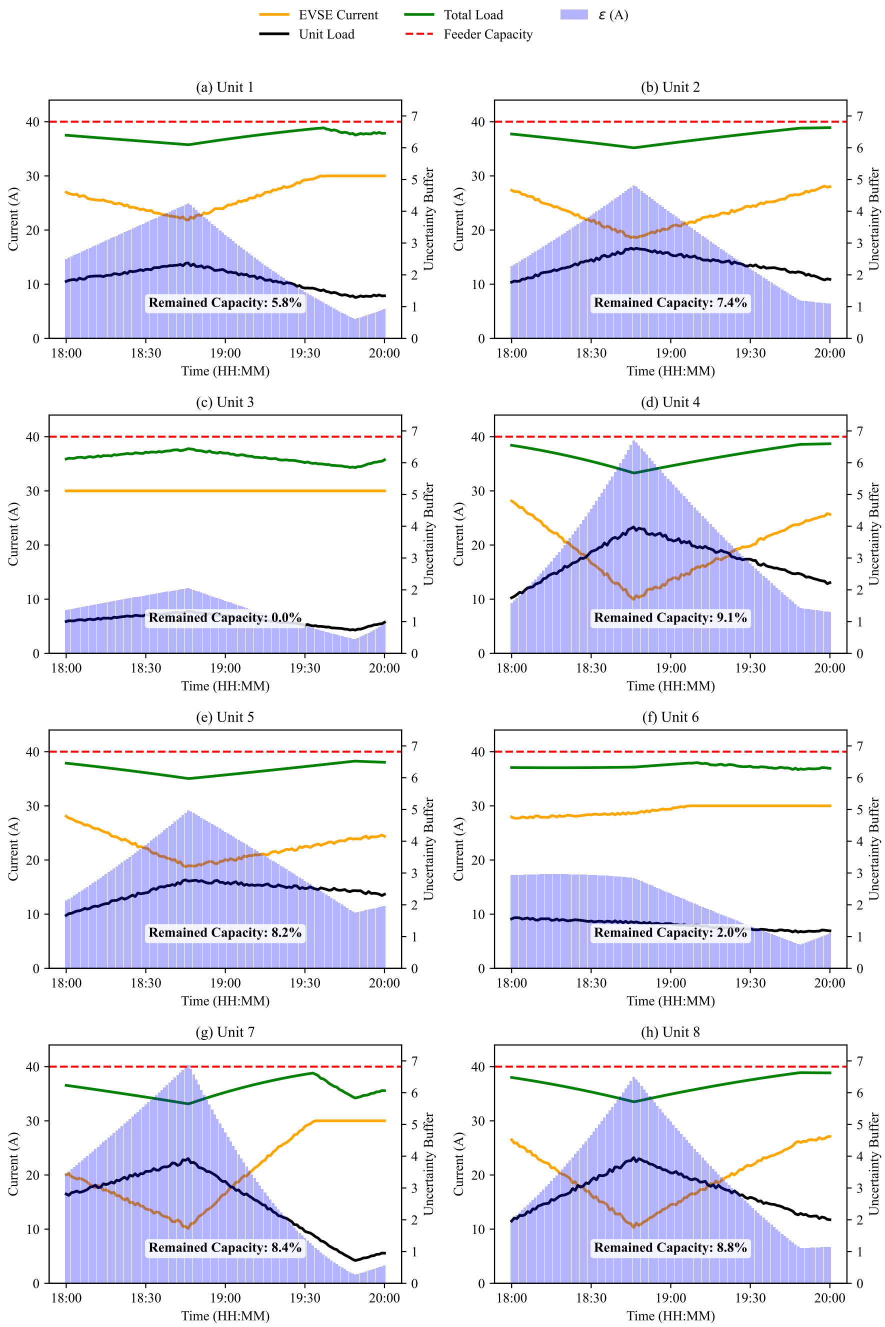

Figure 5.4: Minute-level EMS operation for all units between 6:00 P.M. and 8:00 P.M., showing EVSE current, non-EV load, total load, and feeder capacity for each sub-feeder.

Figure 5.5 illustrates the comparison between our DRO approach and two other common optimization methods for handling uncertainties, namely SO and RO. For each method, the optimization was executed 100 times under varying realizations of EVSE availability and non-EV load fluctuations. The line graphs represent the average total feeder load obtained across all runs, and the surrounding shaded regions correspond to ± 1 standard deviation to indicate the variability of total load due to uncertain conditions. From the figure, it can be observed that the RO curve consistently lies below the others, showing its conservative nature and leaving much of the feeder capacity unused. During the early morning hours, the shaded area for SO and DRO shows low variation because non-EV demand and uncertainty are small, and most EVs are connected overnight. The DRO and SO almost overlap in this period, indicating that the uncertainty buffer has little impact when prediction errors are small. Between hours 8 and 16, all three methods show a significant drop in total load as most EVs are disconnected and non-EV consumption dominates. During this period, curtailment does not occur, and all strategies respond almost similarly to minor fluctuations in non-EV load. At night hours, both SO and DRO exhibit higher mean loads and wider shaded regions as more EVs reconnect, and non-EV demand and uncertainty increase. During this period, specifically hour 18, when uncertainty is high, DRO adopts a more conservative approach by increasing the buffer and limiting variations in EV load consumption, which results in a thinner band compared to SO. As it is demonstrated in the figure, the SO curve occasionally surpasses the main panel capacity limit, indicating potential overload risks when uncertainty is high, whereas the proposed DRO maintains operation below the limit by adaptively adjusting its buffer, achieving a balanced trade-off between the conservatism of RO and the aggressive utilization of SO.

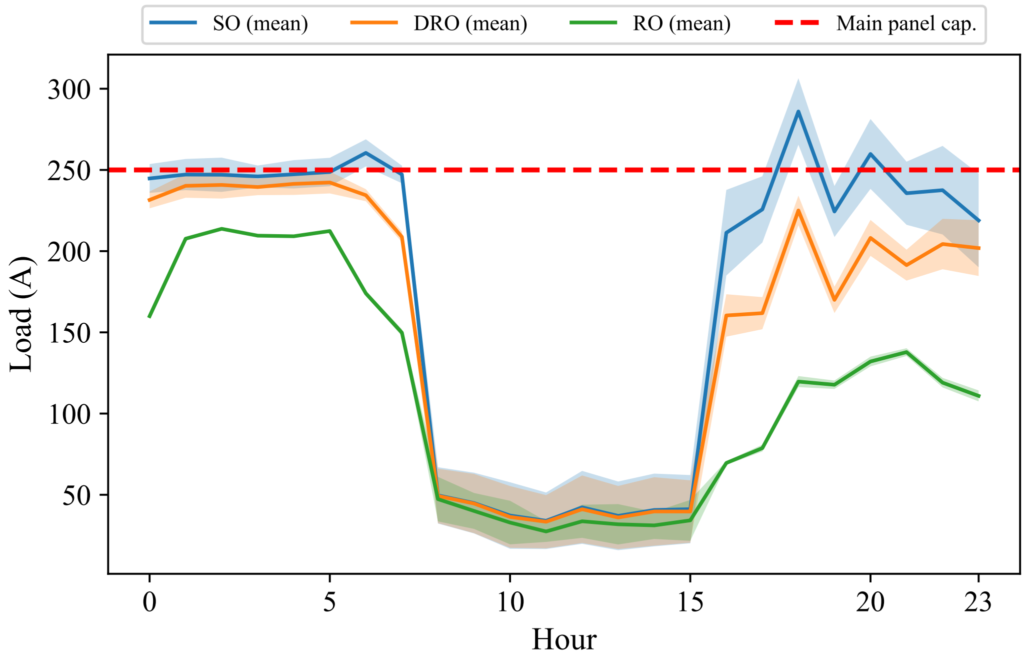

Figure 5.5: Comparison of total feeder load under SO, RO, and DRO over a 24-hour period. The shaded regions represent the ± 1 standard deviation across 100 simulation runs.

5.4 Conclusion

This chapter proposed an EMS based on a DRO framework to manage uncertainty in EVSE consumption within MURBs. A Wasserstein ambiguity set was introduced to model uncertainty in EVSE availability and non-EV residential loads. To make the problem computationally tractable, the infinite-dimensional DRO formulation was reformulated into a finite convex program. The NARX forecasted model was utilized to compute the uncertainty set and offer valuable insights for the curtailment of EVSE consumption. The proposed framework was validated through a case study of a residential building in Vancouver, Canada. Results demonstrate that the DRO-based EMS can effectively reduce EVSE consumption during periods of peak power demand while respecting feeder constraints. Accounting for the uncertainty at each sub-feeder, it generates EVSE setpoints that ensure the total load remains within the capacities of each sub-feeder as well as the main feeder. Finally, the comparison with RO and SO methods shows that DRO is less conservative than RO and more risk-averse than SO, which makes it a balanced trade-off between robustness and performance.

To capture the hierarchical interaction between the main panel and the sub-feeders, a decentralized EMS architecture is required in which sub-feeder decisions are coordinated with the main panel capacity limits. Therefore, the next chapter introduces an EMS based on a Stackelberg game formulation to model this leader–follower interaction.

Chapter 6

Hierarchical EMS with Stackelberg Game for Multi-Tiered EVSE Panels

To capture the heterogeneous and hierarchical structure of MURB electrical networks, this chapter introduces a real-time EMS based on a Stackelberg game framework. In this formulation, the main panel acts as the leader, regulating capacity limits, while the sub-feeders operate as followers that maximize their local consumption within the imposed constraints. The existence of a Stackelberg equilibrium is established to ensure the feasibility and stability of the proposed model.

A case study is conducted on a representative MURB to evaluate the performance of the Stackelberg-based EMS. The results demonstrate that the proposed approach effectively maximizes panel utilization without compromising high-priority loads. During peak periods, the EMS prioritizes non-EV loads and dynamically adjusts EV charging rates to prevent overloading. The computational analysis confirms that the proposed control algorithm computes optimal set-points rapidly, validating its suitability for real-time operation of EVSEs. Furthermore, the integration of the proposed dynamic

Round Robin (d-RR) scheduler within the case study highlights its effectiveness in improving fairness and increasing EVSE penetration when combined with the real-time EMS.

6.1 Stackelberg Game Model

Figure 6.1 illustrates the multi-tiered electrical system in a MURB application, which can be interpreted as a combination of the hierarchical MURB architecture introduced in Fig. 2.3 and the d-RR sub-feeder scheduling model presented in Fig. 3.2. The variables and notations used in this figure remain consistent with those defined in the System Model chapter. To avoid redundancy, they are not restated here, and the reader is referred to Chapter 2 for detailed definitions.

The sequence diagram in Figure 6.2 shows the hierarchical process for starting an EV charging session. The EV first sends a charge request to its connected EVSE, which results in a demand to the sub-feeder. The sub-feeder checks the available capacity via the non-EV meter and initially sends a zero-current profile to the EVSE. After receiving an acknowledgment, the sub-feeder escalates the demand upstream to the main panel, which returns a feasible power allocation considering overall system constraints. The sub-feeder then updates the EVSE with a non-zero current profile. Once accepted, the EVSE initiates the charging process by sending a start command to the EV, which is confirmed across all levels. The sub-feeder has performed continual non-EV monitoring to ensure the demand profile allocated has not exceeded a safe operating status. In the next section, we demonstrate how optimal energy management can be achieved using a Stackelberg game while preserving this process flow.

The aim is to create a holistic EMS that integrates EVSE into existing building infrastructure while managing limited electrical capacity, adjusting EV demand in response to non-EV load changes, and ensuring optimal and

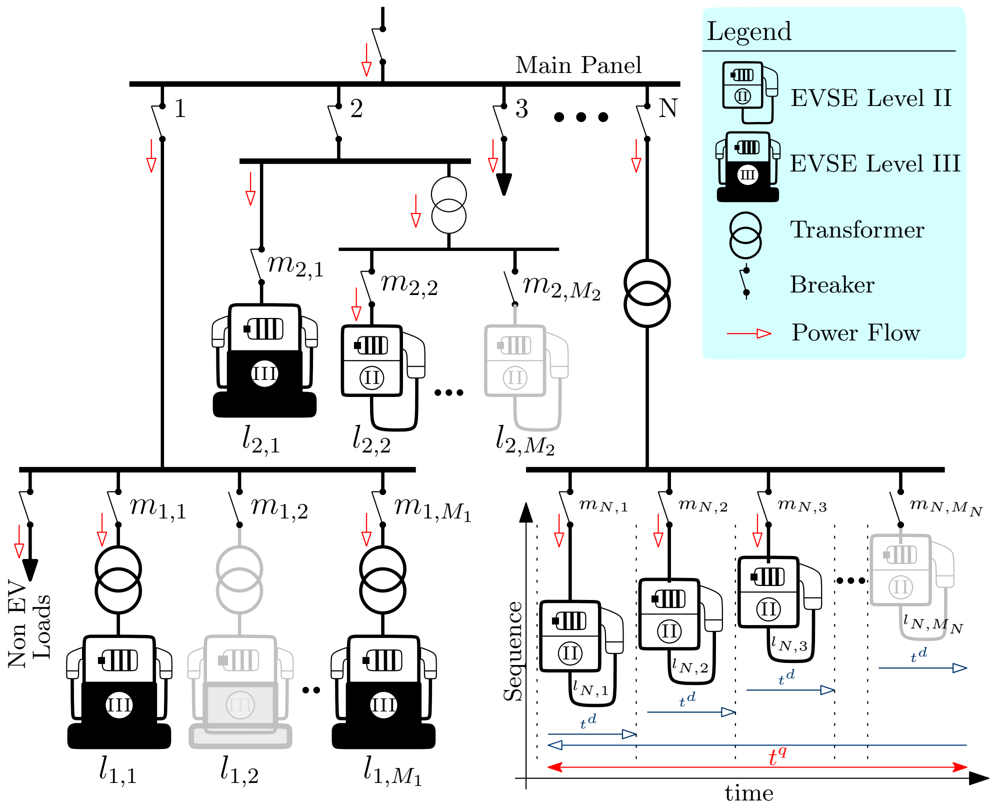

Figure 6.1: Schematic diagram of a hypothetical multi-tier electrical system of a MURB with d-RR scheduling applied at the sub-feeder level.

fair operating. The sequence diagram shown in Figure 6.2 aligns well with a non-cooperative game model between the main panel and sub-feeders. The core regulatory principle of this model is to initially fulfill the requirements of non-EV loads and subsequently adjust the current to EVSEs based on real-time demands. This prioritization strategy is essential for ensuring that consumers' primary needs are adequately met before allocating resources to EVSEs.

As depicted in Figure 2.3, the main panel serves as the leader, sourcing energy for the entire system at the highest level, while the sub-feeders function as followers, determining initial demands. This structure facilitates mod-

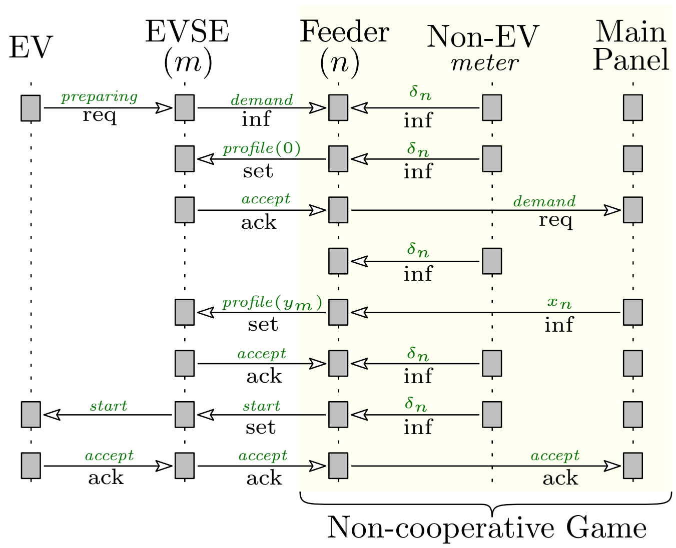

Figure 6.2: Sequence diagram illustrating the message flow between different components of the system during the initiation of an EV charging session.

eling demand-supply interactions as a Stackelberg game. In a Stackelberg game, the leader makes decisions first, and the remaining players (followers) react accordingly. The leader assumes rationality among the followers, anticipating their best possible responses after observing the leader's decision. Consequently, the leader can influence the situation such that the best response of the followers aligns with the leader's interests.

Solving Stackelberg games involves backward induction, where the followers' actions are computed as a function of the leader's decision. These actions, known as the best response, guide the leader in making subsequent decisions, resulting in a dynamic and strategic decision-making process. As outlined in Figure 6.2, the main panel (as the leader) makes final decisions, while individual sub-feeders focus on increasing customer satisfaction by incorporating more connected consumers. This can be scaled through a hierarchical scheduling mechanism that operates at different voltage levels with unique limits.

We introduce a profitability objective function to maximize each EVSE's operating rate while maintaining the main panel's strategy. Each sub-feeder aims to maximize its local operating rate under the ampacity limit x_n set by the main panel, with respect to the operating demand $y_m \in Y$ assigned to the m^{th} EVSE, and the individual (i_m) and average $(\bar{i})$ requested demands. The variable χ_m is defined as a binary indicator of EVSE type, where $\chi_m = 1$ for DC fast chargers and $\chi_m = 0$ for AC chargers. The coefficient α reflects the priority assigned to different charger types, allowing the model to favor higher-priority circuits (e.g., fast chargers) when allocating limited capacity.

$$\max_{y_m \in \mathcal{Y}} G(y_m) = \sum_{m=1}^{M} \left(-\frac{i_m}{\bar{i}} \left(\alpha\chi_m + (1 - \chi_m) \right) y_m^2 + \beta y_m \right) \tag{6.1}$$

subject to:

$$\sum_{m=1}^{M} y_m + \delta_n \leq x_n \tag{6.1a}$$

$$\sum_{m=1}^{M} \chi_m y_m \leq I_n^{dc} \tag{6.1b}$$

$$\sum_{m=1}^{M} (1 - \chi_m) y_m \leq I_n^{ac} \tag{6.1c}$$

$$I_m^{\min} \leq y_m \leq I_m^{\max} \tag{6.1d}$$

$$\sum_{m=1}^{M} z_m = q \tag{6.1e}$$

$$y_m \leq z_m I_m^{\max} \quad \text{for all } m \in M \tag{6.1f}$$

$$y_m \geq z_m I_m^{\min} \quad \text{for all } m \in M \tag{6.1g}$$

Here, the coefficient β is used to ensure non-zero charging allocations. In practice, β acts as a soft constraint on the allowed maximum capacity of the panels based on operational considerations of the applicable safety standards, where the larger values of β promote a more aggressive utilization. δ_n denotes the non-EV baseload at sub-feeder n, and $x_n \in X_n$ is the total ampacity available from the main panel. Constraints (6.1a) through (6.1c) ensure that the total sub-feeder load (both EVSE and non-EV demand) remains within capacity, and that DC and AC sub-feeders do not exceed their respective rated limits, I_n^{dc} and I_n^{ac}. The parameters $I_m^{\min}$ and $I_m^{\max}$ in (6.1d) define the minimum and maximum allowable current for each EVSE. The binary variable z_m represents whether a circuit is active, and q defines the number of simultaneously active chargers per scheduling round. Constraints (6.1e) to (6.1g) ensure that only selected EVSEs are assigned demand within their operational limits. The coefficient α provides a degree of fairness by allowing users with more urgent demands, such as those returning with low SoC or needing a quicker turnaround, to be favored in scheduling decisions through higher α values. In this work, α does not equate to giving unlimited preference to certain users, but rather integrates a configurable policy-based prioritization. In practice, α can also be extended to account for user-specific attributes (e.g., declared trip urgency) to enhance fairness while preserving system efficiency. The z_m in (6.1e)-(6.1g) is a binary variable that determines whether circuit m and its connected EVSEs are active. Therefore, $\forall m \in \{1, 2, \ldots, M\}$, the rule for selecting EVSEs in a d-RR manner can be defined by:

$$z_m = \begin{cases} 1 & \text{if } m = \mathcal{G}_g[\imath], \\ 0 & \text{otherwise,} \end{cases} \tag{6.2}$$

where $\mathcal{G}_g$ is the list of circuit indices assigned to group g, for all $g \in \{1, 2, \ldots, q\}$. The index of the activated circuit within group $\mathcal{G}_g$ in round R is computed by:

$$\imath = (R - 1) \bmod |\mathcal{G}_g| + 1,$$

where R is the round index starting from 1, and $|\mathcal{G}_g|$ represents the size of group g. The list $\mathcal{G}_g$ contains either $\lfloor M/q \rfloor$ or $\lceil M/q \rceil$ circuits, depending on how evenly M is divisible by q. This rule ensures that one circuit is activated per group per round, rotating cyclically within each group. As is outlined in Table 6.1, For $M = 8$ and $q = 3$, which implies three groups: $\mathcal{G}_1 = \{1, 2, 3\}$, $\mathcal{G}_2 = \{4, 5, 6\}$, and $\mathcal{G}_3 = \{7, 8\}$. In round $R = 1$, the first member from each group is activated; in round $R = 2$, the second members are selected; in round $R = 3$, it continues rotating circuits to 3, 6, and 7.

The details of the d-RR scheduler have been discussed earlier in Chapter 3; here, we proceed with the main sub-feeder objective function used in the EMS formulation.

The objective is to optimize a hierarchical process by minimizing the main panel's overall consumption while maximizing each sub-feeder's operating consumption. Thus, the main panel's utility function can be simply defined as:

$$\min_{x_n \in X_n} U = r \sum_{n=1}^{N} p_n x_n \tag{6.3}$$

subject to:

$$\sum_{n=1}^{N} x_n \leq \mathcal{I}^{\max} \tag{6.3a}$$

$$i_n \leq x_n \leq \mathcal{I}^{\max} \tag{6.3b}$$

$x_n \in X_n$ represents the calculated optimal demand for sub-feeder n, p_n is the nominal rating of sub-feeder n, $\mathcal{I}^{\max}$ denotes the maximum capacity of the main panel, r is a positive coefficient ensuring that the main panel capacity is

Table 6.1: Circuit activation sequence in d-RR manner for $M = 8$ and $q = 3$

Round R	**Actived index** ($\imath$)	**Circuit index** m $\mathcal{G}_1$	$\mathcal{G}_2$	$\mathcal{G}_3$
1	1	1	4	7
2	2	2	5	8
3	3	3	6	7
4	1	1	4	8

restricted by the upstream utility sub-feeder, and i_n is the required amperage for sub-feeder n. The summation of optimal currents x_n for all sub-feeders should be less than or equal to $\mathcal{I}^{\max}$ (6.3a). Additionally, x_n must be greater than or equal to the required amperage i_n and less than or equal to $\mathcal{I}^{\max}$ (6.3b) to ensure the system operates within its capacity limits.

Algorithm 2 outlines the proposed Stackelberg game model, which initiates when there is a detected change in demand, either from the metered amperage of non-EV loads or an EVSE request to start a charging session. The game is an iterative process, where the values of i_m and $\bar{i}$ may be updated in each iteration. During each iteration, the sub-feeders set the operating limits of each EVSE and assess the new demand from the EVSEs. The sub-feeder calculates the current desired amperage i_m demanded by a set of EVSEs and submits it to the main panel without any constraints, ensuring maximum satisfaction for the EV owners regardless of the main panel's limitations. These updated demands are then sent to the main panel and compared against the setpoint calculated in the previous iteration. The process continues until the aggregated new demand from all sub-feeders matches the setpoint from the last iteration, and players have no incentive to change their strategy. Next, we prove the feasibility of the Stackelberg game through the governing utility functions (6.1) and (6.3), and show the existence and uniqueness of a global Nash equilibrium that optimizes energy usage across all EVSEs.

6.2 Proof of Game and Equilibrium

A Stackelberg game is a sequential game system in which one player (as a leader) has the power to choose the first move, and all other players (as followers) move after [104]. This process repeats till there is no temp for players to change their strategies. This set of strategies is called the Stackelberg equilibrium (SE). The proposed Stackelberg game is used to model the

Algorithm 2 Managing EVSE energy using a Stackelberg game

```
1: if A new session or demand is registered then
2:     Forward EVSE demand to the corresponding sub-feeder
3:     Sub-feeder queries local non-EV loads and updates available capacity
4:     Sub-feeder aggregates demands and sends the total to the main panel
5:     while Sub-feeder allocation ≠ received setpoint do
6:         Main panel minimize (6.3) to find sub-feeders optimal setpoint
7:         Main panel broadcasts optimal setpoints to sub-feeders
8:         Each sub-feeder maximizes (6.1) and sets EVSEs' setpoints
9:         Sub-feeder updates its demand and iterates to Step 5
10:    end while
11:    Sub-feeder sends the final profile to each EVSE
12:    EVSE acknowledges and starts charging session
13: else
14:    Monitor for new charge session and non-EV demand
15: end if
```

interaction between a finite n-player game, defined by:

$$\Gamma = (\mathcal{H}, \{S^h\}_{h\in\mathcal{H}}, \{\mathcal{U}^h\}_{h\in\mathcal{H}}) \tag{6.4}$$

where $\mathcal{H}$ is a finite set of players and $|\mathcal{H}|$ is the number of players. We have N sub-feeders and one main panel where $|\mathcal{H}| = N + 1$. The S^h is the space of pure strategies, and $\mathcal{U}^h$ is the utility function of player $h \in \mathcal{H}$. Γ is a finite game with a finite number of pure strategies for players. Therefore, for each sub-feeder $n \in N$, we have strategy space $y^n_m \in S^n = \{s^n_1, s^n_2, \ldots, s^n_M\}$. We also have strategy space for the main panel as $x_n \in S^1 = \{s^1_1, s^1_2, \ldots, s^1_N\}$.

In our proposed Stackelberg game model, when the main panel selects $S^1 = \{s^1_1, s^1_2, \ldots, s^1_N\}$ strategies for sub-feeders as the first move, then the sub-feeder chooses the best strategy ${s^*}^n_m, \quad \forall n \in \mathcal{N}$ for the connected EVSE m using;

$$s^{*n}_m = \arg \max_{s^n_m \in S^n} G(s^1_n, s^n_m), \quad \forall m \in \mathcal{M},\ \forall n \in \mathcal{N} \tag{6.5}$$

Then, the main panel updates its strategy ${s^*}^1_n$ using;

$$s_n^{*1} = \arg\max_{s_n^1 \in S^1} U(s_n^1, s_m^{*n}), \quad \forall n \in \mathcal{N} \tag{6.6}$$

These steps repeat till there is no incentive for players to change their strategies. Finally, the best responses of the main panel and sub-feeders, S^{1*} and S^{n*}, would be the equilibrium results [105, 106].

The existence of a Stackelberg equilibrium (SE) has been proven in several works [107, 108, 109]. Following these studies, we divide the game model into sub-games (one at the main panel level and one at the sub-feeders level). Then, based on Kakutani's fixed-point theory [110], the Nash equilibrium (NE) can be proven for each subgame. To prove the existence of NE, the terms of the Kakutani theorem must be satisfied. The set of strategies S^h is a compact and convex set in Euclidean space, $\mathcal{U}^h(s^h)$ is non-empty for all $s^h \in S^h$, and for all $s^h \in S^h$, $\mathcal{U}^h(s^h)$ is a continuous and convex set. We analyze a Stackelberg game where the followers (sub-feeders) choose actions $y_m \in Y$, and the leader (main panel) subsequently chooses a strategy $x_n \in X_n(y_m)$, aiming to optimize its utility given the equilibrium response of the followers.

Theorem 6.2.1. *There exists a Stackelberg equilibrium in the proposed hierarchical game between the sub-feeders (followers) and the main panel (leader), with respect to their optimal solutions of* (6.1) *and* (6.3)*.*

Proof. The Stackelberg equilibrium (SE) is a strategy pair (y^*, x^*) such that $y^* \in Y$ solves the followers' equilibrium problem, and $x^* \in X(y^*)$ minimizes the leader's cost function given that follower behavior.

We begin by establishing the existence and continuity of follower best responses. Each follower solves the problem defined in equation (6.1), where $Y \subset \mathbb{R}$ is compact and convex. The first derivative of the utility function is

$$\frac{\partial G}{\partial y_m} = -2M \frac{i_m}{\bar{i}} \left(\alpha \chi_m + 1 - \chi_m\right) y_m + \beta, \tag{6.7}$$

and the second derivative is

$$\frac{\partial^2 G}{\partial y_m^2} = -2M\frac{i_m}{\bar{i}}\left(\alpha\chi_m + 1 - \chi_m\right) < 0, \quad \text{for } 1 \leq \alpha \leq 1.5, \tag{6.8}$$

Which shows that the utility function G is continuous and strictly concave on y_m. Since G is strictly concave and continuous over a compact set, a unique optimal solution $y_m^* \in Y$ exists for each follower. Furthermore, because the utility is differentiable and the second-order condition is satisfied, the followers' best-response mapping is continuously differentiable in any parameters on which it depends.

Next, we analyze the leader's problem. After observing y_m^*, the leader chooses $x_n \in X_n(y_m^*)$ to minimize the cost function defined in equation (6.3):

$$\min_{x_n \in X_n(y_m^*)} U(x_n; y_m^*).$$

The leader's cost function U is assumed to be continuous and convex in x_n. Explicitly, its first and second derivatives are

$$\frac{\partial U}{\partial x_n} = Nrp_n > 0, \quad \text{for } r > 0, \tag{6.9}$$

and

$$\frac{\partial^2 U}{\partial x_n^2} = 0, \tag{6.10}$$

which shows that U is linear in x_n. Since the feasible set $X_n(y_m^*)$ is compact and convex, and U is continuous and linear, an optimal solution $x_n^*(y_m^*) \in X_n(y_m^*)$ exists. The upper hemicontinuity of the followers' best-response mapping follows from the strict concavity and continuous differentiability of their utility function G. Given that the leader's cost function U is continuous and defined over a compact, convex feasible set, Kakutani's fixed-point theorem [110] ensures the existence of a fixed point, and thus a SE $(y_m^*, x_n^*(y_m^*))$ exists. □

6.3 Case Study

To evaluate the efficacy of the proposed model, we analyzed an MURB with the configuration outlined in Table 6.2. Sub-feeder 1, which powers a combination of AC and DC chargers (EVSEs), Sub-feeder 2, designated for other non-EV loads, and Sub-feeder 3, supplying power to a mix of EVSEs and non-EV loads. The integrated EVSEs in Sub-feeder 1 necessitate management by an EMS to ensure compliance with electrical regulations and safety requirements. Sub-feeder 1 further divides its supply into two sets of EVSE sites. One set includes two DC fast chargers with a maximum rating of 150A at 480V, while the other set comprises seven Level II EVSEs with a rating of 80A at 208V. The load on sub-feeder 2 fluctuates between 200A and 600A at 600V over time. In sub-feeder 3, there is one DC fast charger with a rating of 100A each and eight Level II chargers with a rating of 80A each. Additionally, there is a variable non-EV load supplying common site loads, ranging between 80A and 200A at 600V.To account for actual peak and off-peak periods, we used the Ontario Time-of-Use (ToU) time slots [111] to enhance the realism of our model. For this analysis, we assigned priority coefficients α between 1 and 1.5 and $\beta < \alpha$ in (6.1). The coefficient χ_i is set to 1 for the fast DC charger and 0 for the AC Level II chargers.

Table 6.2: Case study configuration and assumptions for the Stackelberg-based EMS model.

Item	Assumption
Main Panel Rating	1250A (1000A after safety margin deduction)
EVSEs of Sub-feeder 1	2 DC fast chargers (150A, 480V) and 7 Level II chargers (80A, 208V)
EVSEs of Sub-feeder 3	1 DC fast charger (100A) and 8 Level II chargers (80A, 208V)
Non-EV Loads on Sub-feeder 2	200–600A
Non-EV Loads on Sub-feeder 3	80–200A
Priority Coefficient (α)	1–1.5
Pricing Model	Ontario Time-of-Use (ToU)
Static Safety Margin	20% of the nominal panel rating

Figure 6.3 illustrates the real-time charging profile of sub-feeder 1 over 24 hours, from 5 PM to 5 PM the following day. In this scenario, sub-feeder 1 adapts to the main panel strategy while ensuring that the breakers connected to the DC fast chargers and AC Level II chargers operate at their maximum setpoints. As DC demand increases, the demand from AC Level II chargers decreases to balance the total load, giving priority to the DC charger. Conversely, when the DC charger has no load (i.e., zero) or less load, the AC Level II chargers operate at maximum capacity. Figure 6.4 presents a more challenging scenario with the presence of non-EV loads on sub-feeder 3, where demand dynamically fluctuates over 24 hours. The default priority is assigned to non-controllable non-EV loads, followed by the two fast DC chargers, which are prioritized to ensure rapid EV fleet charging. To provide a comprehensive view of the system, Figure 6.5 displays the cumulative load profile of all three sub-feeders over a 24-hour real-time interval. Note that the main panel's actual capacity is 1000A (1250×0.8), and all loads have been normalized for the main sub-feeder voltage (600 V). This demonstrates the effectiveness of the proposed method in fully utilizing the panel capacity of the existing electrical infrastructure without curtailing high-priority loads. As depicted in Figures 6.3 to 6.5, during mid-peak and peak times (7 AM to 5 PM), the load on sub-feeder 2 (non-EV load) increases, leading sub-feeders 1 and 3 to manage their demand by reducing their total load. Consequently, during peak times, most of the capacity is allocated to non-EV loads on sub-feeders 2 and 3 (green lines), followed by the DC fast chargers (red lines), with the Level II chargers (blue lines) receiving the least capacity. In contrast, during off-peak times, the load for non-EV and Level II chargers is nearly equal. To demonstrate the efficacy of our game model, the computation time for calculating the optimal setpoints using the proposed multi-level Stackelberg game is presented in Figure 6.6b. Increasing the number of EVSEs results in a logarithmic increase in processing time, indicating that the algorithm is both fast and efficient.

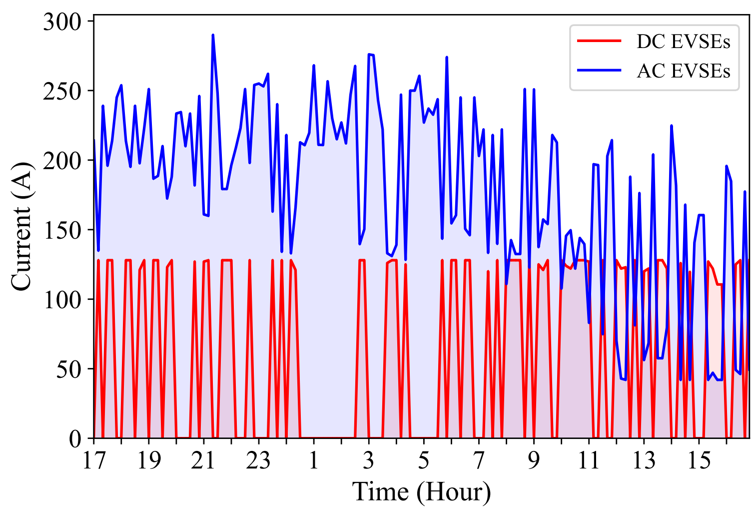

Figure 6.3: The optimal current assigned to different loads of the sub-feeder 1.

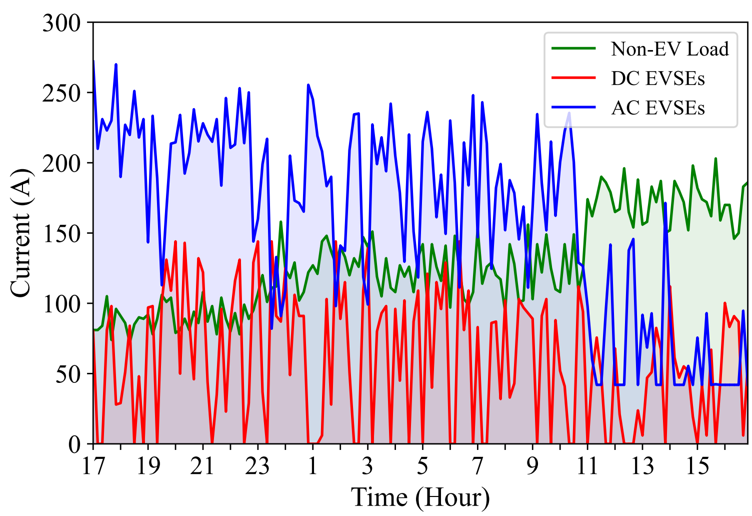

Figure 6.4: The optimal current assigned to different loads in the sub-feeder 3.

Figure 6.6a shows the sensitivity of the utility function (6.1) to the parameters β, x_n, and M. The strong impact of β reflects its direct role in the linear

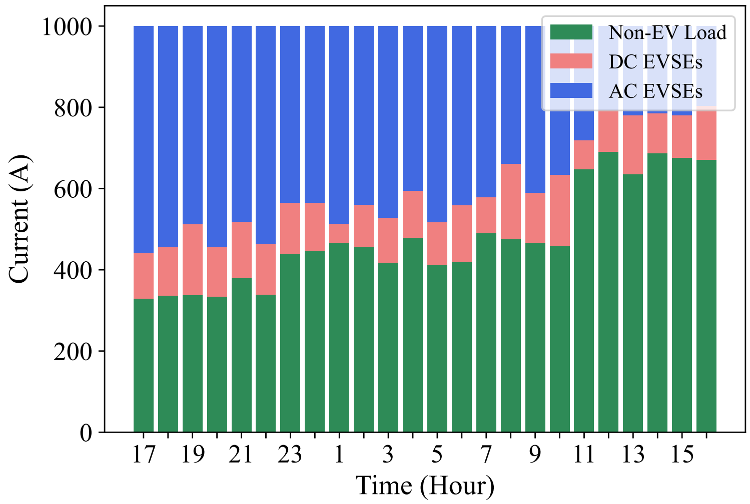

Figure 6.5: The cumulative load profile of all three sub-feeders throughout a day, real-time interval.

benefit of the first term in constraint (6.1a), which dominates when larger y_m values are permitted. The sensitivity to x_n indicates how the resource bound in constraint (6.1a) alters the optimal total dispatch. The number of devices M scales both the objective and the constraints, effectively changing the problem dimensionality. The α that modulates the penalty in (6.1), and q, which governs the activation constraints (6.1e)–(6.1g), show low influence under the operating conditions. Thus, system performance is mainly shaped by reward-driven allocation subject to resource and scaling constraints.

To demonstrate the effectiveness of the proposed d-RR scheduling coupled with Stackelberg-based EMS, and to enable a comparison against scheduling without EMS, the same MURB configuration, EV behavior assumptions, and parameter settings used in the d-RR case study (Chapter 3) are adopted here. The initial and final SoC calculations follow the same formulations and equations presented in Chapter 3. Likewise, the customer satisfaction metric and overall satisfaction score are defined according to Eqs. (3.3)–(3.4). The main distinction in this case study is that, since EMS exists, the charging

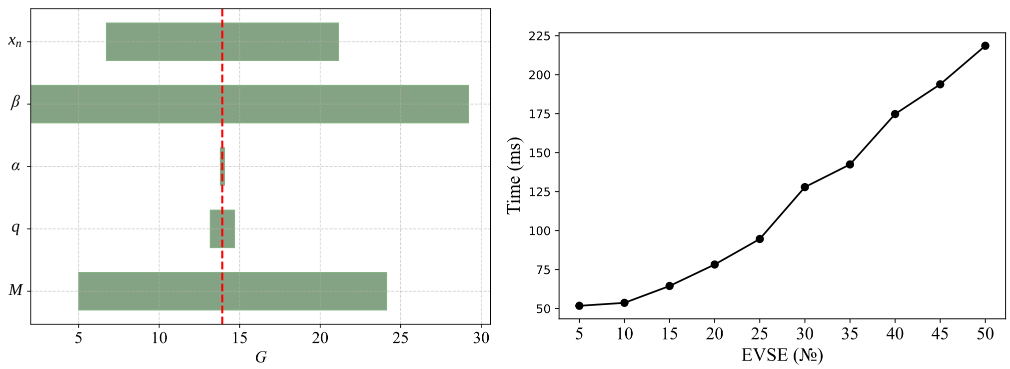

(a) (b)

Figure 6.6: (a) Tornado diagram showing sensitivity of the sub-feeder utility function to system parameters; (b) computation time for optimal set-point calculation using the proposed multi-level Stackelberg game.

power E_c assigned to each active EVSE is dynamically and randomly selected within the range of 1.5 kW to 10 kW to reflect the EMS's ability to reallocate unused power from non-EV loads.

Figures 6.7 to 6.9 show the yearly satisfaction score ($\mathcal{S}^{+}$) with a minimum satisfaction threshold of $\mathcal{S}^{\text{min}} = 30\%$ and a satisfaction threshold $\mathcal{S}^{\text{thr}} = 30\%$, with 56 EVSEs ($E$) over 365 days ($T$) for the Regular, FCFS, and d-RR scenarios, respectively. By comparing this figure with the results obtained in the d-RR case study (Figures 3.3 to 3.5 in Chapter 3), it can be observed that integrating the scheduler with the EMS significantly enhances overall customer satisfaction. When the EMS exists, it dynamically reallocates the unused feeder capacity, which is left over by non-EV loads, to the EVSEs, particularly during off-peak hours. This allows the active chargers to operate with a higher charging profile and improved utilization of available capacity. In contrast, when scheduling operates without EMS support, the system must assume that non-EV loads may be active across all circuits. As a result, a conservative power allocation is enforced to prevent overloading, which limits the maximum available charging power and leads to a noticeable reduction in the yearly satisfaction score.

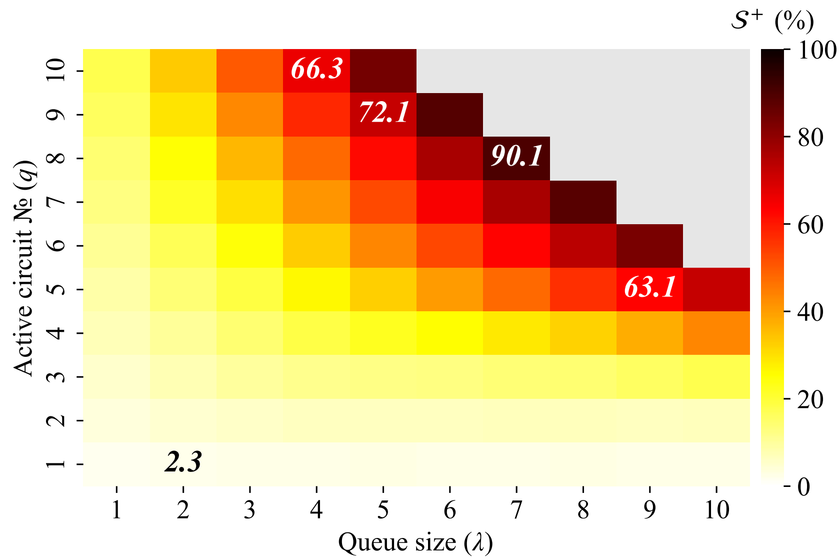

Figure 6.7: Customer satisfaction S^+ as a function of the number of installed EVSEs and queued EVSEs for the regular case.

Figure 6.7 illustrates a heatmap that captures the overall customer satisfaction score ($\mathcal{S}^+$) in the Regular scenario, where no centralized scheduling algorithm is used, and EVs are charged based on availability. This method is all about a first-available, non-prioritized service model, which can lead to less-than-ideal resource use, especially when demand is high. The figure reveals that the peak satisfaction score of 90.1% is achieved when there are 8 active EVSEs and a queue size of 7. This queue is not a physical queue; rather, it reflects the average number of daily charging requests happening throughout the year. In this setup, the number of EVs competing for service is modest relative to the available infrastructure, allowing most vehicles to achieve a final SoC above the minimum satisfaction threshold. However, if the number of active EVSEs drops or the queue size increases, the system's ability to meet customer charging needs takes a significant hit. For instance, when we cut the active EVSEs down to 5 and with the best queue $\lambda = 9$, the satisfaction score drops to 63.1%. Thus, without a scheduling system in place, resources can't be allocated dynamically based on demand, resulting in a higher frequency of charging sessions that fall short of the required SoC threshold.

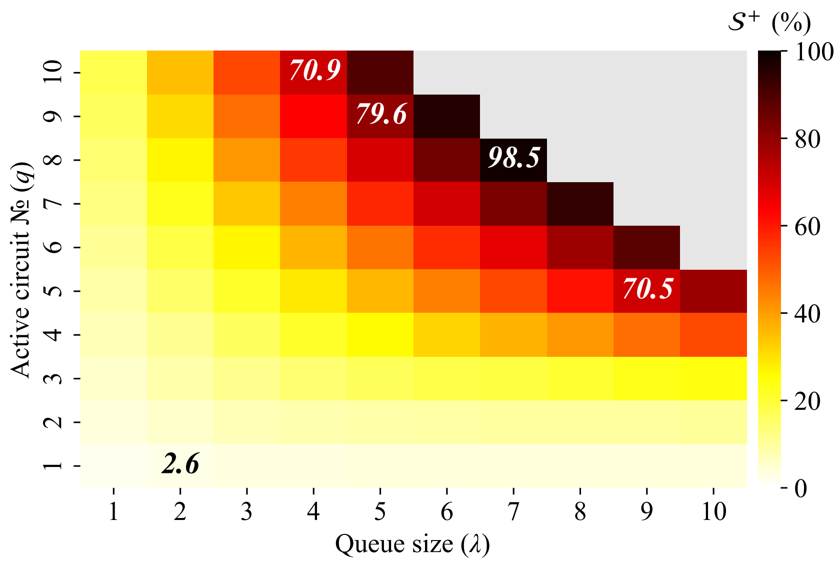

Figure 6.8: Customer satisfaction S^+ as a function of the number of installed EVSEs and queued EVSEs for the FCFS scheduling

Figure 6.8 shows the satisfaction for the FCFS scheduling case, which is a common central scheduling approach for managing EV fleets. This scenario requires a central system to manage charge requests and loitering, which might necessitate a more complex integration with the local real-time EMS. Assuming the existence of such integration and coordination, FCFS shows a significantly better satisfaction score compared to the Regular case. With 8 active EVSEs and an EV queue size of 7, an average satisfaction score of around 98.5% can be achieved. In this setting, the number of concurrent charging requests is slightly below the available infrastructure, allowing the FCFS scheduler to allocate chargers to vehicles with minimal delay. As EVs are served in arrival order and the demand stays within system limits, waiting times remain short, and most vehicles can achieve their target SoC before departure, and therefore resulting in high satisfaction. For all other cases, enabling such scheduling enables the efficient use of available time and power resources, making it feasible to install and dedicate up to twice as many EVSEs to individual users compared to the Regular case. Figure 6.9 presents the results for the d-RR scheduling strategy, which distributes charging time fairly across EVs. It manages to achieve a slightly higher satisfaction score of 99.0% under the same conditions (with 8 EVSEs and a queue size of 7) and demonstrates better resilience during periods of light demand. In both d-RR and FCFS setups, a total of 56 EVSEs are installed and ready to plug upon arrival, while only 8 are enabled at a time. Taking the availability of a charger upon arrival and sufficient SoC for the next day as a measure of convenience and satisfaction, this indicates the value of coordinated scheduling in maximizing perceived service quality with limited infrastructure.

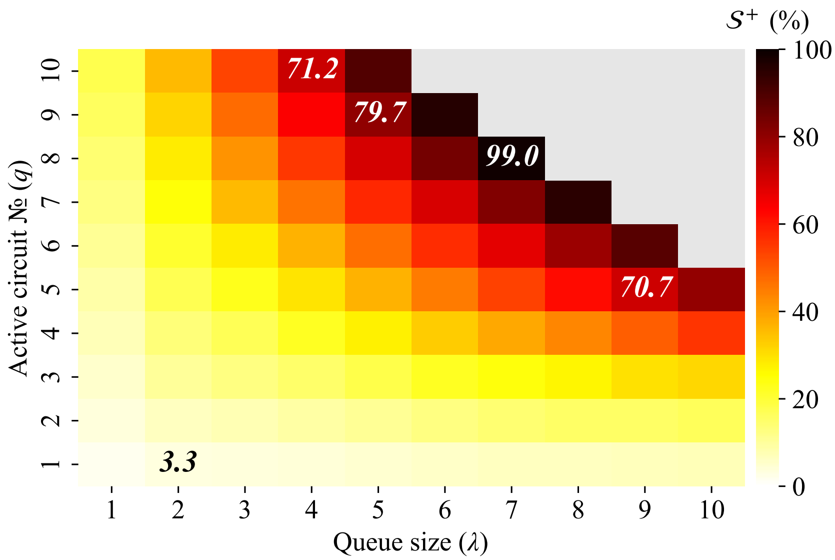

Figure 6.9: Customer satisfaction S^+ as a function of the number of installed EVSEs and queued EVSEs under the d-RR scheduling.

Although the FCFS and d-RR approaches achieve similar satisfaction

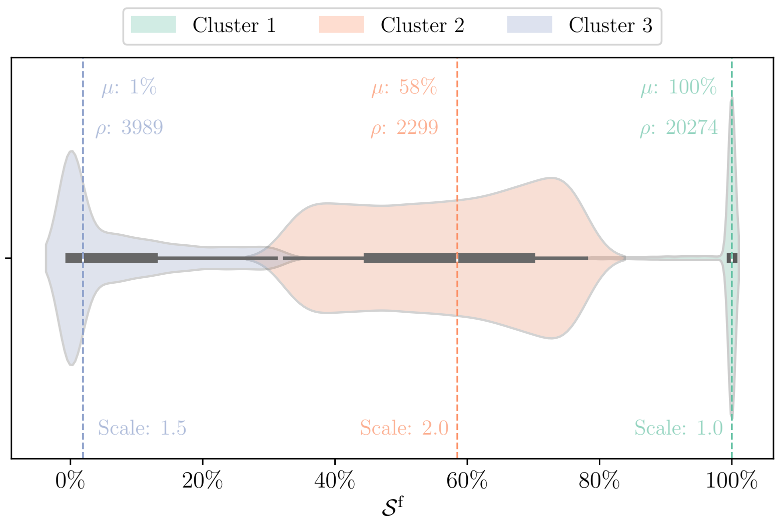

(a)

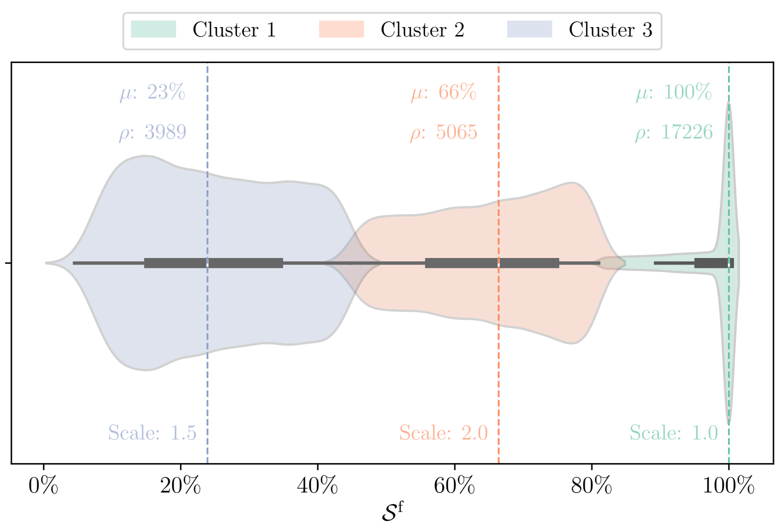

(b)

Figure 6.10: Distribution of daily received charge $\mathcal{S}^{\mathrm{f}}$ for (a) FCFS and (b) d-RR scheduling methods with a queue size $\lambda = 8$, shown using three K-means clusters with their corresponding medians and population sizes.

scores as defined in (3.4), it should be noted that in FCFS scheduling, an EV requiring a long charge duration while in the queue can cause other EVs to wait for an extended time or depart without receiving a charge, leading to customer dissatisfaction. In extreme cases, this can result in customers not receiving any charges for several consecutive days. Conversely, the d-RR algorithm ensures that all EVs in the queue receive a fair amount of charge, effectively preventing the starvation phenomenon.

Therefore, the satisfaction score defined in (3.4) may mask the number of cases where the SoC is less than $\mathcal{S}^{\min}$ and obscure the distribution of the points. To address this, we next analyze the distribution of customer satisfaction as defined in (3.3), considering the daily received charge $\mathcal{S}^{\mathrm{f}}$ and no penalty ($\kappa = 0 \therefore \mathcal{S} = \mathcal{S}^{\mathrm{f}}$). We employed a K-means clustering method with three distinct clusters. Figure 6.10 presents the violin plots of the clustering of $\mathcal{S}^{\mathrm{f}}$ for both the FCFS scheduling and d-RR methods for the EV size in the same MURB with a queue size (λ) of 8. The clusters shown in the figure are scaled up for better representation, and the median of each cluster is indicated by a dashed line. The cluster median (μ) and population (ρ) are displayed for each corresponding cluster.

As shown in Figure 6.10a, for FCFS scheduling, a large data density of 3989 points is clustered around a median of 1%, indicating a relatively high likelihood of receiving zero charge. This suggests that on certain days, a significant number of EV owners were unable to receive any charge. Unlike the FCFS method, Figure 6.10b shows that the median for the first cluster in the d-RR approach is around 23%, indicating that this scheduling provides a more equitable resource allocation. Additionally, the median for the other clusters is relatively higher in the d-RR method compared to FCFS scheduling, suggesting that the d-RR method more effectively distributes charging opportunities, resulting in a higher overall $\mathcal{S}^{\mathrm{f}}$ for EVs.

Furthermore, we compared the number of incurred penalty events, as defined in (3.3), over a full year for the Regular, FCFS, and d-RR schedul-

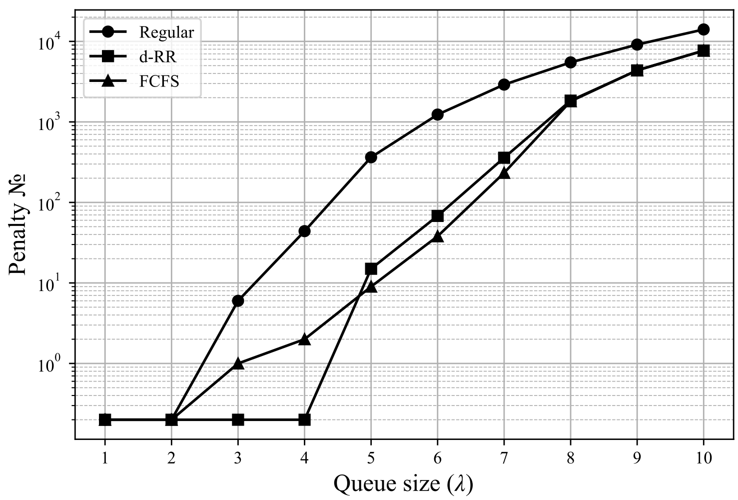

Figure 6.11: Number of penalties incurred by Regular, FCFS, and d-RR methods over a year for different queue sizes.

Table 6.3: Skewness and Kurtosis values for data points with $\mathcal{S}^{\mathrm{f}}$ values ranging from 0 to 30% (1st) and from 30% to 100% (3rd cluster)

	$0\% < \mathcal{S}^{\mathrm{f}} \leq 30\%$				$30\% < \mathcal{S}^{\mathrm{f}} \leq 100\%$			
	Skewness		Kurtosis		Skewness		Kurtosis	
Queue Size (λ)	FCFS	d-RR	FCFS	d-RR	FCFS	d-RR	FCFS	d-RR
6	0.02	-0.48	-1.23	-0.62	-4.32	-3.89	19.312	15.61
8	1.16	-0.07	0.15	-1.08	-3.28	-1.51	10.28	1.06
9	1.76	0.43	2.12	-0.93	-3.23	-1.1	10.14	-0.13

ing methods across various queue sizes. Figure 6.11 shows that the d-RR method is more risk-averse in deploying additional EVSEs in MURBs with limited electricity services. In particular, placing 4 EVSEs per queue is an effective configuration under the d-RR method, as it results in no penalty events. This outcome is primarily due to the method's efficient utilization of available charging time and its fair allocation of charging opportunities among EVs. The Regular method, however, exhibits a steep increase in penalties as queue sizes grow, demonstrating its inefficiency in managing charging demands compared to the other two approaches. Although increasing the number of EVSEs in a queue leads to higher penalty rates in all cases, the d-RR scheduling method shows a clear advantage over the Regular case, with a relatively lower number of penalties for larger queue sizes. For queue sizes exceeding 4, the number of penalties for the FCFS and d-RR methods converges, demonstrating similar performance.

To further analyze the distribution of data points for these two methods, we calculated Skewness and Kurtosis for various values of $\mathcal{S}^{\mathrm{f}}$, focusing on data points with SoC values ranging from 0 to 30% (1^{st} cluster) and from 70% to 100% (3^{rd} cluster). Table 6.3 presents the Skewness and Kurtosis values for these two clusters. For the first cluster, the FCFS method consistently exhibits higher positive Skewness values compared to the d-RR method, indicating a greater concentration of the population toward lower SoC values, closer to 0% SoC. Moreover, FCFS shows increasing positive kurtosis as the group size λ increases, reflecting the emergence of a higher number of extreme outliers with very low SoC values. On the other hand, the d-RR method consistently shows negative Kurtosis values, suggesting a flatter and more uniform distribution with fewer such extreme cases.

In the third cluster, the analysis shows that as the group size λ increases, there is a decreasing concentration of data points around higher SoC values and a reduction in extreme values. However, kurtosis values for FCFS remain significantly high across all queue sizes, revealing a sharp concentration of SoC values near 100%. By comparing the first and third clusters, we can realize that FCFS produces a polarized outcome, meaning that some EVs are left near 0% SoC while others are charged close to 100%, reflecting the system's starvation behaviour. In contrast, d-RR avoids extreme SoC values on both ends of the spectrum and promotes a fairer allocation of charge across all EVs. These statistical results demonstrate that d-RR is more effective in maintaining fairness and mitigating long-term inequalities in EV charging under limited capacity constraints. It is worth mentioning that when the queue size is set to nine, then the d-RR method exhibits negative Kurtosis in the third cluster, combined with positive Skewness in the 1^{st} cluster. This suggests that data points are no longer concentrated around high SoC values but are instead leaning towards lower SoC values. Therefore, the d-RR algorithm becomes less effective at this queue size, with the maximum $\mathcal{L}_{\mathcal{A}}$ for optimal performance being eight.

6.4 Conclusion

In this chapter, we introduced a real-time EMS for EVSE energy curtailment in MURBs based on a multi-level Stackelberg game, which captures well the hierarchical structure of electrical systems in multi-unit buildings. In this framework, the main panel acts as the leader, while the sub-feeders serve as followers. Each sub-feeder seeks to maximize its local operating rate within the ampacity constraints imposed by the main panel. The objective of the proposed model is to optimize this hierarchical interaction by minimizing total energy consumption at the main panel while maximizing utilization across sub-feeders. Furthermore, the existence of a Stackelberg equilibrium was proven using Kakutani's fixed-point theorem, guaranteeing the feasibility and stability of the proposed scheme.

A case study on a representative MURB demonstrated that the proposed EMS effectively manages sub-feeder demand and enables coordinated energy allocation among EVSEs. The system implements a prioritization mechanism that gives precedence to non-EV loads, followed by DC fast chargers and then Level II AC chargers. The computational efficiency analysis indicated that increasing the number of EVSEs results in a logarithmic growth in processing time, confirming that the proposed EMS operates efficiently in real time. Furthermore, the integration of the dynamic Round Robin (d-RR) scheduler was demonstrated within the case study, illustrating its effectiveness in managing on-demand EV charging requests. The results showed that coupling the d-RR mechanism with the Stackelberg-based EMS can increase

EVSE installation penetration by up to fourfold.

Chapter 7

Discussion and Conclusion

7.1 Concluding Remarks

Convenient access to a charging station is a decisive factor for EV adoption in the ongoing electrification transition. Since MURBs comprise a large share of urban housing, providing affordable and reliable EV charging within these buildings is essential. However, MURBs were mostly built decades ago in Canada without considering the additional electrical demand of EVs, and upgrading their infrastructure is often costly. A practical and scalable alternative is deploying EMS, which allows EVSEs to operate within existing building capacity (ampacity) by intelligently adjusting charging power based on real-time non-EV load conditions.

This thesis developed a suite of real-time cloud-based EMS for integrating EVSEs in MURBs, addressing both power allocation and time scheduling under real-world electrical and behavioral constraints. Adopting a cloud software approach avoids certification burdens required for systems that directly control electrical hardware, while remaining interoperable with certified devices and metering over secure protocols; this makes large-scale residential deployment far more feasible in practice.

We first introduced a d-RR algorithm as a lightweight scheduler to handle real-time charging coordination among multiple EVSEs in MURBs. The d-RR algorithm dynamically adjusts its time quantum based on the number of active EVSEs, ensuring fair access to limited feeder capacity while maintaining responsiveness to new charging requests. Compared to conventional scheduling methods such as FCFS, the d-RR approach effectively mitigates long waiting times and prevents charging monopolization by individual users. Simulation results showed that the d-RR scheduler enhances energy utilization, improves fairness in energy allocation, and enables higher EVSE penetration within existing electrical constraints.

Secondly, a Mixed-Integer Linear Programming (MILP)-based EMS was proposed to coordinate EVSE power allocation in MURBs with Mixed and Dedicated topology of sub-feeders. MILP is particularly well-suited for modeling the elastic behavior of EVSEs and the binary decisions associated with their phase connections in a three-phase network. The proposed EMS optimizes charging current distribution while respecting feeder ampacity and maintaining phase balance. By integrating short-term forecasts of non-EV building loads through an NARX model, it proactively adjusts charging levels to avoid overloads and improve phase utilization. Simulation results using real MURB data confirmed that this method maintains safe operation under variable load conditions, achieves high SoC levels for connected EVs, and operates within millisecond-level computation times, demonstrating its suitability for real-time applications.

In Chapter 5, an EMS based on DRO was developed for scenarios where EVSEs are distributed across multiple feeders within the MURB electrical system. Unlike the deterministic MILP model, the DRO framework explicitly accounts for uncertainties such as non-EV load consumption and EV availability variations across feeders. The proposed formulation constructs a Wasserstein ambiguity set, enabling the EMS to make decisions that remain feasible across a range of plausible probability distributions. Simulation results demonstrated that this EMS maintains feeder ampacity limits and achieves higher capacity utilization compared to purely robust methods, without relying on the assumption of a known true distribution as in stochastic optimization approaches.

Finally, a decentralized EMS based on a Stackelberg game model was proposed to coordinate energy allocation in multi-tier MURB electrical systems. The Stackelberg formulation captures the leader–follower interaction between the main panel and sub-feeders, where the main panel acts as the leader that allocates capacity limits, and each sub-feeder operates as a follower optimizing its local EVSE utilization within those limits. This hierarchical structure reflects the physical and operational characteristics of real MURB distribution systems. The existence of a Stackelberg equilibrium was proven using Kakutani's fixed-point theorem, ensuring the feasibility of the proposed model. Simulation results demonstrated that the Stackelberg-based EMS effectively manages sub-feeder demand and maintains computational efficiency suitable for real-time operation. Moreover, the integration of the d-RR scheduler within this framework showed that it can further increase EVSE penetration and lead to higher user satisfaction.

7.2 Future Work

Electrification in the residential sector comprises upgrading thermal and transportation loads. This thesis has focused on developing EMSs that enable the integration of EVSE into existing MURB infrastructures to facilitate an affordable path toward residential electrification. Thermal loads, particularly heat pumps, represent another significant source of electrical demand in MURBs. Owing to their operational flexibility, heat pumps could be integrated into the EMS formulation to proactively curtail or restore their consumption in coordination with EV charging while adhering to feeder capacity constraints. Achieving this integration would require modeling the dynamic behavior of heat pumps under uncertainties in temperature variations and comfort preferences, which could serve as a direction for future work.

In this work, the NARX forecasting model for non-EV load prediction was trained offline using historical consumption data and then deployed for real-time EMS operation. While offline training offers low computational overhead during deployment, it presents inherent limitations. Since the model parameters remain fixed after training, the forecasting model cannot adapt to evolving building consumption patterns, occupancy changes, or long-term electrification trends. Future research may investigate adaptive NARX architectures with recursive parameter estimation or online backpropagation to update model weights continuously. Such extensions would enable the EMS to mitigate concept drift and maintain predictive reliability under dynamic operating conditions.

The cloud-based EMS framework used in this work relies on stable internet communication. In practice, underground or enclosed parking areas often experience poor connectivity, which can introduce delays or temporary communication losses. Such disruptions may prevent real-time commands from reaching the EVSEs on time, which is in conflict with the fast response requirements of a real-time EMS and may reduce the effectiveness of overload prevention. Future implementations may therefore benefit from redundancy mechanisms or enhanced communication reliability to ensure consistent EMS performance in challenging deployment environments.

The Wasserstein radius, utilized in DRO formulation, is tuned based on empirical forecasting errors and remains fixed during operation. Although this approach provides robustness, it does not capture variations in uncertainty that naturally occur over time due to changing load patterns or fluctuations in EV availability. A potential improvement is to determine the radius through data-driven techniques that adapt to new observations. This would allow the ambiguity set to adjust to real-time fluctuations in non-EV load and EVSE availability, and enable the EMS to allocate charging currents more accurately under stable conditions and increase conservativeness only when uncertainty grows.

The Stackelberg EMS developed in this thesis assumes that both the main panel and the sub-feeders have perfect knowledge of system conditions, including non-EV loads and EVSE availability. However, in reality, these quantities are uncertain and may only be partially known to each agent. In other words, the main panel may not have full visibility into the real-time load of each sub-feeder, and sub-feeders cannot perfectly predict future EV arrivals or user behavior. A useful direction for future work is to relax this perfect-information assumption and explore probabilistic game models that allow agents to make decisions when information is uncertain, offering a more realistic representation of how multi-tier electrical systems operate in practice.

Bibliography

[1] Government of Canada, "Net-zero emissions by 2050," https://www.canada.ca/en/services/environment/weather/climatechange/climate-plan/net-zero-emissions-2050.html, 2024, accessed: Oct. 21, 2025.

[2] S.-L. Penttinen, K. Kallioharju, J. Sorri, J. Heljo, and P. Harsia, "Electrification and energy efficiency in buildings: Policy implications and interactions," in *Electrification*. Elsevier, 2021, pp. 175–196.

[3] K. Ajeigbe and W. Holt, "Government policies and incentives for ev manufacturing," 2025.

[4] A. Bui, P. Slowik, and N. Lutsey, "Power play: Evaluating the u.s. position in the global electric vehicle transition," 06 2021.

[5] International Energy Agency, "Global ev outlook 2024: Catching up with climate ambitions," 2024, accessed: October 2025. [Online]. Available: https://www.iea.org/reports/global-ev-outlook-2024/outlook-for-electric-mobility

[6] Canada Energy Regulator, "Market snapshot: Zero-emission vehicles now account for over 10% of all new vehicles in canada," https://www.cer-rec.gc.ca/en/data-analysis/energy-markets/market-snapshots/2024/market-snapshot-zero-emission-vehicles-now-account-for-over-10-percent-of-all-new-vehicles-in-canada.html, 2024, accessed: 2025-09-21.

[7] H. S. Das, M. M. Rahman, S. Li, and C. W. Tan, "Electric vehicles standards, charging infrastructure, and impact on grid integration: A technological review," *Renewable and Sustainable Energy Reviews*, vol. 120, p. 109618, 2020.

[8] A. Khandakar, A. Rizqullah, A. Ashraf Abdou Berbar, M. Rafi Ahmed, A. Iqbal, M. E. Chowdhury, and S. A. Uz Zaman, "A case study to identify the hindrances to widespread adoption of electric vehicles in qatar," *Energies*, vol. 13, no. 15, p. 3994, 2020.

[9] S. LeVasseur and J. Situ, "Condominium dwellings in canada: Nhs 2011," 2014.

[10] G. Bauer, C.-W. Hsu, M. Nicholas, and N. Lutsey, "Charging up america: Assessing the growing need for us charging infrastructure through 2030," *White Paper ICCT*, 2021.

[11] M. August, "The financialization of canadian multi-family rental housing: From trailer to tower," *Journal of Urban Affairs*, vol. 42, no. 7, pp. 975–997, 2020.

[12] H. O. E. Price, "Independent electricity system operator (ieso)," *Retrieved May*, 2014.

[13] M. Samadi and J. Fattahi, "Effective self-committed v2g for residential complexes," *Sustainable Energy, Grids and Networks*, vol. 35, p. 101114, 2023.

[14] R. Rice and G. W. Stagg, "Application program design criteria for the southern company control system," in *Proceedings of the 8th IEEE PICA Conference*, Minneapolis, MN, USA, 1973, pp. 128–134.

[15] S. C. Savulescu, *Computerized operation of Power systems.* Elsevier Amsterdam, 1976.

[16] A. Monticelli, “The role and implementation of state estimation in an energy management system,” *Electric Power Systems Research*, vol. 16, no. 1, pp. 1–10, 1990.

[17] D. Mariano-Hernández, L. Hernández-Callejo, A. Zorita-Lamadrid, O. Duque-Pérez, and F. S. García, “A review of strategies for building energy management system: Model predictive control, demand side management, optimization, and fault detect & diagnosis,” *Journal of building engineering*, vol. 33, p. 101692, 2021.

[18] I. Gomes, K. Bot, M. G. Ruano, and A. Ruano, “Recent techniques used in home energy management systems: A review,” *Energies*, vol. 15, no. 8, p. 2866, 2022.

[19] G. Srihari, R. Krishnam Naidu, P. Falkowski-Gilski, P. Bidare Divakarachari, and R. Kiran Varma Penmatsa, “Integration of electric vehicle into smart grid: a meta heuristic algorithm for energy management between v2g and g2v,” *Frontiers in Energy Research*, vol. 12, p. 1357863, 2024.

[20] S. Ahmad, M. Shafiullah, C. B. Ahmed, and M. Alowaifeer, “A review of microgrid energy management and control strategies,” *IEEe Access*, vol. 11, pp. 21 729–21 757, 2023.

[21] C. L. Bhattar and M. A. Chaudhari, “Centralized energy management scheme for grid connected dc microgrid,” *IEEE Systems Journal*, vol. 17, no. 3, pp. 3741–3751, 2023.

[22] M. Elkholy, H. Metwally, M. Farahat, T. Senjyu, and M. E. Lotfy, “Smart centralized energy management system for autonomous microgrid using fpga,” *Applied energy*, vol. 317, p. 119164, 2022.

[23] M. Yan, F. Teng, W. Gan, W. Yao, and J. Wen, "Blockchain for secure decentralized energy management of multi-energy system using state machine replication," *Applied Energy*, vol. 337, p. 120863, 2023.

[24] S. L. L. Wynn, T. Boonraksa, P. Boonraksa, W. Pinthurat, and B. Marungsri, "Decentralized energy management system in microgrid considering uncertainty and demand response," *Electronics*, vol. 12, no. 1, p. 237, 2023.

[25] V. Boglou, C.-S. Karavas, A. Karlis, and K. Arvanitis, "An intelligent decentralized energy management strategy for the optimal electric vehicles' charging in low-voltage islanded microgrids," *International journal of energy research*, vol. 46, no. 3, pp. 2988–3016, 2022.

[26] E. Gümrükcü, J. R. A. Klemets, J. A. Suul, F. Ponci, and A. Monti, "Decentralized energy management concept for urban charging hubs with multiple v2g aggregators," *IEEE Transactions on Transportation Electrification*, vol. 9, no. 2, pp. 2367–2381, 2022.

[27] Y. Sabri, N. El Kamoun, and F. Lakrami, "A survey: Centralized, decentralized, and distributed control scheme in smart grid systems," in *2019 7th mediterranean congress of telecommunications (CMT)*. IEEE, 2019, pp. 1–11.

[28] T.-Y. Chen, F.-F. Wei, and W.-N. Chen, "Multi-agent swarm optimization for decentralized energy management considering game behaviors of electric vehicles," in *Proceedings of the Genetic and Evolutionary Computation Conference*, 2025, pp. 1337–1344.

[29] A. Umar, D. Kumar, T. Ghose, T. A. Alghamdi, and A. Y. Abdelaziz, "Decentralized community energy management: Enhancing demand response through smart contracts in a blockchain network," *IEEE Access*, vol. 12, pp. 80 781–80 798, 2024.

[30] T. D. de Lima, P. Faria, and Z. Vale, "Optimizing home energy management systems: A mixed integer linear programming model considering battery cycle degradation," *Energy and Buildings*, vol. 329, p. 115251, 2025.

[31] R. Faia, P. Faria, and Z. Vale, "Optimizing house energy management with milp considering shifting of electric appliances and battery storage system," in *2023 IEEE PES Innovative Smart Grid Technologies Europe (ISGT EUROPE)*. IEEE, 2023, pp. 1–5.

[32] G. Liu, M. F. Ferrari, T. B. Ollis, and K. Tomsovic, "An milp-based distributed energy management for coordination of networked microgrids," *Energies*, vol. 15, no. 19, p. 6971, 2022.

[33] S. García, S. Bracco, A. Parejo, M. Fresia, J. I. Guerrero, and C. Leon, "Cost-effective operation of microgrids: A milp-based energy management system for active and reactive power control," *International Journal of Electrical Power & Energy Systems*, vol. 165, p. 110458, 2025.

[34] A. Imran, G. Hafeez, I. Khan, M. Usman, Z. Shafiq, A. B. Qazi, A. Khalid, and K.-D. Thoben, "Heuristic-based programable controller for efficient energy management under renewable energy sources and energy storage system in smart grid," *IEEE Access*, vol. 8, pp. 139 587–139 608, 2020.

[35] H. E. Oliveira Farias, C. A. Sepulveda Rangel, L. Weber Stringini, L. Neves Canha, D. Pegoraro Bertineti, W. da Silva Brignol, and Z. Iensen Nadal, "Combined framework with heuristic programming and rule-based strategies for scheduling and real time operation in electric vehicle charging stations," *Energies*, vol. 14, no. 5, p. 1370, 2021.

[36] V. Suresh, P. Janik, M. Jasinski, J. M. Guerrero, and Z. Leonowicz, "Microgrid energy management using metaheuristic optimization algorithms," *Applied Soft Computing*, vol. 134, p. 109981, 2023.

[37] A. Jindal, N. Kumar, and J. J. Rodrigues, "A heuristic-based smart hvac energy management scheme for university buildings," *IEEE Transactions on Industrial Informatics*, vol. 14, no. 11, pp. 5074–5086, 2018.

[38] Z. Mahmood, B. Cheng, N. A. Butt, G. U. Rehman, M. Zubair, A. Badshah, and M. Aslam, "Efficient scheduling of home energy management controller (hemc) using heuristic optimization techniques," *Sustainability*, vol. 15, no. 2, p. 1378, 2023.

[39] R. Liemthong, C. Srithapon, P. K. Ghosh, and R. Chatthaworn, "Home energy management strategy-based meta-heuristic optimization for electrical energy cost minimization considering tou tariffs," *Energies*, vol. 15, no. 2, p. 537, 2022.

[40] M. Cannon, V. Deshmukh, and B. Kouvaritakis, "Nonlinear model predictive control with polytopic invariant sets," *Automatica*, vol. 39, no. 8, pp. 1487–1494, 2003.

[41] F. Simmini, T. Caldognetto, M. Bruschetta, E. Mion, and R. Carli, "Model predictive control for efficient management of energy resources in smart buildings," *Energies*, vol. 14, no. 18, p. 5592, 2021.

[42] S. Sen and M. Kumar, "Mpc based energy management system for grid-connected smart buildings with evs," in *2022 IEEE IAS Global Conference on Emerging Technologies (GlobConET)*. IEEE, 2022, pp. 146–151.

[43] D. Zhao, D. Watari, Y. Ozawa, I. Taniguchi, T. Suzuki, Y. Shimoda, and T. Onoye, "Data-driven online energy management framework for hvac systems: An experimental study," *Applied Energy*, vol. 352, p. 121921, 2023.

[44] T. Schmitt, J. Engel, and T. Rodemann, "Regression-based model error compensation for a hierarchical mpc building energy management system," in *2023 IEEE Conference on Control Technology and Applications (CCTA)*. IEEE, 2023, pp. 1–8.

[45] G. Bruni, S. Cordiner, V. Mulone, V. Rocco, and F. Spagnolo, "A study on the energy management in domestic micro-grids based on model predictive control strategies," *Energy Conversion and Management*, vol. 102, pp. 50–58, 2015.

[46] F. Mueller, S. de Jongh, C. A. Cañizares, T. Leibfried, and K. Bhattacharya, "Comparison of machine learning and mpc methods for control of home battery storage systems in distribution grids," *Applied Energy*, vol. 400, p. 126465, 2025.

[47] A. Saifoddin, N. Mirzaei, M. Allahrabbi Shirazi, and H. Yousefi, "Comparative applications of supervised and unsupervised machine learning models in energy systems," *Journal of Energy Management and Technology*, vol. 9, no. 4, pp. 284–290, 2025.

[48] G. E. Okereke, M. C. Bali, C. N. Okwueze, E. C. Ukekwe, S. C. Echezona, and C. I. Ugwu, "K-means clustering of electricity consumers using time-domain features from smart meter data," *Journal of Electrical Systems and Information Technology*, vol. 10, no. 1, p. 2, 2023.

[49] J. Liu, X. Xu, F. Zhang, Y. Gao, and W. Gao, "Modeling of spatial distribution characteristics of high proportion renewable energy based on complex principal component analysis," in *2020 IEEE Sustainable Power and Energy Conference (iSPEC)*, 2020, pp. 193–198.

[50] S. Akhtar, S. Shahzad, A. Zaheer, H. S. Ullah, H. Kilic, R. Gono, M. Jasiński, and Z. Leonowicz, "Short-term load forecasting models:

A review of challenges, progress, and the road ahead," *Energies*, vol. 16, no. 10, p. 4060, 2023.

[51] E. Vianita and H. Tantyoko, "A comparative study of machine learning models for short-term load forecasting," *Jurnal Masyarakat Informatika*, vol. 16, no. 1, pp. 93–103, 2025.

[52] W. Guo, L. Che, M. Shahidehpour, and X. Wan, "Machine-learning based methods in short-term load forecasting," *The Electricity Journal*, vol. 34, no. 1, p. 106884, 2021.

[53] A. E. Muñoz-Zavala, J. E. Macías-Díaz, D. Alba-Cuéllar, and J. A. Guerrero-Díaz-de León, "A literature review on some trends in artificial neural networks for modeling and simulation with time series," *Algorithms*, vol. 17, no. 2, p. 76, 2024.

[54] I. Khabbouchi, D. Said, A. Oukaira, I. Mellal, and L. Khoukhi, "Machine learning and game-theoretic model for advanced wind energy management protocol (awemp)," *Energies*, vol. 16, no. 5, p. 2179, 2023.

[55] M. Movahednia, H. Karimi, and S. Jadid, "A cooperative game approach for energy management of interconnected microgrids," *Electric Power Systems Research*, vol. 213, p. 108772, 2022.

[56] S. Malik, M. Duffy, S. Thakur, B. Hayes, and J. Breslin, "A priority-based approach for peer-to-peer energy trading using cooperative game theory in local energy community," *International Journal of Electrical Power & Energy Systems*, vol. 137, p. 107865, 2022.

[57] Y. Huang, Y. Wang, and N. Liu, "A two-stage energy management for heat-electricity integrated energy system considering dynamic pricing of stackelberg game and operation strategy optimization," *Energy*, vol. 244, p. 122576, 2022.

[58] Y. Li, B. Wang, Z. Yang, J. Li, and C. Chen, "Hierarchical stochastic scheduling of multi-community integrated energy systems in uncertain environments via stackelberg game," *Applied Energy*, vol. 308, p. 118392, 2022.

[59] F. González, P. Arévalo, and L. Ramirez, "Game theory and robust predictive control for peer-to-peer energy management: a pathway to a low-carbon economy," *Sustainability*, vol. 17, no. 5, p. 1780, 2025.

[60] L. A. Roald, D. Pozo, A. Papavasiliou, D. K. Molzahn, J. Kazempour, and A. Conejo, "Power systems optimization under uncertainty: A review of methods and applications," *Electric Power Systems Research*, vol. 214, p. 108725, 2023.

[61] Z. Wang, P. Jochem, and W. Fichtner, "A scenario-based stochastic optimization model for charging scheduling of electric vehicles under uncertainties of vehicle availability and charging demand," *Journal of Cleaner Production*, vol. 254, p. 119886, 2020.

[62] A. Alsharif, C. W. Tan, R. Ayop, A. Al Smin, A. Ali Ahmed, F. H. Kuwil, and M. M. Khaleel, "Impact of electric vehicle on residential power distribution considering energy management strategy and stochastic monte carlo algorithm," *Energies*, vol. 16, no. 3, p. 1358, 2023.

[63] X.-J. Dong, J.-N. Shen, Z.-F. Ma, and Y.-J. He, "Stochastic optimization of integrated electric vehicle charging stations under photovoltaic uncertainty and battery power constraints," *Energy*, vol. 314, p. 134163, 2025.

[64] A. Arrigo, C. Ordoudis, J. Kazempour, Z. De Grève, J.-F. Toubeau, and F. Vallée, "Wasserstein distributionally robust chance-constrained

optimization for energy and reserve dispatch: An exact and physically-bounded formulation," *European Journal of Operational Research*, vol. 296, no. 1, pp. 304–322, 2022.

[65] D. Bertsimas, D. B. Brown, and C. Caramanis, "Theory and applications of robust optimization," *SIAM review*, vol. 53, no. 3, pp. 464–501, 2011.

[66] H. Karimianfard, "A robust optimization framework for smart home energy management: Integrating photovoltaic storage, electric vehicle charging, and demand response," *Journal of Energy Storage*, vol. 110, p. 115259, 2025.

[67] B. Tan, H. Chen, X. Zheng, and J. Huang, "Two-stage robust optimization dispatch for multiple microgrids with electric vehicle loads based on a novel data-driven uncertainty set," *International Journal of Electrical Power & Energy Systems*, vol. 134, p. 107359, 2022.

[68] S. Ratanakuakangwan and H. Morita, "Hybrid stochastic robust optimization and robust optimization for energy planning–a social impact-constrained case study," *Applied Energy*, vol. 298, p. 117258, 2021.

[69] H. Rahimian and S. Mehrotra, "Distributionally robust optimization: A review," *arXiv preprint arXiv:1908.05659*, 2019.

[70] F. Aghamohammadi, A. Abbaspour, H. Saber, S. Fattaheian-Dehkordi, and M. Lehtonen, "Decentralized energy management of multiagent distribution systems considering the grid reliability and agent misbehavior," *IEEE Systems Journal*, vol. 18, no. 2, pp. 905–916, 2024.

[71] Y. Cao, D. Li, Y. Zhang, Q. Tang, A. Khodaei, H. Zhang, and Z. Han, "Optimal energy management for multi-microgrid under a transactive energy framework with distributionally robust optimization," *IEEE transactions on smart grid*, vol. 13, no. 1, pp. 599–612, 2021.

[72] P. Mohajerin Esfahani and D. Kuhn, "Data-driven distributionally robust optimization using the wasserstein metric: Performance guarantees and tractable reformulations," *Mathematical Programming*, vol. 171, no. 1, pp. 115–166, 2018.

[73] R. Gao and A. Kleywegt, "Distributionally robust stochastic optimization with wasserstein distance," *Mathematics of Operations Research*, vol. 48, no. 2, pp. 603–655, 2023.

[74] A. Zhou, M. Yang, T. Wu, and L. Yang, "Distributionally robust energy management for islanded microgrids with variable moment information: An misocp approach," *IEEE Transactions on Smart Grid*, vol. 14, no. 5, pp. 3668–3680, 2023.

[75] K. Shariatmadar, A. Arrigo, F. Vallée, H. Hallez, L. Vandevelde, and D. Moens, "Day-ahead energy and reserve dispatch problem under non-probabilistic uncertainty," *Energies*, vol. 14, no. 4, p. 1016, 2021.

[76] A. Arrigo, J.-F. Toubeau, I. Fattahi, Z. De Grève, and F. Vallée, "Distributionally robust power and gas dispatch with multivariate and correlated uncertainty," in *2022 17th International Conference on Probabilistic Methods Applied to Power Systems (PMAPS)*. IEEE, 2022, pp. 1–6.

[77] H. Saberi, C. Zhang, and Z. Y. Dong, "Data-driven distributionally robust hierarchical coordination for home energy management," *IEEE Transactions on Smart Grid*, vol. 12, no. 5, pp. 4090–4101, 2021.

[78] N. Nazir, T. Ramachandaran, S. Kundu, and V. Adetola, "Improved microgrid resiliency through distributionally robust optimization under a policy-mode framework," in *2024 IEEE Power & Energy Society General Meeting (PESGM)*. IEEE, 2024, pp. 1–5.

[79] H. T. Nguyen and D.-H. Choi, "Distributionally robust model predictive control for smart electric vehicle charging station with v2g/v2v capability," *IEEE Transactions on Smart Grid*, vol. 14, no. 6, pp. 4621–4633, 2023.

[80] T. Wang, X. Zhang, X. Zheng, J. Wang, S. Ma, J. Chen, M. Liu, and W. Wei, "Data-driven distributionally robust optimization for solar-powered ev charging under spatiotemporal uncertainty in urban distribution networks," *Energies*, vol. 18, no. 15, p. 4001, 2025.

[81] S. P. Boyd and L. Vandenberghe, *Convex optimization.* Cambridge university press, 2004.

[82] S. Pemasinghe and S. Rajapaksha, "Comparison of cpu scheduling algorithms: Fcfs, sjf, srtf, round robin, priority based, and multilevel queuing," in *2022 IEEE 10th Region 10 Humanitarian Technology Conference (R10-HTC).* IEEE, 2022, pp. 318–323.

[83] S. M. Tabatabaee, J.-Y. Le Boudec, and M. Boyer, "Interleaved weighted round-robin: A network calculus analysis," *IEICE Transactions on Communications*, vol. 104, no. 12, pp. 1479–1493, 2021.

[84] X.-X. Ren and G.-H. Yang, "Multi-sensor kalman filtering over packet-dropping networks subject to round-robin protocol scheduling," *Journal of the Franklin Institute*, vol. 358, no. 15, pp. 7938–7954, 2021.

[85] F. Han, Z. Wang, G. Chen, and H. Dong, "Scalable consensus filtering for uncertain systems over sensor networks with round-robin protocol," *International Journal of Robust and Nonlinear Control*, vol. 31, no. 3, pp. 1051–1066, 2021.

[86] Y. Xu, W. Lv, W. Lin, R. Lu, and D. E. Quevedo, "On extended state estimation for nonlinear uncertain systems with round-robin protocol," *Automatica*, vol. 138, p. 110154, 2022.

[87] Z. Feng, W. Xu, and J. Cao, "Distributed nash equilibrium computation under round-robin scheduling protocol," *IEEE Transactions on Automatic Control*, vol. 69, no. 1, pp. 339–346, 2023.

[88] B. Shen, Z. Wang, D. Wang, and H. Liu, "Distributed state-saturated recursive filtering over sensor networks under round-robin protocol," *IEEE Transactions on Cybernetics*, vol. 50, no. 8, pp. 3605–3615, 2019.

[89] Y. Chen, Z. Wang, L. Wang, and W. Sheng, "Finite-horizon h_∞ state estimation for stochastic coupled networks with random inner couplings using round-robin protocol," *IEEE Transactions on Cybernetics*, vol. 51, no. 3, pp. 1204–1215, 2020.

[90] Y. Li, L. Wang, K. Liu, W. He, Y. Yin, and R. Johansson, "Distributed neural-network-based cooperation control for teleoperation of multiple mobile manipulators under round-robin protocol," *IEEE Transactions on Neural Networks and Learning Systems*, vol. 34, no. 8, pp. 4841–4855, 2021.

[91] M. Sanaj and P. J. Prathap, "An enhanced round robin (err) algorithm for effective and efficient task scheduling in cloud environment," in *2020 Advanced Computing and Communication Technologies for High Performance Applications (ACCTHPA)*. IEEE, 2020, pp. 107–110.

[92] M. Iqbal, Z. Ullah, I. A. Khan, S. Aslam, H. Shaheer, M. Humayon, M. A. Salahuddin, and A. Mehmood, "Optimizing task execution: The impact of dynamic time quantum and priorities on round robin scheduling," *Future Internet*, vol. 15, no. 3, p. 104, 2023.

[93] N. Ghazy, A. Abdelkader, M. S. Zaki, and K. A. ElDahshan, "A new round robin algorithm for task scheduling in real-time system." *International Journal of Intelligent Engineering & Systems*, vol. 15, no. 5, 2022.

[94] W. Kempton, R. T. McGee, and G. A. Ejzak, "A universal electric vehicle outlet and portable cable for north america," *World Electric Vehicle Journal*, vol. 15, no. 8, p. 353, 2024.

[95] SAE International, *SAE Electric Vehicle and Plug-in Hybrid Electric Vehicle Conductive Charge Coupler*, SAE International Std. SAE J1772, Oct. 2017, table 5.

[96] D. Elmo, G. Fragkos, J. Johnson, K. Rohde, S. Salinas, and J. Zhang, "Disrupting ev charging sessions and gaining remote code execution with dos, mitm, and code injection exploits using ocpp 1.6," in *2023 Resilience Week (RWS)*. IEEE, 2023, pp. 1–8.

[97] SWTCH Energy. (2023) Open charge point protocol (ocpp) explained: What it is, how it works, and why it matters for ev charging. Accessed: 2025-08-19. [Online]. Available: https://swtchenergy.com/blog/ev-insights/open-charge-point-protocol-ocpp-explained-what-it-is-how-it-works-and-why-it-matters-for-ev-charging/

[98] M. Samadi and J. Fattahi, "Evse effectiveness in multi-unit residential buildings using composite optimization and heuristic search," *IEEE Transactions on Power Systems*, vol. 39, no. 2, pp. 3523–3536, 2023.

[99] P. Pradhan, P. K. Behera, and B. Ray, "Modified round robin algorithm for resource allocation in cloud computing," *Procedia Computer Science*, vol. 85, pp. 878–890, 2016.

[100] R. J. Fernandes, "Queue fundamentals, implementation and its applications in round robin scheduling," *Int. J. Adv. Sci. Eng*, vol. 9, pp. 2556–2566, 2022.

[101] T. Balharith and F. Alhaidari, "Round robin scheduling algorithm in cpu and cloud computing: a review," in *2019 2nd international con-*

ference on computer applications & information security (ICCAIS). IEEE, 2019, pp. 1–7.

[102] J. Smart, W. Powell, and S. Schey, "Extended range electric vehicle driving and charging behavior observed early in the ev project," SAE Technical Paper, Tech. Rep., 2013.

[103] S. Makonin, B. Ellert, I. V. Bajic, and F. Popowich, "Electricity, water, and natural gas consumption of a residential house in Canada from 2012 to 2014," *Scientific Data*, vol. 3, no. 160037, pp. 1–12, 2016.

[104] T. Başar and G. J. Olsder, *Dynamic noncooperative game theory.* SIAM, 1998.

[105] A. A. Kulkarni, "Stackelberg game," https://www.sc.iitb.ac.in/~ankur/docs/SC631Notes/SC631_2014_Lecture23.pdf, 2014.

[106] R. Johari, "Lecture notes | MS&E 246: Lecture 7 Stackelberg games | Stanford University," http://web.stanford.edu/~rjohari/teaching/notes/246_lecture7_2007.pdf, 2007.

[107] J. Fattahi, D. Wright, and H. Schriemer, "An energy internet derms platform using a multi-level stackelberg game," *Sustainable Cities and Society*, vol. 60, p. 102262, 2020.

[108] J. Watson, *Strategy: An Introduction to Game Theory.* W.W. Norton, 2008.

[109] M. Samadi, H. Kebriaei, H. Schriemer, and M. Erol-Kantarci, "Stochastic demand response management using mixed-strategy Stackelberg game," *IEEE Systems Journal*, 2022.

[110] S. Kakutani, "A generalization of brouwer's fixed point theorem," *Duke Mathematical Journal*, vol. 8, no. 3, pp. 457–459, 1941.

[111] O. E. Board, “Electricity rates,” http://www.oeb.ca/rates-and-your-bill/electricity-rates, 2020.